Reorganization of the Senescent Genome *via* Spatial CTCF Clustering

Dissertation

for the award of the degree

Doctor rerum naturalium (Dr. rer. nat.)

of the Georg-August-Universität Göttingen

within the doctoral program

International Max Planck Research School for Genome Science

of the Georg-August University School of Science (GAUSS)

submitted by

Spyridon Palikyras

from Corfu, Greece

Göttingen 2023

Thesis Advisory Committee

Prof. Dr. Argyris Papantonis (Supervisor)

Institute of Pathology, University Medical Center Göttingen, 37075 Göttingen, Germany

Dr. Ufuk Günesdogan

Göttingen Center for Molecular Biosciences, Department of Developmental Biology, 37077, Göttingen, Germany

Prof. Dr. Markus Zweckstetter

German Center for Neurodegenerative Diseases, 37075 Göttingen, Germany

Members of the Examination Board

1st Referee: **Prof. Dr. Argyris Papantonis** (Supervisor)

Institute of Pathology, University Medical Center Göttingen, 37075 Göttingen, Germany

2nd Referee: **Dr. Ufuk Günesdogan**

Göttingen Center for Molecular Biosciences, Department of Developmental Biology, 37077, Göttingen, Germany

Further members of the Examination Board

Dr. Marieke Oudelaar

Max Planck Institute for Biophysical Chemistry, Göttingen, Germany

PD. Dr. Laura Zelarayán-Behrend

Institute of Pharmacology and Toxicology, University Medical Center Göttingen

Dr. Nico Posnien

Department of Developmental Biology, Johann-Friedrich-Blumenbach-Institute of Zoology and

Anthropology, Georg-August-University Göttingen

Date of oral examination: May 31st, 2023

Table of contents

Acknowledgements

Here comes the time that you need to fit the last four years into one page. A task harder than writing this dissertation itself. At the same time the limited space forces the mind to extract the very essence of the PhD life and avoid a stream of idle chatter. Undoubtedly, during the course of these years I grew as a person and I could not have asked for a better environment to do so, than the one that I found here in Göttingen at Akis' lab.

Which brings me to the first person that I would like to thank and the main responsible for people, soon, to call me a Dr.. Aki, our first interview was on a summery Saturday morning after being partying the night before. I thought I did well. In matter of fact, you must have been left so amazed that I never heard from you again for the rest of the summer. It was only at the end of September, when I was still looking for a position, you were still looking for a student, so as we were both desperate enough, we agreed on collaborating. I have never regrated that day, not even for a single moment. Being part of your team was a delight. At your face, I found an above average novelist, a great scientist, but mostly, an extraordinaire mentor. You have managed to gather a successful team here and I believe this did not happen accidently. Therefore, thank you for involving me on this.

Out of this team, I managed to create some strong, non-work related, bonds. Kosta, my first impression for you was not the best and honestly little did change the more I got to know you. I compromised so that I can have someone to go out for a beer and I ended up hosting you for a month and helping you countless times to move from place to place, including your establishment to another country! Honestly though, my time here would have been completely different if we had not met and if we had not created all these memories together. Therefore, I should thank you. Nataša, the first time we interacted, I immediately thought to myself what a nice and not-at-all intimidating person! But, I could already foresee what a sensitive person you are and the kind of supportive friend that you would turn to be for me. We spent numerous times discussing about life and things that were bothering both of us and giving each other a push to go forward. Hvala ti puno što si bila tu!

Nadine, I remember a couple of months after I was here we had a discussion and when I referred to you as a friend you turned to me and with a very German way you told me "we're not friends, we're colleagues''! Our retreat in KWT a couple of weeks later and our trip to Greece upgraded our status extremely fast! Since then we have shared a lot of stuff, thoughts and worries.

We were together from day 0 in this PhD journey until the very last moment of submission and your help all this time cannot be put into words. I cannot imagine how different these years would have been if I was by myself!

Of course, throughout this time I met some excellent people in Akis' group. Sia, Ting, Mariano, Adi, Shu, Yajie and Ilia each one of you assisted in your own unique way to make me feel welcomed and that I belong to something bigger than just a working group. Believe me, in the course of time that was the most important emotion that kept me going even when I thought I had enough! Thank you all and each one of you separately!

Lastly, a few words about my family. Ειλικρινά, είναι δύσκολο να διαλέξω μια στιγμή για να ξεκινήσω, μιας και η συμπαράσταση και η βοήθεια που μου έχει προσφερθεί διαρκεί 32 χρόνια! Ίσως η αφετηρία αυτού που σήμερα ολοκληρώνεται να είναι η μητέρα μου. Η δική της παρότρυνση με οδήγησε στη Μοριακή Βιολογία and the rest is history (που λέμε και στην Κέρκυρα). Δυστυχώς, δε βρίσκεται πλέον ανάμεσά μας αλλά είμαι σίγουρος πως θα ήταν πολύ περήφανη αν ήταν εδώ και θα καμάρωνε. Όπως πιθανότατα θα καμαρώνει ο πατέρας μου και ας μην το δείχνει ή το παραδέχεται για να μην πάρουν τα μυαλά μου περισσότερο αέρα. Μέσα σε ένα γενικότερο χαμό το 2014, όταν τελείωσα με το πτυχίο μου στην Αλεξανδρούπολη και δεν ήξερα τι μέλλει γενέσθαι, παρουσιάστηκε μια ευκαιρία για τα Γιάννενα. Τότε, με πενιχρά οικονομικά μέσα, όταν τον ρώτησα τι να κάνω και αν μπορούμε να το υποστηρίξουμε, χωρίς να το σκεφτεί μου είπε «πήγαινε και θα τα καταφέρουμε». Και απ' ότι φαίνεται τα καταφέραμε! Τα Γιάννενα ήταν που, πιθανότατα, με οδήγησαν για μεταπτυχιακό στη Χαϊδελβέργη. Κι εκεί Βάγγο, έβαλες μεγάλη πλάτη. Παρά τα παράπονα σου, ειδικά κάθε εξάμηνο που έπεφταν μαζεμένα τα έξοδα, και τις «γλυκές» σου παροτρύνσεις, «άντε πότε θα βρεις καμιά δουλειά», με στήριξες όλα αυτά τα τρία χρόνια, ούτως ώστε το "Project S" να αρχίσει να αποδίδει! Μόνο ευχαριστώ μπορώ να πω και να ξέρεις ότι δεν έχει περάσει απαρατήρητο!

Summary

Cellular senescence is now understood to be a major hallmark of the aging process. Senescence can be induced by many stress factors, including telomere shortening, DNA damage and tumor-suppressor genes activation and is characterized by growth arrest, changes in gene expression and chromatin reorganization. Intensive research in the field has uncovered diverse functional implications for these senescence-inducing cascades. Nowadays, senescence is perceived as a late developmental stage in cell's life, as a protective mechanism against cancer and as a positive contributor in wound healing. On the other hand, senescence can also be implicated in a range of abnormal contexts, for example tumor progression due to the senescence-associated secretome, and many age-related syndromes. Despite its importance, studying senescence *in vitro* remains complex and problematic in practice as, usually, cell population nearing senescence are highly heterogenous and it takes a significant amount of time to drive certain cell types into full-fledged senescence. Therefore, in **Chapter I**, I am discussing the establishment of a novel way for chemically inducing senescence which tackles the aforementioned caveats and allows for robust studies of the replicative senescence cascade.

Chromatin organization is also markedly affected upon senescence entry and aging. These changes in chromatin structure range from very focal ones, for example histone modifications, to alterations in heterochromatin organization and, eventually, higher-order chromatin conformation. CTCF holds a prominent role in 3D genome architecture as it functions as an insulator protein between different chromatin domains and is one of the primary factors driving loop formation. Following senescence entry, CTCF has been found to dramatically reorganize into distinct senescence-associated CTCF clusters (SICCs). In **Chapter II,** I examine how SICCs are formed and maintained in 3D nuclear space, along with their interplay with nuclear speckles, a phase separated repository of RNA-processing related factors. Taken together, this thesis combines the introduction of a new model of chemically-induced senescence with the study of a structural hallmark of senescence entry to offer a new perspective of how genome reorganization crosswalks with cellular aging.

1. Introduction

1.1 *Overview of Senescence*

1.1.1 What is Senescence?

Cellular senescence was firstly described by Hayflick and Moorhead back in the 60's [1,2], when they observed that primary diploid fibroblasts in culture have a limited amount of cell divisions – what was later known as the Hayflick's limit. Since then, great amount of research has been devoted in an effort to further and better explain this phenomenon. It is now understood that different kinds of senescence exist as a response to a variety of different stress stimuli (**Fig.1.1**). These, can include progressive telomere shortening, oncogenic activation, genotoxic stress (e.g. irradiation, chemotherapy), but also chromatin and epigenetic changes [3–5] that subsequently lead to replicative senescence (RS), oncogene-induced senescence (OIS), senescence induced by genotoxic stress and epigenetically induced senescence [6]. Nonetheless, regardless of what the causal trigger might be, all of them share a common characteristic: the irreversible cell cycle arrest. In few occasions, however, mostly tumor-related, it was demonstrated that this arrest can be reversed and cells can re-enter the cell cycle, but these cases represent the minority rather than the norm [7–9].

After intensive research in the field it has been lately shown, that senescence is a far more complicated and dynamic process than just a proliferation arrest stage, which exhibits numerous changes both in cellular and molecular level [10,11]. Maybe the most prominent of them is the initiation of a highly complex cascade that leads to the secretion of senescence-associated proteins (senescence-associated secretory phenotype – SASP, see below for details)[12]. On top of these changes, many microscopically visible phenotypical alterations occur, such as enlarged nuclear size and amend composition of the plasma membrane, just to mention a few [13]. Additionally, senescent cells undergo extreme changes in their metabolic activities, gene expression pattern and chromatin architecture [14–16], thus senescence should not be confused with aging, but it should be consider, and lately it does more and more, as one of its hallmarks [17].

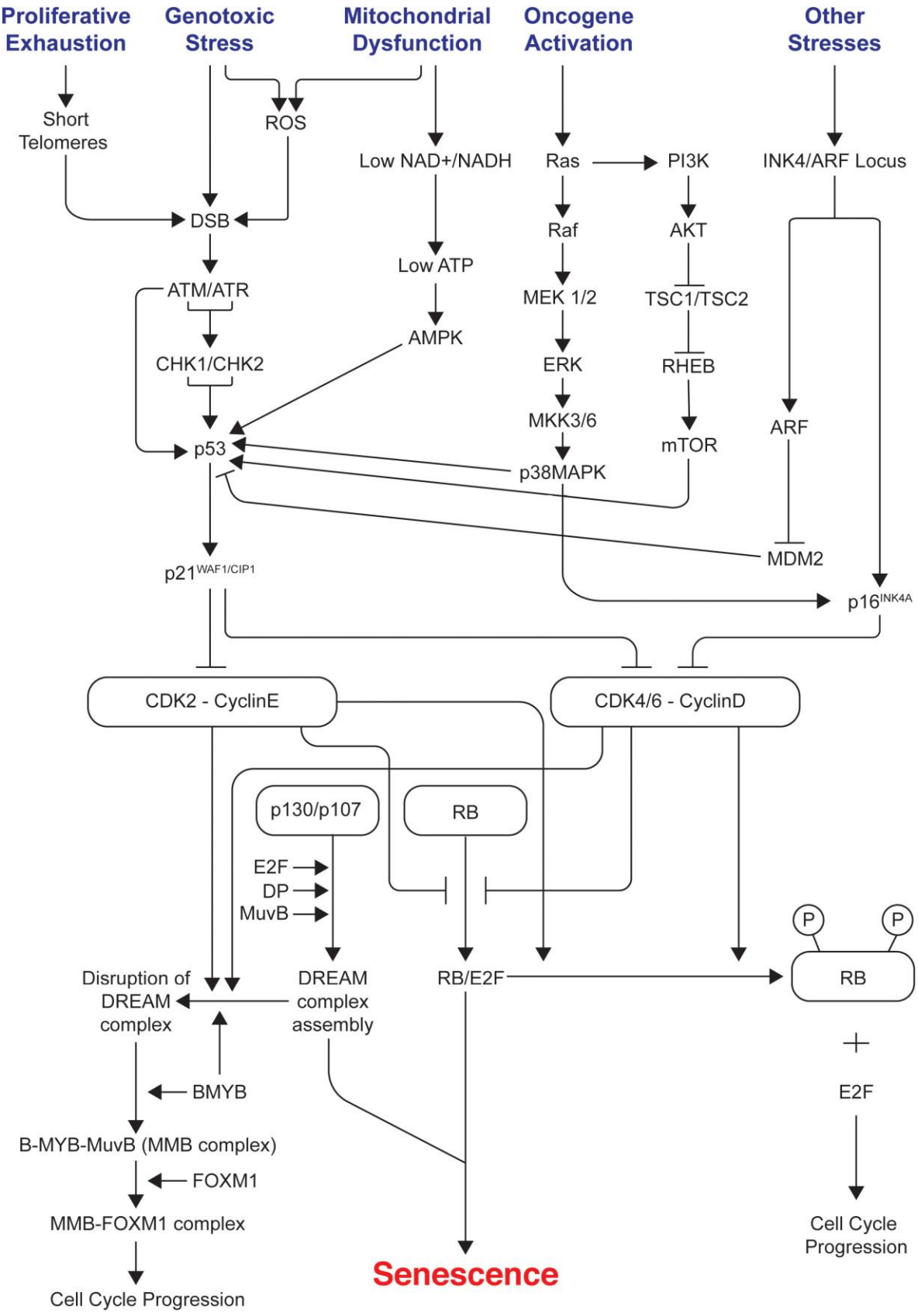

Figure 1.1: A plethora of triggers could initiate different cascades and subsequently lead to cell cycle arrest and cellular senescence (*Adapted from: Kumari R and Jat P (2021) Front. Cell Dev. Biol. 9:645593. doi: 10.3389/fcell.2021.645593*).

1.1.2 Cell Cycle Arrest & Cellular Senescence

Well-orchestrated cell cycle propagation is a vital process during cell's lifespan. Failure to do so contributes, under normal circumstances, to cell cycle arrest. This protective mechanism prevents potentially harmful cells from continuing to proliferate with catastrophic consequences. Usually this arrest happens during G1 or G2 stage of the cell cycle [18]. This key feature is a distinguished characteristic between senescence and other, seemingly similar, kinds of growth arrest, such as quiescent, a phenomenon that occurs in G0 phase [19]. A fundamental difference in the identity of these two forms of arrest is that under the appropriate signals, quiescent cells could procced with proliferation, while senescent cells cannot [13,20]. One of the main signaling pathways that controls this fate is the mTOR cascade. This kinase is key component of two larger complexes, mTORC1 and -2, which combined they heavily control anabolic metabolism [21]. When there is a growth arrest and the mTOR pathway remains active it signals for cellular senescence, while its inhibition marks quiescent cells [22,23]. In addition, it has been demonstrated that downregulation of the mTORC1 complex in different organisms promotes their longevity [24].

Crucial role during cell cycle is held by the telomeres, repetitive sequences found at the end of the chromosomes and are shortened after every cell division (and progressively been left exposed), since DNA polymerase cannot fully replicate the lagging strands. The so-called "end replication problem" was already described during the 70's from Alexei Olovnikov, who first observed that chromosomes are unable to completely replicate their ends. Adding this piece of information to Hayflick's observation, Harley et al. linked the telomere shortening with the appearance of cellular senescence [25]. This theory was later strengthened by the fact that ectopic expression of telomerase, the enzyme responsible for elongating the telomeres, was shown to be sufficient to bypass the initial cell cycle arrest [26]. The problem that this shortening creates is that the exposed telomeric ends are now perceived as double-strand breaks by the DNA repair machinery. A multi-step downstream cascade is alarmed [27] and a vast amount of proteins are accumulated on the spot, as part of the DNA damage response (DDR) [28]. The two most prominent signaling cascades that govern cellular senescence are the tumor suppressor pathways of p53/$p21^{WAF1/CIP1}$ and $p16^{INK4A}$ /pRB, which can be activated either together or individually [29,30].

The p53 pathway has a pleiotropic role in a plethora of cellular processes [31]. One of its many activators is the DDR as a result of telomer attrition, which results to constitutive activation of p53 and, consequent, induction of senescence. Ataxia Telengectasia Mutated kinase (ATM), which is also recruited to DNA damage point, phosphorylates p53, thus stabilizing it and allowing it to regulate the expression of other anti-proliferative targets [32], such as the key transcription factor Forkhead Box O-4 (FOXO4) [33]. Similarly, p21, a cyclin-dependent kinase inhibitor (CDKI), is regulated by p53 and plays an important role in telomere-induced senescence. Its upregulation leads to the inhibition of cyclinD/CDK4,6 complexes causing cell cycle arrest [34]. As a result of its two cyclin binding motifs (Cy1/Cy2), p21 can interact and inhibit cyclin complexes [35] and this exact ability allows it to inhibit phosphorylation of the Retinoblastoma (RB) proteins. This inhibition hinders, at a later point, the downstream formation of the dimerization partner, RB-like, E2F and multi-vulval class B (DREAM) complex, hence prompting cell cycle arrest, too [36].

The RB family of proteins consists of three member: RB1 (pRB), RBL1 (p107), and RBL2 (p130). On its dephosphorylated form, pRB binds to transcription factors E2Fs and then, this newly-formed complex binds to E2F target genes promoters and inhibits them. Many of these targets are genes participating in cell cycle progression [37]. Additionally, RB1 inhibits E2F targets by interacting with the Argonaute 2 (AGO2) and miRNA let-7 in the nucleus [38]. The other member of the pathway, $p16^{INK4A}$, is also a CDKI and participates in the cell cycle by binding to and inhibiting CDK4,6. Thus the assembly of cyclinD/CDK4,6 complexes is prevented and RB phosphorylation is impeded leading to the expression of E2F targets [39]. As it has already mentioned above, there are different kinds of senescence. $p16^{INK4A}$ expression is induced upon epigenetically-induced senescence, which is usually chemically induced by a large number of compounds targeting, for example, DNA methyltransferases, histone deacetylases and/or acetyltransferases, and so on [40]. Interestingly, it has been shown that during replicative senescence the CDKN2A locus is derepressed resulting in an upregulation of its expression [41]. Even though the exact mechanism rendering this phenomenon is not yet clear, it has been suggested that what might contribute to it is the loss of some Polycomb-group proteins [42]. The proteins which belong to this group are highly conserved and their main function is to stably repressing specific genes through histone modifications [43]. Knocking-down PRC1/PRC2 complexes led to decreased levels of H3K27me3, followed by $p16^{INK4A}$ induced senescence [42,44]. Despite the fact that epigenetic modifications are rather cell type specific the above case serves as a nice example of how they can possibly regulate and affect cellular senescence.

1.1.3 Senescence-associated Secretome

Despite being in a state of growth arrest, senescent cells are still metabolically active, at least to some extent, and present extreme alterations in their transcriptome. One of the hallmarks during this state is the secretion of a mixture of factors, such as cyto- and chemo-kines, extracellular matrix components, growth modulators and proteases, which collectively are termed as senescence-associated secretory phenotype (SASP) [12,14,45,46]. Through this secretome, senescent cells can communicate with their surroundings and state to neighboring cells their 'special nature', while simultaneously modulating their microenvironment [47,48]. Still, in this complex 'molecular soup' there are factors that are more dominant and studied compared to others.

Insulin-like growth factor-binding proteins -3, -4 and -7 (IGFBP-3,-4 and -7) are well-characterized SASP components [49–51]. They have been found to induce senescence via interaction with the plasminogen activator inhibitor-1 (PAI-1), which is a downstream component of the p53 pathway and they cause senescence through the PI(3)K-PKB-GSK3β-cyclin D1 pathway [52,53]. Additionally, pro-inflammatory factors, like IL-1A, IL-6 and IL-8, which are components and directly dependent from the NF-κB pathway, are over-represented in SASP [54]. Usually, their elevated expression is a result of DNA damage and prolonged activation of the DDR, marking this response as a significant moderator of SASP [5,14,55]. Upregulation of these protein creates a positive feedback loop enhancing NF-κB activity and strengthening the SASP signaling [14,55,56]. The importance of these factors becomes apparent since it has been demonstrated that ectopic expression of IL-1A can, up to a certain degree, recapitulate the SASP effect [57,58]. The components of SASP have the ability to act in a cell-autonomous manner (autocrine) in order to spread senescence, but also in a paracrine manner, thus affecting the microenvironment around the senescent cells and influencing healthy, proliferating neighbors [55,58].

It was shown, that DDR can be induced in adjoining healthy cells by senescent cells, through active transfer of reactive oxygen spices (ROS) via direct cell contact [59,60]. In addition, extracellular vesicles have been recently described as 'transporters' of the 'senescence message' to more distal areas [61]. Another such 'commissionaire' is the complex secretome which is organized by inflammasomes and on its core the senescent signals are mediated by IL-1A and TGF-β [58]. Inflammasomes consists of large cytosolic complexes and their main role is to detect stress-related stimuli and activate an inflammatory response mediated by caspase-1 [62].

SASP expression and secretion can be caused and regulated by many different factors that are both cytoplasmic and nuclear (**Fig. 1.2**). These factors can include, among others, DNA damage, as it has been discussed so far, transposable elements, the presence of cytoplasmic DNA and toll like receptors (TLR). Due to so many and diverse stimuli, equally diverse is the respective response and the included signaling pathways. Recently, it has been shown that there is a cross-talk between transposable elements and cytoplasmic chromatin fragments. Collectively, they can activate the cyclic GMP– AMP synthase linked to stimulator of interferon genes pathway (cGAS-STING), tuning the production of SASP [63–65]. The progressive loss of Lamin B1 from the nucleus [63] and the downregulation of a group of DNases from the cytoplasm [66] upon senescence are the leading factors for the cytoplasmic chromatin accumulation. It was shown, that the activation of the retrotransposable element L1 results in the accretion of cDNA in the cytoplasm, as L1 holds great reverse transcriptase activity. These accumulated cDNA fragments cause the activation of the cGAS-STING pathway and the production of SASP factors [67]. Epigenetic alterations can also affect the expression of SASP genes. Loss of G9a and GLP methyltransferases, due to DNA damage, has as a consequence the general reduction in H2K9me2 levels and upregulation of IL-6 and -8 [68]. Another epigenetic example is that of GATA-4. In proliferating cells GATA-4 binds to p62, an autophagy regulator, and is marked for degradation. Initiation of senescence blocks autophagy, thus stabilizing GATA-4 and enhancing SASP through the NF-κB pathway activation [69].

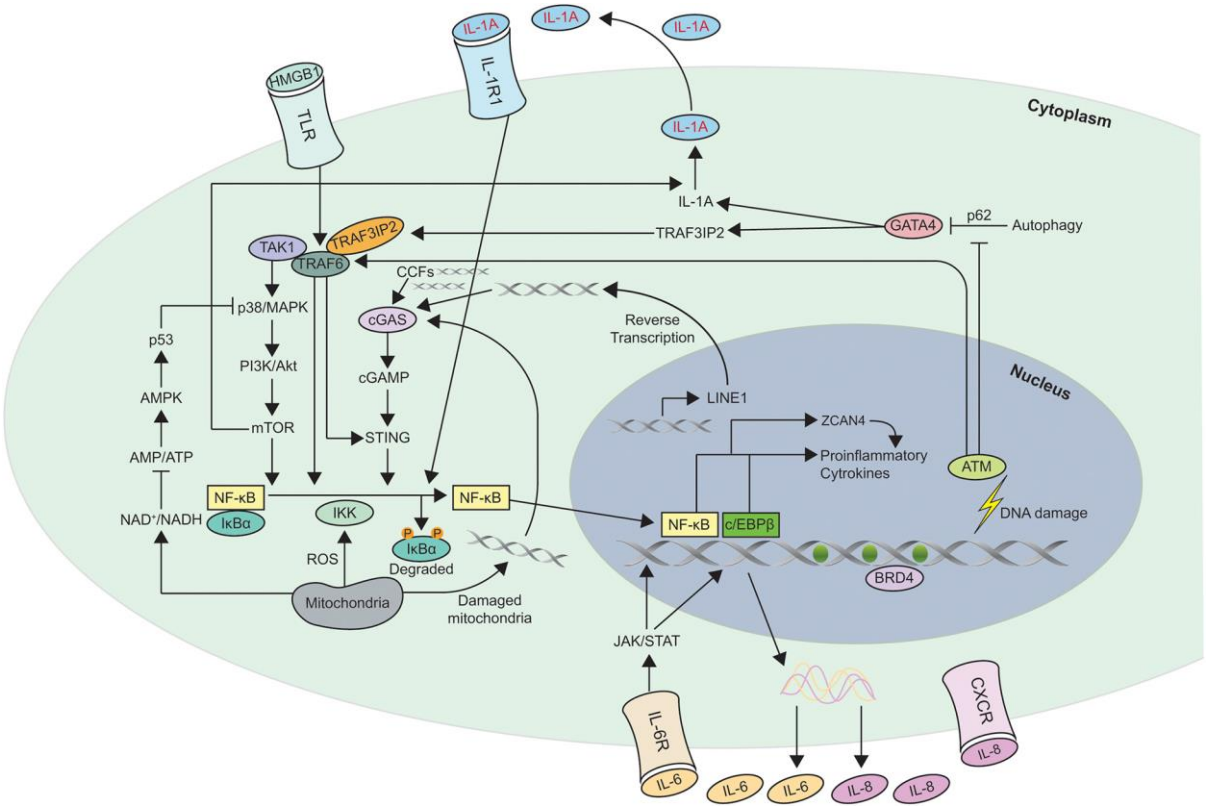

Figure 1.2: Nuclear and cytoplasmic triggers of SASP production (*Adapted from: Kumari R and Jat P (2021) Front. CellDev. Biol. 9:645593. doi: 10.3389/fcell.2021.645593*).

1.1.4 The Diverse Nature of Cellular Senescence

As cellular senescence is an active field of research it becomes continuously obvious its pleiotropic effects; some beneficial, some deleterious (**Fig. 1.3**). On the positive site, senescence is seemed to be a protective mechanism against tumor progression [45,70,71]. In OIS mutations in RAS and/or BRAF oncogenes has been shown to cause growth arrest and prevent tumor expansion [72,73]. In addition, p53-mediated senescence and the respective SASP have been demonstrated to play a beneficial role in limiting fibrotic effects in mice after excessive liver damage [74]. Wound healing is also a process where senescence has a positive contribution. The matricellular protein CCN1, a cysteine-rich protein, has been shown to induce senescence in fibroblast cells [75]. Through binding to integrin $\alpha_6\beta_1$ and activating p53 pathway it gives raise to ROS, resulting in $p16^{INK4a}$/pRb pathway activation.

This cascade leads to the expression of antifibrotic genes and acceleration of wound healing. In another study [76], senescent fibroblasts appeared rapidly upon wound presence and hastened the healing process upon secretion of platelet-derived growth factor AA (PDGF-AA). Lastly, senescence has been attributed an additional role, as the programmed end of differentiation. More specifically, it was shown that mature megakaryocytes acquire a senescent state and they stop dividing through activation of the ERK/MAPK pathway and induction of $p21^{CIP1}$ expression [77].

As beneficial as it could be, senescence has and its dark side. The senescent secretome might be beneficial in many cases, but it does not cease to be the causal factor in many abnormal situations. The inflammatory components of SASP together with immunosuppressive tumor cells can lead to aberrant tumorigenesis by propagating cell migration and progressively tumor metastasis [78–81]. An accurate example of what is described above is the case of immature myeloid cells (iMC) [82]. In early tumor stages, SASP has the ability to recruit iMCs, drive their differentiation to macrophages, thus preventing cancer initiation by eliminating the abnormal cells. However, in later stages this maturation is blocked by the malignance and the consequent accumulation of immature IMCs, blocks the function of the NK cells, promoting the formation and appearance of hepatocellular carcinoma. Accumulation of senescent cells can also be supervised by SASP after chemotherapy treatment, due to local inflammation [80]. Being able to understand which SASP components hold beneficial, and which not, characteristics would probably offer a useful tool in dealing with age-related diseases, but also cancer treatment.

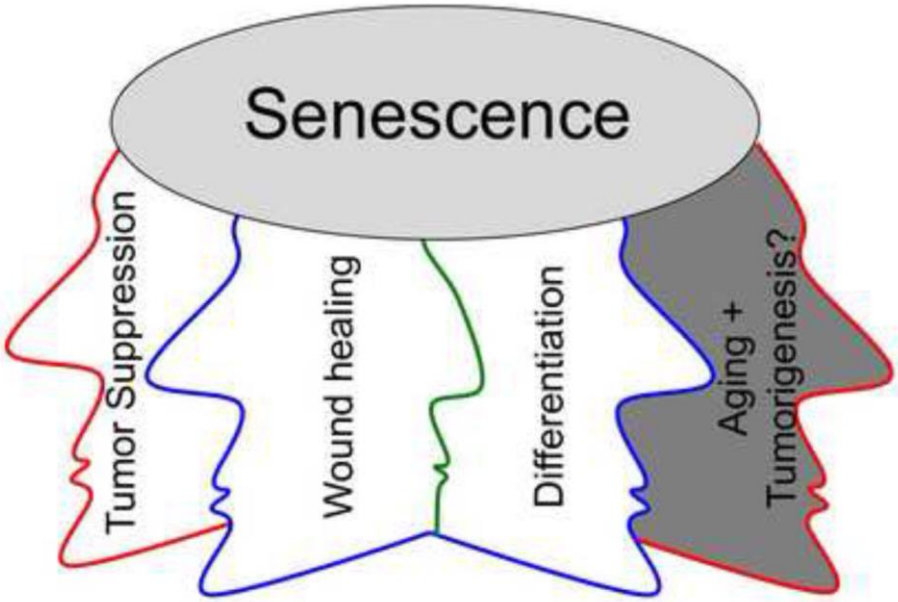

Figure 1.3: The diverse profile of senescence. Cellular senescence and its SASP could have beneficial role in many processes, but also deleterious effects. (*Adapted from: Taranjit Singh Rai and Peter D. Adams (2012) Biochim Biophys Acta. doi:1 0.1016/j.bbagrm.2011.07.014).*

1.2 *Genome Organization in Senescence*

Along the lines with cellular senescence, extremely dynamic and complex is the eucaryotic genome, too. Therefore, it has been extensively studied and shown that it undergoes dramatic changes upon senescence entry ranging from nucleosome positioning and histone modifications to global chromatin alterations [16,17,83–92]. The following chapter will glean and discuss the most pronounced of them in an increasing order of architectural magnitude.

1.2.1 Histone Alterations During Senescence

Compacting DNA inside the nucleus is a meticulous multistep process involving various levels of compaction. The simplest unit of compaction is the nucleosome, an octamer of paired histone proteins, with the 146 bp DNA wrapped around it. The N- and C-terminus of these proteins (histone tails) are subjected to a wide range of post-translational modifications (PTMs) and significantly impact the chromatin structure [93].

In recent times, it has become apparent that histone proteins, H2A, H2B, H3 and H4, serve a critical role during aging processes. The budding yeast was shown to suffer a dramatic loss of histone proteins upon replicative senescence [94,95]. As a result of this, an overall transcriptional upregulation was observed most probably due to massive chromatin derepression. However, despite the unsurprising increase in histone transcripts as well, the old yeast presented low levels of protein synthesis, explaining the reduction of histone proteins. The importance of this loss is better depicted by the fact that overexpression of histone proteins H3/4, or deletion of genes expressing histone repressors or genes expressing proteins that are involved in histones degradation, increases the lifespan of yeast [95,96]. The impact of the core histone loss in not restricted only to yeast, but it extends to other organisms, such as mammals. The aging process of muscle stem cells includes the downregulation of histone genes [97]. Replicative senescent fibroblasts also present reduced synthesis of histone proteins as a result of telomere shortening and excess DNA damage. Another mechanism, apart from the lowered synthesis, that might explain the curtailed levels of histones is the presence of cytoplasmic chromatin fragments. These fragments are handled by the autophagy/lysosomal pathway and this action is connected with reduced histone levels in senescent cells [98].

It has been already mentioned, that histone tails are imposed to a broad number of PTMs (so far over 1000). The most preeminent ones regarding senescence are acetylation and methylation of lysine residues. Acetylation of histone H3 on lysine 56 (H3K56ac) and H4 on lysine 16 (H4K16ac), respectively, are both influencing replicative senescence in yeast [94,95]. H3K56ac levels are significantly dropping upon senescence entry. At the same time, completely removing H3K56ac has the opposite of the expected effects, as its loss advances genome instability and shortens the lifespan of yeast [94]. The mechanism behind the exact regulation of this event is not yet fully understood. Deletion of genes coding for histone deacetylases (HDACs) that remove H3K56ac and Hst3/4 shortens lifespan, but also deletions on histone acetyltransferases (HATs) has similar effect. Addition of an extra copy of either *HST3* or *HST4* genes, extends lifespan [95,99]. The fact that H3K56ac has a diverse role in cells, from driving chromatin assembly to regulating aspects of DNA replication [100,101], shows that there might be a 'golden' expression ratio that could promote longevity. While H3K56ac levels are dropping in senescence, H4K16ac ones are rising.

This increase is due to the downregulation of the Sir2 deacetylase in aged yeast [94] and it has been demonstrated that, if overexpressed, it can contribute to life extension [102]. In a similar manner, depletion of the *SAS2* gene, which encodes for a H4K16 acetyltransferase, extends lifespan [94].

Differences in histone methylation status have also been extensively studied so far. Methylation alterations in key lysines of H3 histone have been observed upon senescence entry, with the most important to be in the trimethylation levels of H3-K4, -K9, -K27 and -K36. Most of these changes are connected with repressed states of chromatin, like heterochromatin, and a global interchange between states with aging [103]. H3K4me3 levels, which is an activating marker, are elevated in old worms and have been shown to control longevity, since deletion of the SET-2 methyltransferase increased lifespan, while deletion of the rdr-2 demethylase decreased it [104]. In the contrary, the levels of the repressive marker H3K27me3 are decreased with time. Active role in this reduction plays the increased expression of *utx-1,* which encodes for a demethylase. Knocking-down *utx-1* results to extended longevity [105]. Moving from worms, and in an effort to set more global hallmarks for histone methylation changes with aging, a similar heterochromatic reorganization was observed in mesenchymal stem cells (MSCs) derived from Werner syndrome patients, a premature aging disorder due to WRN protein defect. A general loss of H3K9me3 was reported, accompanied by decreased levels of HP1 protein, a fundamental component for heterochromatin packaging and an interactor of H3K9me3 [106].

In line with this observation, fibroblasts taken from patients with Hutchinson–Gilford progeria syndrome (HGPS), where mutations in the nuclear protein lamin A cause premature aging [107], were shown to also suffer from a general heterochromatic loss [108,109]. There, levels of H3K9me3, HP1 and H3K27me3 were significantly decreased, supported by a decrease in the H3K27me3 methyltransferase EZH2. Taken together the above observations, it becomes clear that the levels of histone modifications are altered during aging and the reorganization of heterochromatin contributes to an increased genome instability.

1.2.2 Histone Variants & Senescence

Apart from the canonical histones mentioned above, there are also variants of these forms. These variants can have differences in their sequences, compared to canonical ones, and very distinct functions [110,111]. Taken for example the H3 histone variant H3.3. This variant is continuously expressed throughout the cell cycle and its incorporation into the genome is replication-independent [112]. Therefore, its role when cells are no longer dividing is crucial in maintaining the chromatin structure. It has been demonstrated, that H3.3 variant together with H3.3cs1 (N-terminal cleaved product of H3.3) are over-represented in senescent cells and their ectopic expression can induce senescent-like chromatin alterations without any other stimulus. Responsible for this deposition is the histone cell cycle regulator (HIRA) complex [113]. The importance of this complex is stressed in experiments conducted in yeast, where deletion of Hir complex (yeast's ortholog gene) increased its lifespan [95]. Additional organisms show similar correlation between the accumulation of H3.3 variant and progressive aging. In mice brains, levels of H3.3 are increased by age and an elevated number of nucleosomes bear this new variant. Surprisingly though, chromatin remains highly dynamic in these sites and continuous to express genes responsible for neuronal plasticity, stressing the importance that senescence-related alterations might have in tissue homeostasis [114].

Similarly to H3 variants, macroH2A histone variant (H2A histone variant) holds a prominent role during aging as a key piece of the senescence-associated heterochromatic foci, or SAHFs (see below for details) [115]. The main role of this variant is to repress transcription [116] and its levels are increasing following replicative senescence arrest in human fibroblasts [117]. Recently, it has been shown that sites of SASP genes are enriched for macroH2A upon oncogenic trigger. Stress coming from the endoplasmic reticulum (ER) creates an increase in ROS and constant DDR, which activates ATM and causes microH2A variant to be removed from SASP genes, which in turn are repressed. This negative loop feeds a positive loop that leads again more microH2A to SASP genes creating a paracrine senescent signal for neighboring cells [118]. In a more general picture, there is a huge relocalization of microH2A taking place upon senescence entry, resulting in microH2A leaving SASP genes and going to SAHF, alongside with additional histone marks [118,119]. Even though, it has shown not to be essential per sei for SAHF formation, macroH2A holds pivotal role on keeping these sites transcriptionally inactive [120].

1.2.3 Heterochromatic Alterations in Senescence

It has been demonstrated that senescent cells suffer huge changes to higher-order chromatin structure. The most prominent of these alterations is the creation of senescence-associated heterochromatic foci, or SAHFs (**Fig. 1.4)** [115,121]. These dense DAPI-stained formations are a hallmark of oncogene-induced senescence, but they have also been observed, not that often though, in replicative senescent cells and in patients suffering from aging syndromes [107,122]. SAHF, as their name indicates, are enriched for heterochromatic markers such as HP1 proteins, the variant macroH2A, H3K9- and H3K27-me3 marks of facultative heterochromatin, the high-mobility group A proteins (HMGA) and the DNA damage marker and histone H2 variant, γ-H2AX [121–124].

Different ways of SAHF formation have been proposed [120,125]. It was shown that knocking-down retinoblastoma proteins and p16, their upstream activator, inhibits the formation of SAHF, implying the importance of this pathway, at least in the initial establishment [121]. Another approach suggests that formation of these foci is initiated by a chromatin compaction step assisted by the histone chaperone complex HUCA, which brings the variant H3.3 to chromatin [126]. Lately, Promyelocytic leukemia bodies (PMLs), which become rather apparent in senescence [127,128], are gaining some interest as it has been proposed that they might act as a gathering point for a variety of SAHF factors. Rb protein complexes, HP1 proteins, the HIRA complex and others, have been shown to gathered in PMLs prior to SAHF establishment [115,129]. In addition, an E3 ubiquitin ligase adaptor, SPOP, has recently being identified as a possible upstream candidate for SAHF formation. SPOP is upregulated during senescence, which results in SENP7 deSUMOylase degradation, leading to HP1α sumoylation. This increase in sumoylation drives HP1α partially to SAHF and partially to PMLs. Lastly, key role in the formation and maintenance of SAHF play the HMGAs, which are architectural proteins that bind to the minor groove of DNA, especially between nucleosomes [130]. Diminished levels of other proteins that also preferentially bind to linker DNA (e.g. histone H1), allows more binding loci for HMGAs, propagating SAHF formation [131,132].

Regardless of the high presence of H3K9me3 and H3K27me3 in SAHF, the global displacement and repositioning of these marks, as measured by chromatin immunoprecipitation sequencing (ChIP-Seq), are not so profoundly altered between proliferating and senescent cells [125,133].This observation gave birth to the hypothesis that SAHF are created from pre-existing heterochromatin reorganization, rather than a newly emerging program of heterochromatic spread [133]. Thus, there was an open question how heterochromatin could be shuffled in order SAHF to start to appear.

It is now quite well understood the crucial function nuclear lamina carries in the transition between proliferation and senescence **(Fig. 1.5)**. Key proteins for the lamina function are Lamin-group proteins A and B, which constitute a scaffold in inner nuclear membrane. Lamin B1 in specific, has been shown to be downregulated in senescence [134,135] through mechanisms including (post)-translational regulation and the involvement of autophagy [136–138]. Chromatin nuclear positioning and transcription regulation are main features of nuclear lamina. Mapping of Lamin B1 protein across the genome has identified distinct regions in the (sub)megabase scale, known as Lamin-associated domains (LADs), which are augmented with repressive histones [139]. The H3K9me3 mark was shown to associate mostly with the central part of LADs, a space where Lamin B1 is significantly lost upon senescence. This preferential reduction from H3K9me3-rich regions assist the reorganization of heterochromatin into SAHF [140]. The importance of lamina proteins in the proper function and architecture of chromatin, but also in finetuning the senescence process, becomes obvious also from the fact that almost all of progeria syndromes have some short of lamina-deficiency on their core [91,106–108].

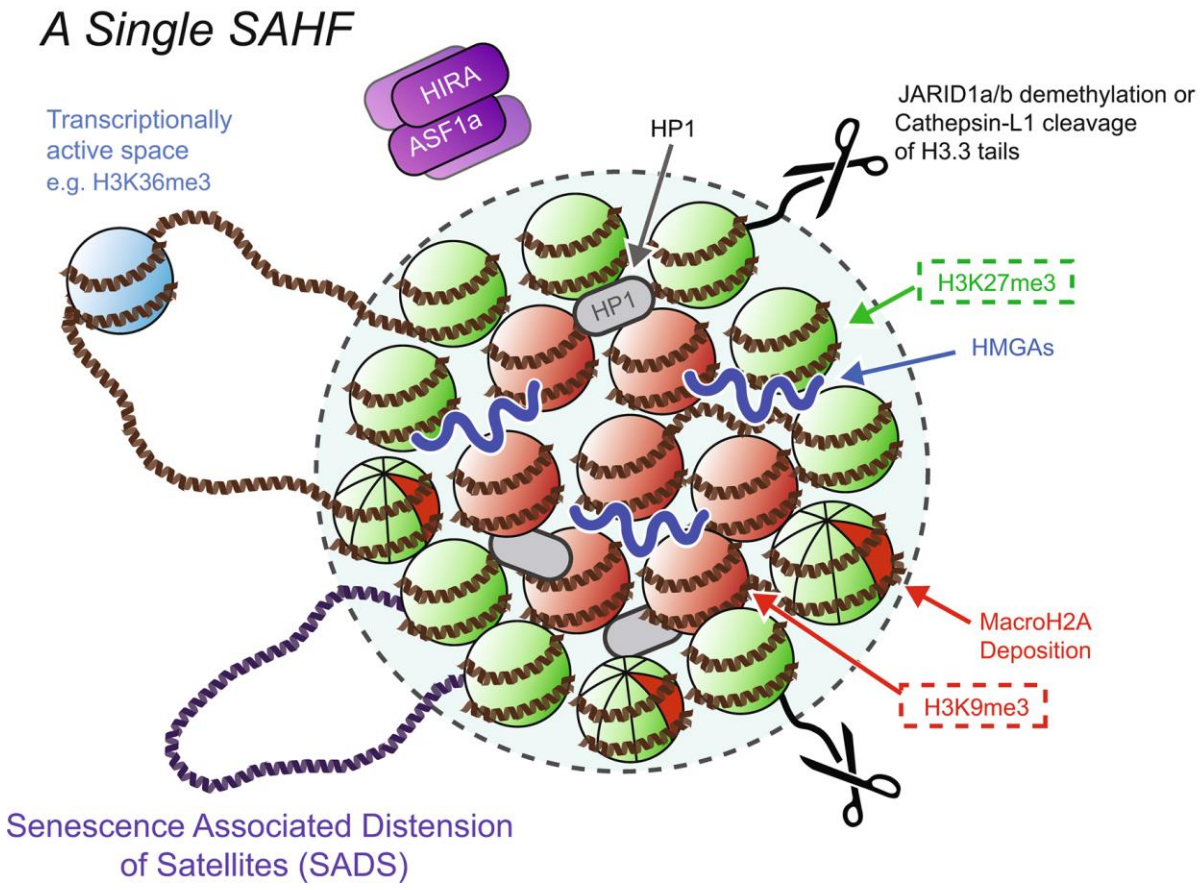

Figure 1.4: Representation of a single SAHF. The core (in red) is enriched for the histone mark H3K9me3 and the periphery (in green) for H3K27me3. Additional key components of the SAHFs are depicted in the cartoon. *(Adapted from: A. J. Parry, M. Narita (2016) Mamm Genome. doi: 10.1007/s00335-016-9628-9).*

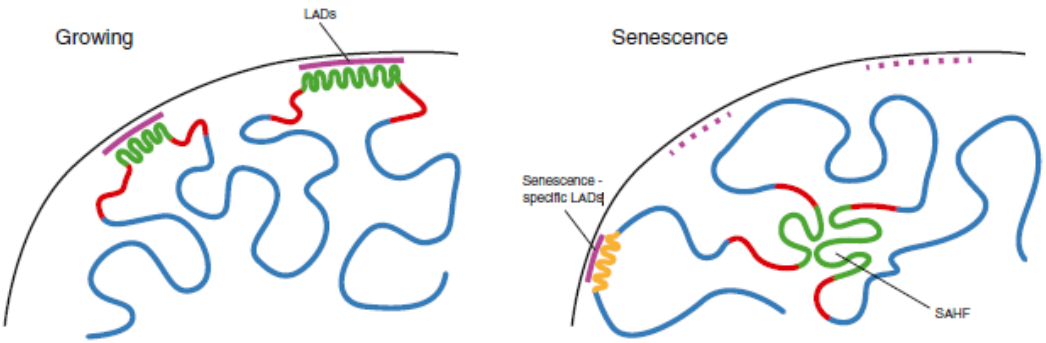

Figure 1.5: Model depicting the change of the chromatin architecture. *(Adapted from: Chandra et al. (2015), Cell Reports. doi: 10.1016/j.celrep.2014.12.055).*

1.2.4 Nucleosome Remodeling in Senescence

The structure of nucleosomes is rather stable, while their positioning across chromatin varies and it is regulated by remodeling complexes, which are ATP-dependent, causing the appearance of more dense or more accessible areas. In senescence, nucleosomes can be repositioned on DNA, which can affect gene expression. It can be caused by changes in the levels and modifications of the histone proteins that make up the nucleosomes, as well as changes in the enzymes that help to remodel chromatin. It was shown in yeast, that upon depletion of the ISW2 chromatin remodeler the lifespan was extended [141]. Upon ISW2 loss, stress- related genes are derepressed and the homologous recombination (HR) damage pathway is activated. The above described state mimics a response similar to the calorie restriction (CR) pathway, where RAD51, also involved in HR, is upregulated leading to yeast longevity [141]. The SWI/SNF remodeling complex also seems to play a role in senescence. Many pathways in worm, including mTOR signaling and AMP-activated kinase (AMPK) pathway, have been found to have a common downstream component; the transcription factor DAF-16/FOXO [142]. DAF-16/FOXO-target genes activation, which promote longevity, is occurring in a SWI/SNF-dependent manner through direct interaction with the chromatin remodeling complex and, subsequent binding to the respective gene promoters. Knocking-down SWI/SNF complex, compromises the lifespan of the worm. The nucleosome remodeling and deacetylase complex (NuRD) is yet another remodeler involved in aging. In skin fibroblasts from HGPS patients, the RBBP-4 and -7 subunits of the complex are reduced, causing downregulation of HP1 and global chromatin reorganization [143]. Similarly, cells derived from old healthy adults, presented comparable reduction in these two subunits, implying the significance of NuRD complex in both physiological and premature aging. From the above, it becomes obvious that the correct nucleosomal positioning is of high importance in smooth regulation of senescent processes.

1.2.5 Higher-order Chromatin Changes in Senescence

Throughout years, studying chromatin architecture has been proven a challenging task. Over the last decade, significant progress has been made towards this direction and now high-throughput chromosomal capture techniques (Hi-C, Micro-C, etc.) have allowed the more in depth study of chromatin organization [144,145]. It is now generally accepted that chromatin can be divided into two large compartments: the active, A, compartment and the inactive, B, compartment, describing the euchromatin and heterochromatin, respectively [144]. Self-interacting fragments of chromatin, in megabase sizes, have also been identified and named topologically associated domains (TADs) [146,147].

One of the first models to study potential changes in higher-order chromatin was fibroblasts derived from HGPS donors [148]. There, it was shown that the borders between compartments A and B were significantly lost and a sub-set of regions had switched compartments. This switch was accompanied with alterations in H3K27me3 levels, in LADs and – ultimately - in gene expression. Similar compartments switching and transcriptional differences have also been observed during differentiation processes in embryonic stem cells (ESCs) [149].

In another form of senescence, the OIS, Hi-C experiment showed a reduction in short-range interactions, which were more prominent at heterochromatic regions and an increase in longer-range association with neighboring repressed regions, but not any larger scale changes [16]. This observation served as a potential explanation on how SAHF could spatially spread by reforming the surrounding environment [133]. Regions of LADs dissociate from the nuclear envelope (NE) and after reassociation in the nuclear interior they build the SAHF core. This loss of local interactions has not only been seen in OIS cells, but also in ESCs and somatic cells assisted with an advancing loss of differentiation capacity. Thus, it was proposed that senescence can be an endpoint of chromosome remodeling during differentiation [16].

Hi-C in RS models, revealed an intermediate state between them and HGPS and/or OIS cells [87]. The global genome architecture was mainly unaltered, as compartments and TADs were overall conserved among proliferating and replicative arrested cells. Intriguingly, however, in cell undergoing RS it was found that there was a genome-wide loss of long-range interactions and a gain of short-range ones [87].

In addition, it was also observed a limited compartment switching, similarly to HGPS, following by a difference in expression levels for the involved genes. Thus, even though the changes in higher-order chromatin are relatively mild in most of the senescent models studied, still the differences that they can create in the transcriptional program of an organism can be of high importance [93].

1.3 *CTCF in Shaping the Genome*

Chromatin packaging within the nucleus is a complex and delicate process as at least two things need to be fulfilled simultaneously; compaction and accessibility. As it was briefly discussed above, nowadays there are the necessary experimental means (Hi-C, Micro-C, etc.) that allow for delineation of this procedure and improvement of the knowledge on how chromatin fiber acquires its 3D organization. It is generally understood and accepted that interphase chromatin is hierarchically organized at different levels: i) chromosome territories, ii) A/B compartments, iii) TADs and iv) chromatin loops **(Fig. 1.6)** [150,151]. Fundamental role in this case of events, but also in the maintenance of genome architecture, is held by CCCTC-binding factor (CTCF). Here, it will be discussed how CTCF assists in genomic organization and its significance under stress conditions.

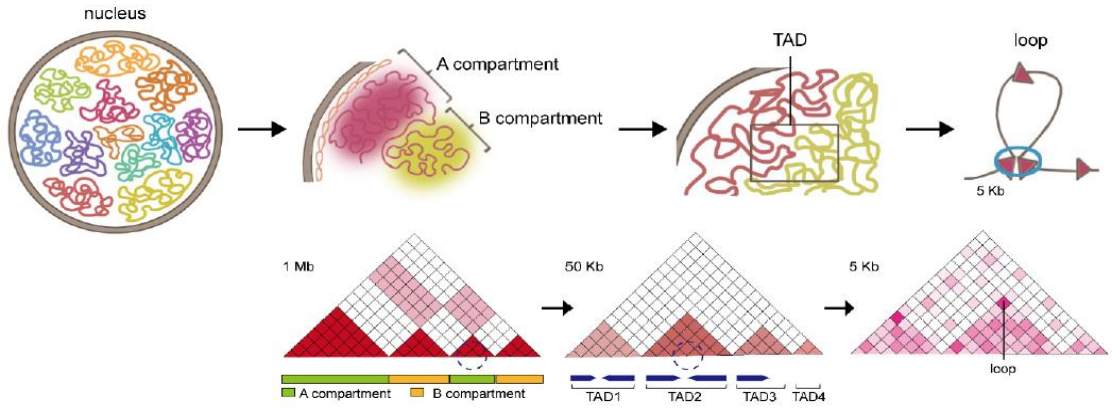

Figure 1.6: The four levels of 3D genome organization. Chromosome territories, A/B compartments, TAD, and chromatin loops. *(Adapted from: Sun, X.; Zhang, J.; Cao, C. (2022), Genes. doi: 10.3390/genes13081383).*

1.3.1 Higher-order Chromatin & CTCF

Chromatin compartments could be partitioned further into TADs. TADs are considered as keystones for genomic structure and organization and consist of self-interacting chromatin fragments. These fragments have higher propensity to interact with one another other than with fragments from a different TAD. They are insulated from their surrounding by TAD boundaries [146,152]. These self-interacting chunks of DNA, chromatin loops, are long-range interactions between distal genomic loci [153–155]. Usually these interactions are found between promoters and/or enhancers, and CTCF binding sites. However, there are limitations on their length, possibly due to limitations by the linear distance [156,157].

There are plentiful binding sites for CTCF across genome. Around half of them are intergenic and the rest are either intragenic or proximal to promoters [158]. CTCF is a highly conserved factor across vertebrates [159] and plays an important role in 3D chromatin organization. The full-length protein accommodates an 11 zinc-finger domain, which assists in DNA-binding, and is named after the ~20mer DNA recognition motif. Studies have shown that it has also an RNA binding capacity which greatly influences its organizational properties [160–163].

Commonly, CTCF was perceived as an insulator protein preventing the spread of heterochromatin [159,164], but over the last decades its role in loop formation and genome topology has become apparent [159]. Both loop anchors and TAD boundaries have been found to carry CTCF binding sites [146]. In order to form either a loop or a boundary, however, these sites need to be oriented properly, as the two motifs that later on will form the respective structure must be positioned in a convergent orientation [154]. This orientation is not random, but it has been shown to greatly assist in the formation and establishment of loops, through a mechanism which is known as ‘loop extrusion model’ [165–168]. On average, CTCF has been found to co-localize in these anchors together with the cohesin complex [169]. Cohesin, on its core, consists of four proteins; structural maintenance of chromosomes protein 1 and 3 (SMC1, SMC3), double-stand-break repair protein 21 (RAD21) and stromal antigen 1 (STAG1) protein, and forms a ring-shaped structure [170]. SMC proteins work like a motor and pull the chromatin fiber through the cohesin ring in order to form loops, until this process is blocked by properly oriented CTCF [165]. The length of the respective loop is directly related to the extrusion time before cohesin meets a barrier that will block the process [171].

Nonetheless, the exact mechanism through which CTCF acts as an obstacle to this procedure is not fully understood, yet. It has been shown that CTCF binding induces conformational changes to chromatin, by largely repositioning nucleosomes [172]. Naked DNA was shown to wrap around bound CTCF protein and form a round structure with a diameter of ~75nm, significantly bigger than the one needed to block cohesin in vitro (~20nm) [173]. Howbeit, this model provides some answers, but fails to answer some others. One thing that seems to be unchanged though is the importance that CTCF has in properly structured chromatin.

1.3.2 CTCF in "Distress"

Apart from its prominent position in proliferating cells, CTCF has lately been shown to be a key player in senescence, as well. Its, relatively, decreased expression seems to be enough to initiate a domino effect.

CTCF, among others, is implemented in a process called genomic imprinting [174]. Expression of imprinted genes is following a parental specific pattern and is controlled by DNA methylation in the gametes. Several imprinted regions facilitate CTCF binding sites and they regulate the monoallelic expression in a CTCF-dependent insulation manner [175]. The *H19/Igf2* genomic locus is such an example and the best described model of CTCF action in imprinting. *Igf2* is crucial for embryo development and its control is of high importance for physiological growth. It has been shown that CTCF, together with cohesin, binds to the maternal allele in a H3K4-rich methylated region, provoking chromosomal looping and attraction of the polycomb repressive complex 2 (PRC2). This cascade results in increased methylation of H3K27 and subsequent maternal *Igf2* repression [176–178]. In senescence, the decreased levels of CTCF result in a loss of insulation and a relaxation in this locus, leading to upregulation of *Igf2* [179]. A similar increase in *Igf2* expression has also been observed in prostate cancer cells, where CTCF is downregulated and imprinting is lost [179]. These observations point to the direction that changes in the imprinting pattern might lead to senescence-related gene expression and cancer development.

In a similar pattern, the genomic locus *INK4/ARF*, which encodes for the senescent marker $p16^{INK4a}$, is regulated by CTCF binding, as it has been found to possess at least three binding motifs [180]. In proliferating cells, CTCF binds to these motifs and negatively regulates the expression of $p16^{INK4a}$ through looping formation on its promoter. In OIS, the decreased levels of CTCF cause a disruption in these loops leading to $p16^{INK4a}$ overexpression and senescence propagation [180]. Another protein that its levels are regulated by CTCF binding is POLD1 [181]. POLD1 is the catalytic subunit of DNA Polδ and it participates in DNA synthesis and repair. Its promoter bears two CTCF binding sites and there is an age-dependent regulation of its expression. It was shown that, in contrast to $p16^{INK4a}$, the decreased levels of CTCF upon senescence and its loss from the promoter sites of *POLD1* negatively regulates its expression, leading to accelerated growth arrest [181]. CTCF is also related to a premature aging disease, called Cockayne syndrome. This syndrome is caused by mutations in the ATP-catalytic domain of the chromatin remodeler Cockayne syndrome group B protein (CSB), a part of SWI/SNF2 family, and its main action is to randomize the position of nucleosomes. Cells derived from patients suffering from this syndrome have shown to present increased levels of ROS. Under these condition, there is an interplay between CTCF and CSB, where CTCF increases the genomic occupancy of CSB at promoter sites, resulting in alterations in gene expression [182].

However, the most profound finding regarding CTCF and senescent genome was made by *Zirkel et al.*, where it was shown that CTCF dramatically reorganizes its pattern upon replicative senescence entry and loss of the chromatin binder high-mobility group B protein (HMGB2) [90]. HMGB proteins are highly abundant inside the proliferating nucleus and their DNA binding causes bending, looping or unwinding [183]. In that study, it was shown that HMGB2 can demarcate a number of TAD boundaries and, on average, it was found to co-localize with CTCF binding sites. Moreover, HMGB2 nuclear eviction was enough to initiate a senescent cascade, which included heterochromatic and transcriptional alterations. Interestingly, its loss from the nucleus caused CTCF to form very distinct clusters, which were named senescence-induced CTCF clusters (SICCs). These clusters were not co-localized with HP1a, so there were not of heterochromatin nature and did not come with cohesin reorganization, in spite of their great chromatin overlap [154]. Therefore, it was hypothesized, that the presence of HMGB2 binding sites in proximity with CTCF ones was offering extra insulation to CTCF-CTCF interaction. CTCF Hi-ChIP data seemed to agree on that, since consequent to HMGB2 loss, new longer CTCF loops were emerging.

Nevertheless, the true nature and biological relevance of these clusters remains somehow elusive, as well as their role in genome organization during senescence.

1.4 *Membraneless Organelles & Senescence*

Nucleus is a very compact, but rich environment for a variety of organelles, of which common characteristic is the lack of a traditional lipid membrane (membraneless organelles, MLOs) **(Fig. 1.7)**. Their function and size varies adequately. From the large nucleolus of approximately 3μm, to the microscopic nuclear speckles of roughly 40nm, each one of these structures contains specific proteins and participates in different processes contributing to gene regulation [184]. Inevitably, some of these formations have a direct or indirect role during senescence and aging and the next chapter will discuss the most notable of them.

1.4.1 The Nucleolus

The nucleolus is the most prominent subnuclear organelle within the nucleus of eukaryotic cells. It is primarily and mostly involved in ribosome biogenesis, which is initiated with the transcription of ribosomal RNA (rRNA) by RNA polymerase I (RNA PolI). Because of these functions, the nucleolus is a deterministic factor of cellular metabolic state. Recently, however, it has been shown that this membraneless structure can participate in diverse activities involving stress response, development and aging [185]. While proliferating cells present higher number and smaller in size nucleoli, senescent cells have usually a single enlarged nucleolus [186]. Independent studies point to the direction that changes in nucleolus structure as a consequence of inhibited rRNA synthesis and ribosome biogenesis can, under circumstances, lead to cell cycle arrest [187,188].

The role of nucleolus in senescence becomes even more pronounced by the fact that a myriad of proteins involved in growth arrest are regulated by their localization there, both under normal and irregular conditions. A large number of proteins related to aging syndromes (Werner syndrome, Cockayne syndrome B, Bloom syndrome, etc.) are exhibiting nucleolar localization at some point during the cell cycle [189–192]. Moreover, in physiological aging, p53-stability mediators p14-alternative reading frame (p14ARF) and nucleophosmin (NPM) are found there [193]. Thus, it becomes more that obvious the crucial role that this organelle can play in maintaining senescence.

It has already been discussed the importance of the p53 and RB pathways during cellular senescence. Arrested cells are usually blocked during their G1 to S-phase transition. G1-S and G2-M checkpoints make sure that DNA is properly duplicated and it has been successfully divided into the daughter cells. p53 and RB regulate these checkpoints and upon activation they can promote cell cycle arrest. On top of these two, the nucleolus actively participates in this process. A successful cell division requires increased levels of protein synthesis, therefore elevated levels of ribosome biogenesis [194]. Indications of a crosstalk between p53, ribosome biogenesis and cell cycle progression come from different studies. It was shown that inhibition of block of proliferation protein 1 (Bop1), which participates in rRNA synthesis and assembly, was sufficient to drive a p53-dependent G1 arrest [195]. Likewise, inhibition of the transcription factor which tethers PolI to the rDNA promoters and promotes rRNA synthesis, TIF-IA, has as a result abnormal nucleolar structure and function, G1-S arrest through p53 and apoptosis [196]. Hence, it is evident the close relationship between the nucleolus and senescence (extensively reviewed in [197]).

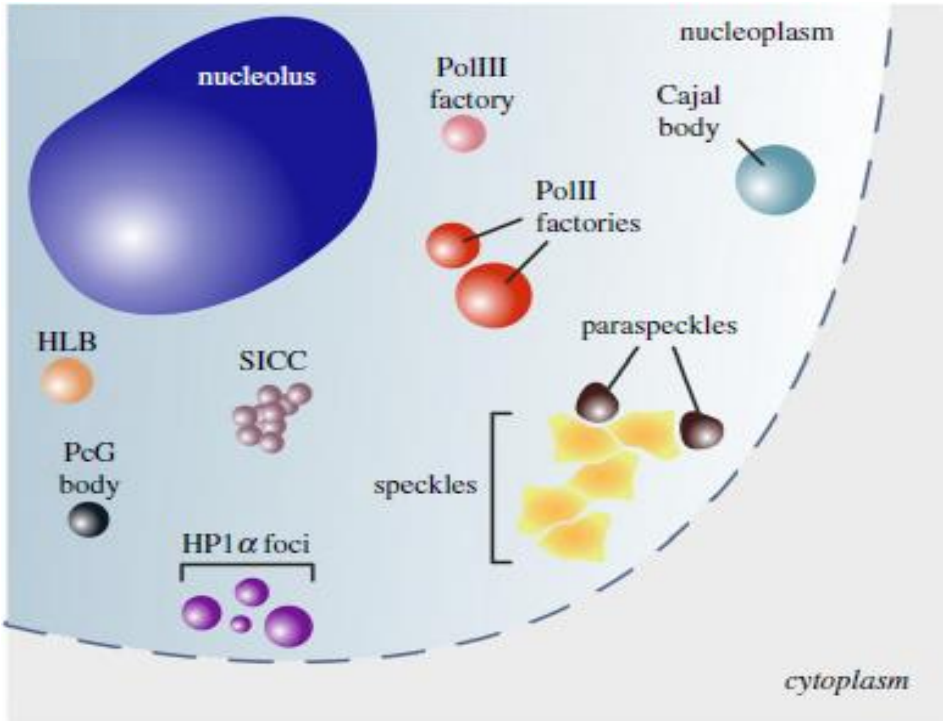

Figure 1.7: Cartoon depicting the variability of membraneless organelles in the nucleus. *(Adapted from: Palikyras S. & Papantonis A. (2019), Open Biology. doi: 1*0.1098/rsob.190167*).*

1.4.2 PML Nuclear Bodies

Promyelocytic leukemia nuclear bodies (PML-NBs) are another example of the importance that MLOs hold in the nuclear environment and how they could contribute and affect multiple processes. PML tumor suppressor protein is highly abundant in the periphery of these bodies, which number some tens inside the nucleus, surrounding a core of many other, unrelated, proteins [198]. PML bodies were mainly studied as tumor suppressor regulators [199], but over the years they have been found to participate in a variety of procedures including gene expression, antiviral immunity and cellular senescence [200,201].

Most of the proteins found in PML bodies are, one way or another, related with stress responses [198]. As it has been shown so far, p53 has a close relationship with stress and a tight connection with senescence. Similarly to many other proteins, post-translational modifications, like acetylation and phosphorylation, can modulate the activity and stability of p53 [202].

Upon activation of the *Ras* oncogene and induction of *Ras*-induced senescence (a form of OIS) it was demonstrated that PML bodies have an active role on it [199]. More specifically, upregulation of Ras leads to PML upregulation and p53-Lys382 acetylation, thus stabilizing the protein and giving it the ability to interact with low-affinity promoters. This process is taking place in PML bodies, where the Cyclic adenosine monophosphate Response Element Binding protein Binding Protein (CREBBP), an acetyltransferase, is also present at the time. The importance of PML bodies' integrity to that process was stressed by the fact that in mutant PML fibroblasts, unable to maintain this structure, there was an oncogene-mediated escape from senescence.

Interestingly, PML-NBs have been associated with the regulation, at least partially, of SAHF, and consequently of chromatin [115,203]. When the cells approach senescence, it was shown that HP1 proteins, formerly to their localization at SAHF, together with HIRA, member of the HUCA complex (HIRA/UBN1/CABIN1/ASF1a), are entering PML bodies. Inability of the HIRA complex to be transferred into these nuclear bodies, has been connected with decreased ability to form SAHF [204]. In agreement with the importance of PML bodies integrity for SAHF formation is the fact that PML mutants with reduced ability to form bodies, disrupt the establishment of SAHF [204]. Apart from the HUCA complex, the chromatin remodeler DAXX/ATRX has also been identified to localize at PML-NBs before induction of senescence [205]. This, strengthens the hypothesis that PML bodies could act as hubs of remodeling and/or preservation of chromatin structure in senescence, through a histone assembly pathway independent of replication [206,207].

1.4.3 Nuclear Speckles

Nucleus is a highly compartmentalized structure with a wide range of bodies with specialized functions. Nuclear speckles (NS) are among the most notable of these, but their exact role is moderately known. Their size is roughly 25nm and they consist, in their majority, of pre-mRNA splicing factors, small nuclear ribonucleoproteins (snRNP) and poly(A)$^+$ RNAs [208–210]. Key components of these speckles are serine/arginine rich proteins, such as SC35, SRRM2 and SON, with disordered domains and related functions; the majority of the known factors are involved in transcription, RNA processing and RNA export [211–216].

As the exact function of nuclear speckles is not precisely determined yet, there have been two main models trying to explain their role inside nucleus. The first model, which is the general understanding of these bodies, implies that nuclear speckles are mainly used as a repository for RNA processing factors [217]. In favor of this idea are data showing that there is no active transcription taking place in the interior of the speckles, they completely lack any DNA and upon transcription inhibition there is an increase in their size [218]. Nonetheless, there are accumulating evidences suggesting a broaden role for these structures and implicating them in the coordination of gene expression and in post-translational RNA processes [219]. Recent high-throughput studies have managed to associate nuclear speckles with certain genomic loci [220–224]. Genome can be highly compartmentalized as it was discussed above. TADs could be further subdivided to A-TADs (active chromatin) and B-TADs (inactive chromatin). A-TADs could be subdivided even further giving rise to Type I and II compartments. Genes which are hyperactive, such as house-keeping genes, could usually be localized in Type I A-TADs [154,222,225,226]. Specifically this type of domains were found to be in close proximity with speckles, in agreement with the observed enrichment of proteins controlling the pause/release circle of RNA PolII (e.g. CDK12) [227].

The importance of NS relative position inside the nucleus is lately becoming evident also in abnormal conditions. A recent study, which used a transgene of the heat shock protein 70 (HSP70), showed that upon heat shock activation, the total and nascent RNA levels of HSP70, adjacent to nuclear speckles, were tremendously upregulated compared to the endogenous one, and its levels were detectable even hours after the shock [228]. In a like manner, another group took advantage of Nutlin-3a, a p53 inhibitor [229], to induce stress in human fibroblasts [230]. Interestingly, upon p53 stabilization and p53-mediated stress response, there was an active association between a subset of p53 targets, e.g. p21, with NS, leading to enhanced transcription.

Lastly, two current studies have made a link between NS and cellular senescence [231,232]. The m^6A methyltransferases METTL-3 and -14, have been found to be localized in nuclear speckles together with Lamin A [224], which is frequently mutated in cells derived from patients with HGPS [107]. It was shown, that Lamin A and METTL-3 and -14 interact in nuclear speckles and in the absence of this interaction, due to lamin A inefficiency, the two m^6A methyltransferases are inclined to proteasome-mediated degradation, in line with their reduced observed levels upon senescence entry [231]. A good fraction of speckles-related components are the nuclear ribonucleoproteins (hnRNPs), which regulate RNA splicing [107].

Part of these processes is alternative splicing, a dominant phenomenon in many age-related diseases, such as Alzheimer's disease (AD) [233]. It was shown that an isoform of hnRNP, which is normally found at NS, is downregulated in aged brain cells, resulting in dysregulation of proper splicing and aberrant alternative splicing events contributing to the decayed phenotype of AD [232]. Therefore, it becomes evident that proper structure maintenance and composition preservation are of high importance for the seamless function of NS. In any other case, there might be severe consequences in organism's well-being.

2. Chapters

Chapter I – Chemical induction of replicative-like senescence via a small molecule inhibitor

My contribution is reflected in the following experiments as outlined below:

• Growing and conducting senescent assays and immunostainings to IMR90 cells

• CUT&Tag experiments for proliferating, ICM-treated and senescent IMR90 cells

• Generating Micro-C data in collaboration with Dovetail Genomics, Ribo-seq data in collaboration with RiboMaps Ltd., and scRNA-seq in collaboration with Active Motif. Micro-C data analysis was performed by A. Stavropoulou on the basis of input by me and Dr. Papantonis

The following figure panels were prepared by myself with the data input from experiments prepared and/or analyzed by me or indicated contributor:

• Figure 2.1.1A. Treatment with 610CP-tagged ICM to validate its subcellular localization

• Figure 2.1.1B. Proliferation rate assessment for control and ICM-treaded IMR90 from experiments performed by me

• Figure 2.1.1D. FACS analysis to identify the stage of cell cycle arrest.

• Figure 2.1.1E-F. Immunofluorescent staining and quantifications

• Figure 2.1.1G. Microscopy quantification with data provided by Dr. A. Zirkel

• Figure 2.1.1I. qPCR in a variety of senescent markers

• Figure 2.1.2C. Volcano plot showing the differentially expressed genes upon ICM treatment with data derived from differential gene expression analysis of RNA-seq data from IMR90

• Figure 2.1.2D. GO term analysis of up- and down-regulated genes between ICM treated and replicative senescent IMR90s

• Figure 2.1.2E, J. GO term analysis of transcription factors regulating up- and down-regulated genes upon ICM treatment

• Figure 2.1.S2. GO term analysis of up- and down-regulated genes upon ICM treatment

• Figure 2.1.3. scRNA-seq panels with data provided by Active Motif

• Figure 2.1.4A. Volcano plot showing the differentially expressed genes upon ICM treatment with data derived from whole-cell proteome from IMR90

• Figure 2.1.4B. GO term analysis of up- and down-regulated genes upon ICM treatment from whole-proteome data

• Figure 2.1.4C-D. Scatter plots comparing mRNA-seq, Ribo-seq and whole-proteome data with data provided by RiboMaps Ltd

• Figure 2.1.S5. Same as in Figure 2.1.4B

• Figure 2.1.5A-C. Micro-C heatmaps, decay plots and saddle plots with data provided by Dovetail Genomics and analysis done by A. Stavropoulou

• Figure 2.1.5D-F CUT&Tag-seq experiment performed by me

• Figure 2.1.5G-I. Micro-C insulation and loop aggregate plots with data provided by Dovetail Genomics and analysis done by A. Stavropoulou

Chemical induction of replicative-like senescence via a small molecule inhibitor

Spiros Palikyras[1], Konstantinos Sofiadis[2], Natasa Josipovic[3], Anne Zirkel[4], Athanasia Stavropoulou[5,6], Argyris Papantonis[1*]

[1] Institute of Pathology, University Medical Center Göttingen, 37075 Göttingen, Germany

[2] Oncode Institute, Hubrecht Institute-KNAW and University Medical Center Utrecht, 3584 CT Utrecht, the Netherlands

[3] Single Cell Discoveries, 3584 CT Utrecht, Netherlands

[4] Center for Molecular Medicine Cologne, University of Cologne, 50931 Cologne, Germany

[5] Institute for Bioinnovation, Biomedical Sciences Research Center "Alexander Fleming", Vari, Greece

[6] Institute for Fundamental Biomedical Research, Biomedical Sciences Research Center "Alexander Fleming", Vari, Greece.

[*]Corresponding author: AP

Abstract

Studying cellular senescence has been proven a keystone in our effort of understanding the aging process. However, studying senescence *in vitro* comes with certain difficulties. Here we describe a novel and robust system of chemically induced senescence, which tackles many of these struggles. The use of Inflachromene (ICM) evicts HMGB1 and HMGB2 from the nucleus and induces a senescence-like phenotype. Comparing ICM-induced and replicative senescence we observed great similarities in both the transcriptional and translational programs of these two mechanisms. In addition, ICM treatment is capable of inducing genome-wide changes to higher-order chromatin, such as strengthened short-range interactions and increased loop length, yet another characteristic of senescence initiation.

Introduction

From the moment of conception and onwards every living organism experiences a variety of developmental programs, leading to progressive cellular decay and aging. Cellular senescence, a process of irreversible growth arrest, is inextricably linked with aging [13,17,20,234]. Different triggers could cause different responses which give rise to three main senescent types: replicative senescence (RS) occurring from telomere exhaustion, oncogene induced-senescence (OIS) due to oncogene overexpression and senescence-induced by genotoxic stress [10]. Senescent cells are communicating with their neighbours and their microenvironment through a complex mixture of pro-inflammatory factors, known as senescence-associated secretory phenotype (SASP) [45], acting in autocrine and paracrine manner [48]. This crosstalk is frequently beneficial, in cases as the wound healing and/or tumor suppression, but the accumulation of senescent cells could lead to chronic inflammation and tumorigenesis [47].

Apart from the focal cellular changes this growth arrest is accompanied by changes in higher-order chromatin, too [6,16,86–88,92]. Genome-wide chromatin capture assays (e.g. Hi-C) in replicative senescence have revealed dramatic changes between active and repressed compartments of chromatin (compartments A and B, respectively) [88]. More striking, a variety of topologically-associated domains (TADs) was switching between compartments, affecting gene expression [87]. The senescence-associated heterochromatic foci (SAHFs) [121], more prominent in some types of senescence, as well with the massive reorganization of lamin-associated domains (LADs) [107,134] are also major alterations occurring upon arrest. The pivotal role of lamins in nuclear architecture and maintenance becomes apparent by the fact that many age-related syndromes bearing lamin deficiencies in their core [108,135]. Thus, identifying proteins that contribute to the senescent phenotype and modulate their action or concentration is of utmost importance.

In an effort to characterize such factors, recent work from our lab shed light into the role of high mobility group box 1/2 (HMGB1/2) proteins in cellular RS [84,90,124]. Depending on their sub-nuclear localization, HMGBs could act either as architectural proteins [90], or as RNA regulators [84], but common characteristic of both is their eviction from the nucleus as an early step in the senescent cascade.

Identifying such factors, however, could prove to be a rather laborious task since a given cell population in culture is heterogenous and asynchronous and, in the case of replicative senescence models, it demands extended periods of culturing, hence, there is the need to tackle these issues.

Here, we describe a novel and robust way of inducing a senescent-like phenotype similar to replicative senescence by using the small benzopyranyl tetracycle compound Inflachromene (ICM). ICM induces senescence within few days of treatment, by evicting HMGB1/2 from the nucleus. Similarly to RS, ICM treatment causes mitotic arrest and produces resembling higher-order chromatin alterations.

Results

ICM treatment induces a senescent-like phenotype

ICM was previously described as a potent inhibitor of HMGBs' nuclear dislodgment [235]. To that end, we had hypothesized that upon ICM treatment the senescent induction would have been halted. To put this into test, we took advantage of an extensively used model on age-related studies; donor-derived human lung fibroblasts (IMR90, I83) [1,25,76,78,236]. Using a 610CP-tagged ICM (offer from the Lukinavicius lab) we were able to confirm the nuclear localization of the compound, in agreement with its, up to that point, characterized function (**Fig 2.1.1A**).

To test for the proliferation rate of cells upon treatment with ICM we took advantage of the Sartorius IncuCyte S3 Live-Cell Analysis System, monitoring the growth of the cells over an extended period of time (**Fig 2.1.1B**). At day 0, IMR90s were treated with either 5uM or 10uM of ICM and were left to grow with the compound for 3 and 6 days. Fresh ICM was added every day, for the respective time period. After these two time points, ICM was removed from the medium and cells were left to grow. Treatment with 5uM of ICM did not majorly affect the proliferation rate of the cells neither during the 3 or 6 days time points, nor after the removal of the compound, as they kept growing similarly to the control cells. On the contrary, and to our surprise, treatment with 10uM of ICM heavily reduced the proliferation rate of the cells, something which was apparent already after 3 days of treatment. Removing the compound after 3 days allowed the cells to re-adopt and start growing again, while removing it after 6 days had minor impact as cells started to die afterwards. Due to this unexpected observation, we thought to assess the senescent state of the cells upon treatment with ICM.

To do so, we exploited the properties of β-galactosidase activity. Senescent-associated β-galactosidase (SA-β-GAL) staining is widely used as a quick microscopic marker to address senescence [237]. Control cells, cells treated with 10uM of ICM for 6 days and replicative arrested cells were stained with β-GAL. The majority of the population of both ICM treated and senescent IMR90s were positive for SA-β-GAL labelling (**Fig 2.1.1C**, 89% and 71%, respectively). In addition, we performed FACS analysis in proliferating, ICM-treated (3 and 6 days) and senescent IMR90s (**Fig 2.1.1D**).

In proliferating fibroblasts only a small fraction of the cells were in S phase (2.4%, **Fig 2.1.1D** left pannel), which upon continuous ICM treatment this fraction was increased (4.4% and 29.2% after 3 and 6 days or treatment respectively, **Fig 2.1.1D** second and third panel), in agreement with the percentage of senescent cells found in S phase (23.6%, **Fig 2.1.1D** right pannel). From the above we were able to conclude that continuous ICM treatment leads IMR90s into a progressive S/G2 arrest similar to the senescent phenotype. On top of that, ICM-treated IMR90s exhibited complete absence of HMGB1 and HMGB2 proteins from their nuclei, indicative for senescence (**Fig 2.1.1E-F** and **Fig 2.1.S1A-B**, Zirkel *et al*, 2018; Sofiadis *et al*, 2021) and upregulation of the senescent marker p21 (**Fig 2.1.1E** and **Fig 2.1.S1B**, Labaer *et al*, 1997; Galanos *et al*, 2016). Additionally, in agreement with what is known for cells undergoing senescence, levels of H3K27me3 were decreased coupled with increased levels of HP1a (**Fig 2.1.1G**, Pal & Tyler, 2016) and senescence-associated CTCF clusters (SICCs) were emerged (**Fig 2.1.1F** and **Fig 2.1.S1A**, Zirkel *et al*, 2018). Western blot analysis confirmed the decrease in HMGB2 protein levels (**Fig 2.1.1H**).

Testing more senescence-related markers by qPCR (**Fig 2.1.1I**) they all agreed for the senscent state of the ICM-treated IMR90s. *HMGB1/2* were found to be downregulated (*pvalue* <0.05) as well as *LMNB1* (*pvalue* <0.05), while on the other hand *HMGA1*, *HDAC9* and *CCND2* were upregulated (*pvalue* <0.05). Moreover, using ChIP-qPCR we were able to confirm the loss of HMGB2 from the nucleus and, thus, from chromatin, upon ICM treatment, as we were able to observe decreased binding of the protein in TAD boundaries and inergenic bodies (**Fig 2.1.1J**). Taken together, all of the aformentioned data, pintpointed to the direction of ICM causing a cellular growth arrest, similar to senescence.

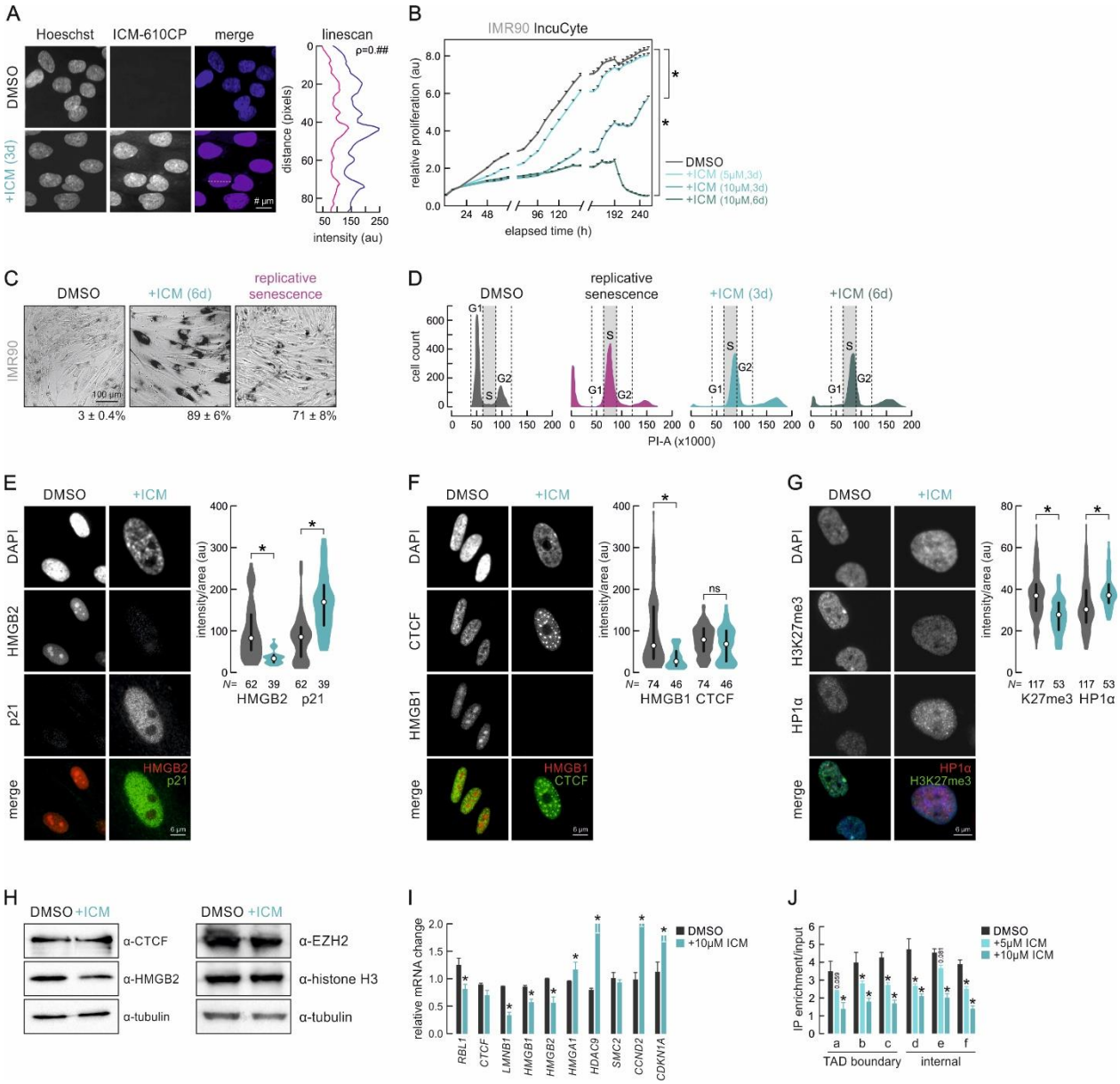

Figure 2.1.1. ICM treatment induces a senescent-like phenotype.

A. Proliferating and ICM-treated IMR90 assayed for proliferation rate using the Sartorius IncuCyte S3 Live-Cell Analysis System.

B. Representative widefield images of proliferating (top panel) and 610CP-tagged ICM-treated (bottom panel) IMR90. DNA is stained with Hoechst dye. On the right side fluorescence signal was used to produce lineplot depicting the overlap between Hoechst and 610CP-tagged ICM. Bar: 5um

C. Proliferating, ICM-treated and senescent IMR90 assayed for β-galactosidase activity. ICM-treated and senescent cells appeared darker, indicative of their senescent state.

D. Cell cycle profiling via FACS in proliferating (upper left panel), senescent (upper right panel) and 3 and 6 days ICM-treated cells (lower left and lower right panel, respectively).

E. Representative immunofluorescence images of IMR90 showing reduced levels of HMGB2 and increased levels of p21. Violin plots quantify this reduction (bottom; N is the number of cells analyzed per each condition/cell type). Bars: 6um. *P<0.05; Wilcoxon–Mann–Whitney test.

F. Same as in E, but for HMGB1/CTCF. SICCs formation is depicted in ICM-treaded nuclei.

G. Same as in E, but for HP1a/H3K27me3

H. Western Blot analysis of CTCF, HMGB2, EZH2 and histone H3 in proliferating and ICM-treated IMR90. a-tubulin serves as a loading control.
I. Representative real time qPCR showing selected senescent markers in proliferating and ICM-treated IMR90. *P<0.05; Wilcoxon–Mann–Whitney test.
J. Mean ChIP-qPCR enrichment (over input and negative controls; $\log_2 \pm$ SD, n=2) in different IMR90 populations (proliferating, 5uM and 10uM ICM-treated) with primers targeting HMGB2.

ICM mimics RS transcriptional pathway

Since our observed data contradicted the previously available literature we wanted to further investigate the effect ICM seemed to have in IMR90s. There were strong indications of a senescent-like phenotype upon ICM treatment and we wanted to see if there would be any resemblance with previously described growth arrests. First, we examined any possible changes at six senescence-predictive CpGs [238]. In contrast to replicative senescence (RS), methylation-aging clock did not seem to apply to ICM treatment (**Fig 2.1.2A**). However, RS and ICM treatment seemed to converge in the reduction of transcription over passaging and period of treatment, respectively, since EU-RNA levels where found to be reduced in both cases (**Fig 2.1.2B**).

To further test for any resemblance, total mRNA from control, ICM-treated (10uM, 6 days) and senescent IMR90s was isolated, enriched for poly(A)$^+$, depleted of rRNA and sequenced to >50mil reads. After *in silico* genomic mapping (hg19), counts were normalized to assess for differences in transcription. A broad range of genes were found to be deferentially expressed upon ICM treatment. In total, 2,212 genes were identified to be differentially expressed (1,265 up- and 947 down-regulated). Notably, genes related to cell cycle progression were found to be downregulated, while the most prominent upregulated genes were part of the NRF2 pathway (**Fig 2.1.S2A-B**). HMGB2 was found to be downregulated, as well as many cell cycle kinases, verifying our FACS results (**Fig 2.1.2C**). Next, using the mRNA-seq data from RS and ICM we looked for changes at the levels of a variety of chromatin factors and, interestingly, both seemed to share great similarities following a similar pattern of up- and downregulated components (**Fig 2.1.2D**).

GO term analysis of the transcription factors governing the expression of either up- or down-regulated genes upon ICM treatment, revealed that p53 is actively engaged in the regulation of both up- and down-regulated genes, consistent with its prominent role in senescence [29], while many pro-inflammatory factors (e.g. RELA, JUN, STAT3) were shown to control downregulated genes (**Fig 2.1.2E**).

Using 'factory' RNA-seq [239] we isolated and analyzed nascent RNA from 3 and 6 days ICM-treated IMR90s. There, we showed that most of the observed alterations are transcriptionally regulated and that upregulated transcripts, apart from being more expressed upon ICM treatment, there are also more stable (**Fig 2.1.2F-G** and **Fig 2.1.S3, S4**). Interestingly, similar to RS [90], the commonly downregulated genes from mRNA-seq and nascent RNA-seq data are related with cell proliferation, DNA metabolism and nuclear and chromatin organization pathways (**Fig 2.1.2I-J**).

Lastly, when we compared mRNA-seq data derived from 3 and 6 days ICM-treated IMR90s with data previously generated in our lab [90] and publicly available [240], it was shown that the ICM-induced arrest shares greater similarity (R^2=0.28 and 0.36 for 3 and 6 days, respectively), with replicative senescence (**Fig 2.1.2H**, left and middle panel), while it demonstrated significantly lower association, (R^2=0.1), with the OIS (**Fig 2.1.2H**, right panel). Summing up, all the above data demonstrated with high confidence that the observed arrest after ICM treatment shares high similarity with RS.

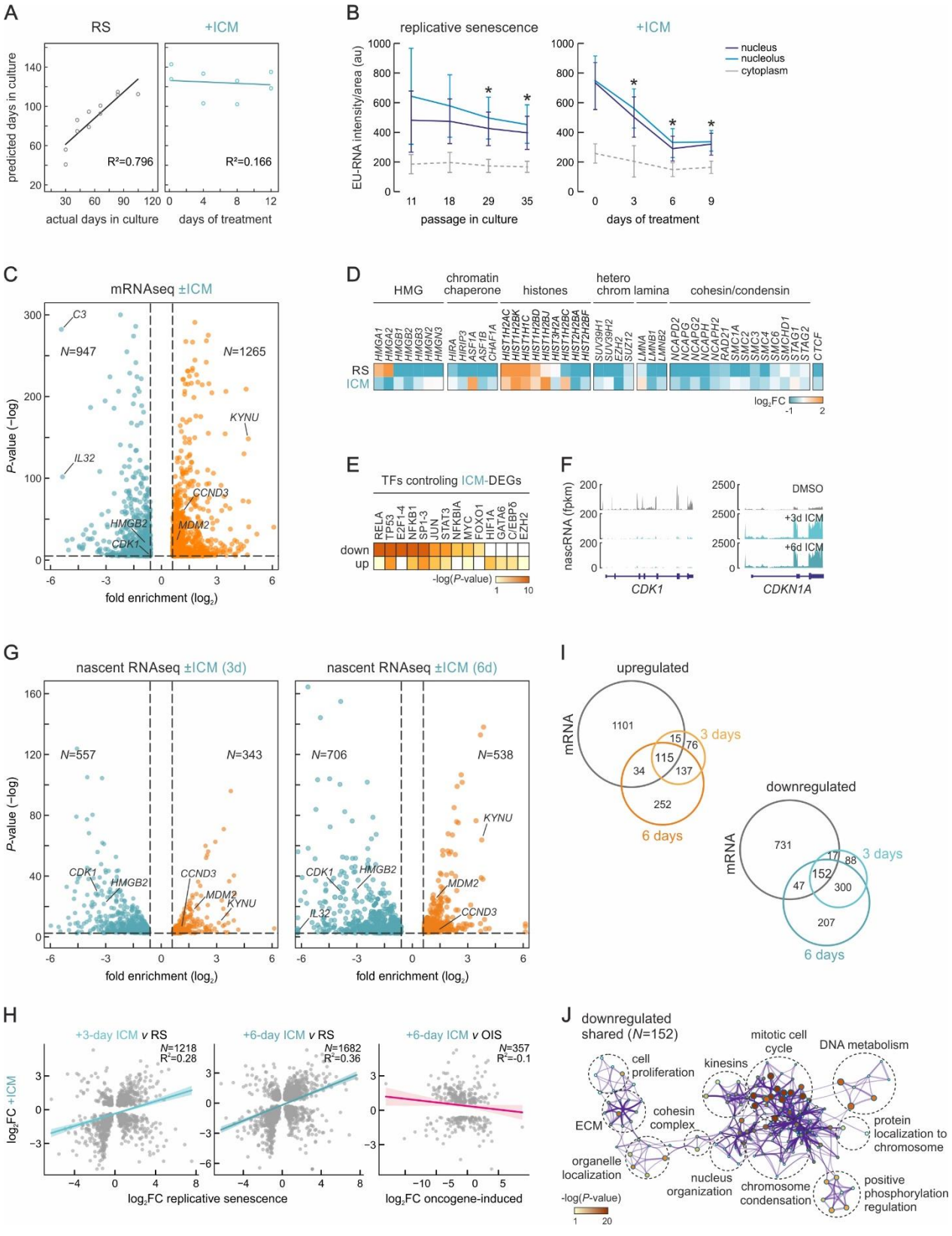

Figure 2.1.2. ICM-induced senescence transcriptionally resembles replicative senescence.

A. On the left: Spearman's correlation (R^2) between actual and predicted IMR90 passage based on the methylation at six CpGs. On the right: same as before, but for days of ICM treatment.

B. Decrease in nascent EU-RNA in IMR90 based on their passage number (on the left) and days of ICM treatment (on the right). *P<0.05, Wilcoxon-Mann-Whitney test.
C. Volcano plot showing differentially expressed genes (fold enrichment) between proliferating and ICM-treated IMR90. In orange, the most significant downregulated genes are shown (< -0.6 log_2-fold change), while in turquoise the most significant upregulated genes are depicted (> 0.6 log_2-fold change). N is the number of the respective genes.
D. Heatmaps showing changes in gene expression levels upon senescence and ICM treatment (log_2FC) of genes encoding selected chromatin-associated factors. For each gene shown, statistically significant expression changes were recorded in at least one condition.
E. Heatmaps showing transcription factors regulating up and downregulated genes upon ICM treatment (log_2FC).
F. *CDK1* and *CDKN1A* loci nascent RNA-seq profiles in proliferating, 3 and 6 days of ICM-treated IMR90s.
G. Volcano plot showing nascent-RNA differences (fold enrichment) between 3 days and 6 days of ICM treatment. In orange, the most significant downregulated genes are shown (< -0.6 log_2-fold change), while in turquoise the most significant upregulated genes are depicted (> 0.6 log_2-fold change). N is the number of the respective genes.
H. Comparison of differentially expressed genes between replicative senescence and 3 and 6 days of ICM treatment (left and middle panel, R^2=0.28 and 0.36, respectively) and oncogene induced senescence and ICM (right panel, R^2=0.1). N is the number of the respective genes
I. Venn diagrams showing commonly up- and down-regulated genes between ICM mRNA-seq and 3 and 6 days ICM nascent RNA-seq.
J. Highlighted in the interaction node are the GO term/pathways of the commonly downregulated targets from panel I.

Single-cell transcriptomic analysis clusters ICM and RS

Having bulk mRNA-seq data indicating the similarity between RS and ICM-induced phenotype, we went on to examine if this holds true also at the single cell level. For that purpose, we used proliferating, ICM-treated and senescent IMR90s. Cells were sequenced and the ones that past the quality control were further analysed and divided into 10 clusters (0-9) (**Fig 2.1.3A-C**). RS and ICM-treated IMR90s were showed to have an extended overlap in clusters with the most prominent to be cluster 0 (**Fig 2.1.3C**). HMGB2 was found to be downregulated in senescence-related clusters (cluster 0,1,5), but overrepresented in all the rest (**Fig 2.1.3D**). GO term/pathway analysis revealed that the majority of gene found in cluster 0 are related with processes which are downregulated upon senescence entry (e.g. cell cycle, chromosome localization), in agreement with the transcription factors that are regulating them (**Fig 2.1.3E-F**). Overall, we were able, also at the single cell level, to show that the arrest which is induced upon ICM treatment matches RS.

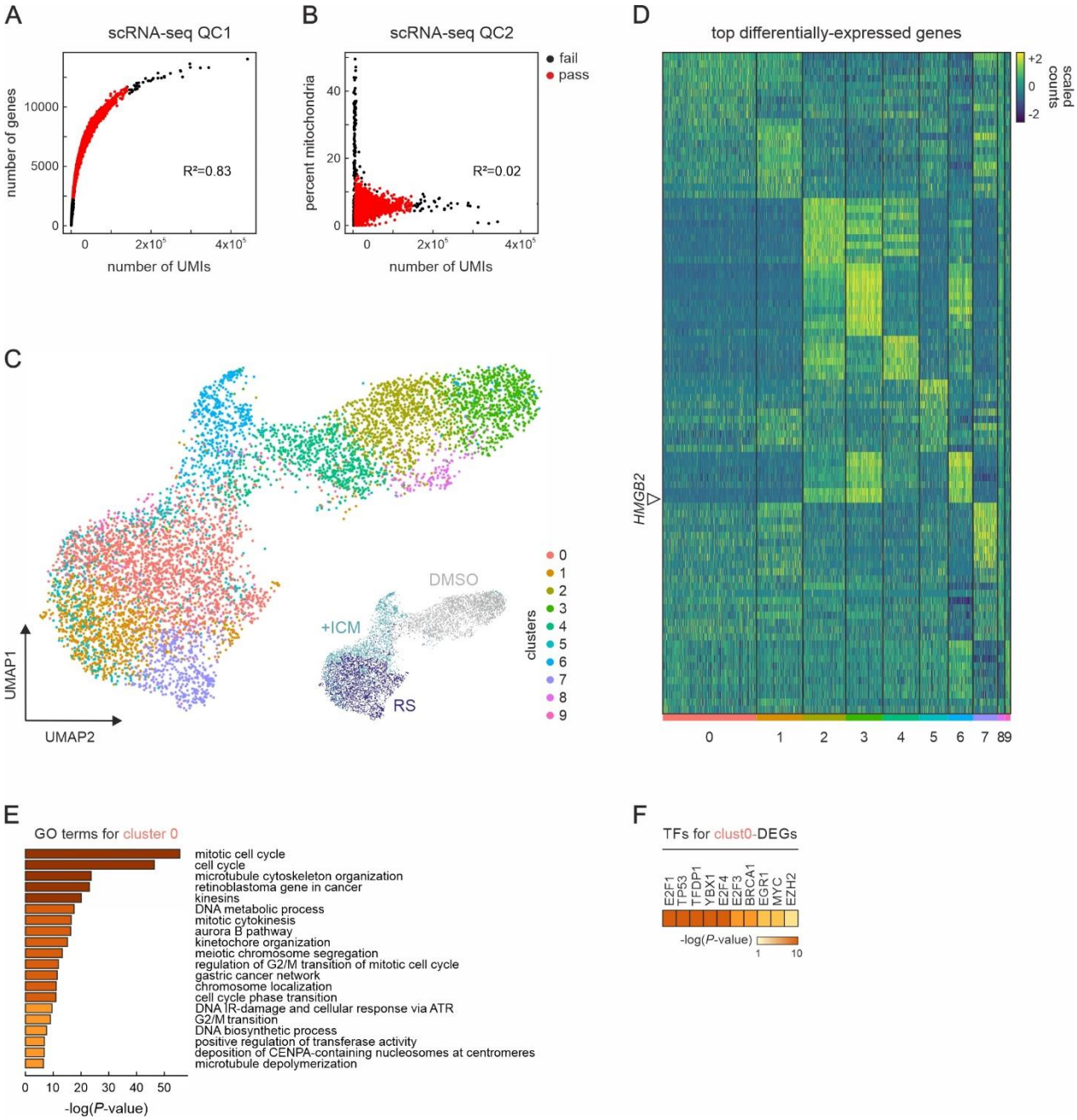

Figure 2.1.3. scRNA-seq clusters ICM and RS together.

A. UMI-Gene: Scatter plot visualizing the relationship between the number of unique molecular identifiers (UMIs) and the number of detected genes for each analyzed cell. Quality control passing cells are displayed in red while those that failed are shown in black.

B. UMI-Mitochondria: Scatter plot showing the relationship between the number of UMIs and the percentage of UMIs in mitochondrial genes. Quality control passing cells are colored in red while those that failed are colored in black.

C. RNA Cluster UMAP: Cells are colored based on their cluster identities and visualized in a two-dimensional uniform manifold approximation and projection for dimension reduction space (UMAP), where UMAP is based on gene expression data alone, and clustering is performed using both gene expression and chromatin accessibility data.

D. Heatmap showing the scaled gene expression of the top markers (top 10) identified for each cluster based on logFC.
E. Heatmap showing GO terms/pathways associated with the gene subgroups of cluster 0 from panel C.
F. Heatmap showing transcription factors associated with the gene subgroups of cluster 0 from panel C.

ICM drives senescence in a transcription-related manner

Having shown that there are significant changes in gene expression, documented by RNA-seq, upon ICM treatment, we thought to further examine in which degree these changes could have had any affect in the transcriptional or translational level. To answer this question, we generated coupled mRNA-seq, Ribo-seq and whole proteomics data from proliferating and ICM-treated IMR90s in biological triplicates.

Whole proteome analysis showed that 642 proteins were found to be downregulated and 565 upregulated upon ICM treatment (Fig 2.1.4A). Pathway analysis demonstrated that the downregulated proteins followed a similar pattern as the mRNA-seq data for ICM, regarding the involved processes, as again nuclear and chromatin organization and cell cycle progression were found among the most prominent targets (Fig 2.1.4B and Fig 2.1.**S5**). Comparing mRNA-seq with Ribo-seq data uncovered that basically the majority of significant changes at the level of mRNA (>$\log_2$ 0.6) could be explained by similar changes in transcription availability (Fig 2.1.4C, E). At the transcriptional level, 504 and 405 genes were found to be commonly ''buffered'' up or down respectively in ICM compared to proliferating IMR90s, leading to a maintenance of consistent protein levels for these genes. Interestingly, the majority of ''buffered'' downregulated transcripts (e.g. *CDK2, RAD51, CDCA5*) are related with pathways such us DNA replication, cell cycle, translation elongation and ribosome biogenesis.

Next, we directly compared how similar or different are the translational and transcriptional programs between ICM-induced senescence and replicative senescence. Following a similar approach as above, Ribo-seq data showed that essentially no genes were found to be differentially regulated exclusively at the translational level between ICM and senescent cells (Fig 2.1.4D).

It is also worth to mention that in the ‘’buffered’’ upregulated transcripts of ICM compared to proliferating IMR90s, there was an over-representation of SASP-related factors, meaning that this increase in the RNA-seq data between conditions was not accompanied by an increase in the Ribo-seq. In addition, dot blot analysis of HMGB1 and HMGB2 in senescent and ICM-treated cells, confirmed the intracellular reduction of both proteins in both cases, but, in contrast to RS [241], in ICM-treated cells HMGB1 was not detected to be secreted (Fig 2.1.4F). Driven by these two observations, we went on and compared our proteome data with publicly available data for fibroblast SASP (http://www.saspatlas.com), where we observed a very small overlap (Fig 2.1.4G). Taken together, the above observations pointing towards a transcriptional regulation of ICM response leading to a SASP-less induction of replicative-like senescence.

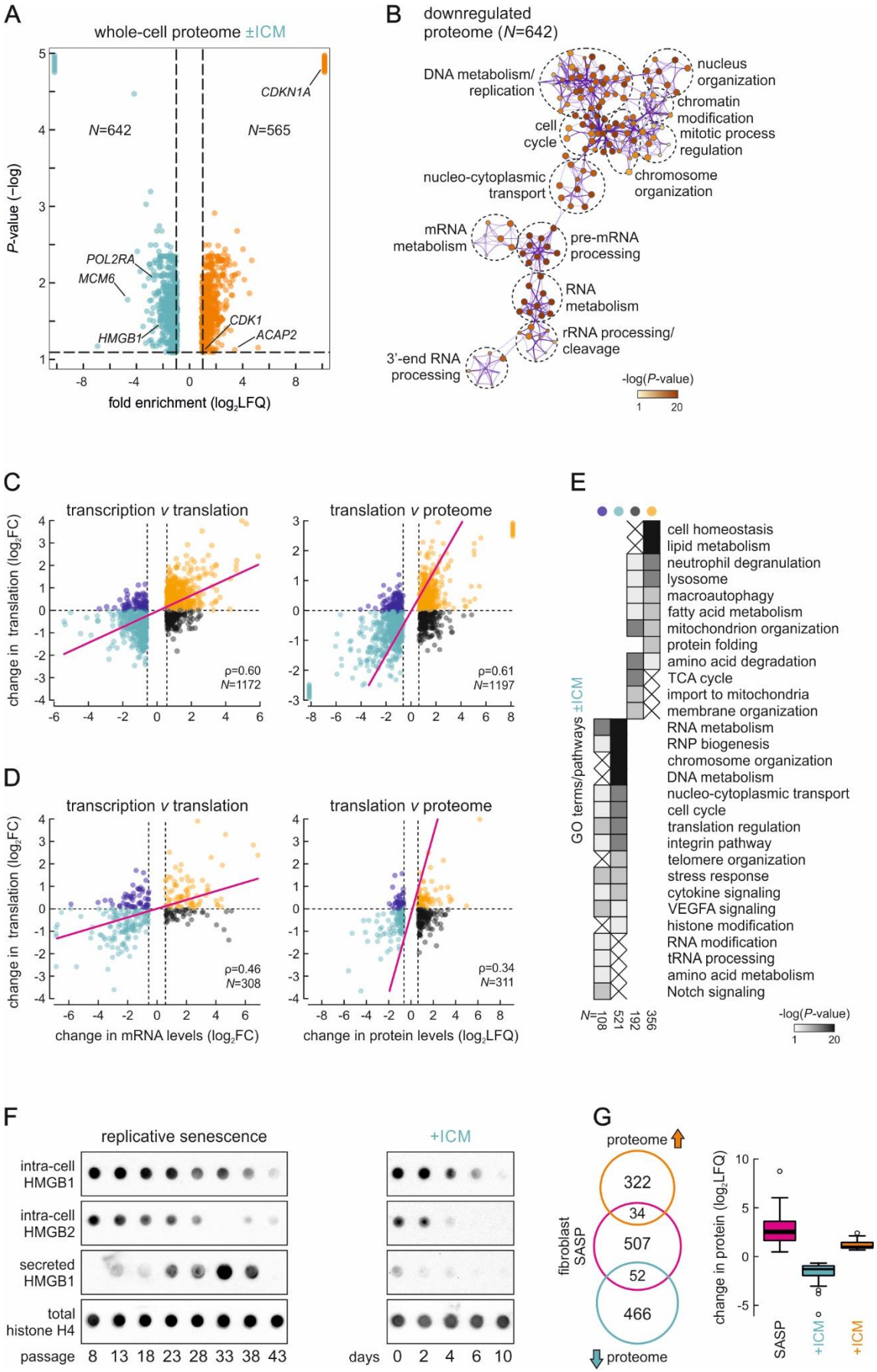
A
whole-cell proteome ±ICM
P-value (−log)
fold enrichment (log2LFQ)
N=642
N=565
CDKN1A
POL2RA
MCM6
HMGB1
CDK1
ACAP2
B
downregulated proteome (N=642)
DNA metabolism/ replication
nucleus organization
chromatin modification
mitotic process regulation
cell cycle
chromosome organization
nucleo-cytoplasmic transport
mRNA metabolism
pre-mRNA processing
RNA metabolism
rRNA processing/ cleavage
3'-end RNA processing
-log(P-value)
C
transcription v translation
translation v proteome
change in translation (log2FC)
ρ=0.60
N=1172
ρ=0.61
N=1197
D
transcription v translation
translation v proteome
change in translation (log2FC)
ρ=0.46
N=308
ρ=0.34
N=311
change in mRNA levels (log2FC)
change in protein levels (log2LFQ)
E
GO terms/pathways ±ICM
cell homeostasis
lipid metabolism
neutrophil degranulation
lysosome
macroautophagy
fatty acid metabolism
mitochondrion organization
protein folding
amino acid degradation
TCA cycle
import to mitochondria
membrane organization
RNA metabolism
RNP biogenesis
chromosome organization
DNA metabolism
nucleo-cytoplasmic transport
cell cycle
translation regulation
integrin pathway
telomere organization
stress response
cytokine signaling
VEGFA signaling
histone modification
RNA modification
tRNA processing
amino acid metabolism
Notch signaling
N= 108 521 192 356
-log(P-value)
F
replicative senescence
+ICM
intra-cell HMGB1
intra-cell HMGB2
secreted HMGB1
total histone H4
passage 8 13 18 23 28 33 38 43
days 0 2 4 6 10
G
proteome
322
34
507
52
466
proteome
fibroblast SASP
change in protein (log2LFQ)
SASP
+ICM
+ICM

Figure 2.1.4. ICM-induced senescence is mostly transcriptionally driven.

A. Volcano plot showing whole proteome difference upon ICM treatment. . In orange, the most significant downregulated genes are shown (< -0.6 log_2-fold change), while in turquoise the most significant upregulated genes are depicted (> 0.6 log_2-fold change). N is the number of the respective genes.
B. Highlighted in the interaction node are the GO term/pathways of the commonly downregulated targets from panel A.
C. Scatter plots showing correlation between mRNA-seq (transcription; log2 > 0.6) and Ribo-seq (translation; log2) (left) and correlation between mRNA-seq and whole proteome (right) in proliferating and ICM-treated IMR90. Coefficient value and the number of genes in each plot (N) are also shown.
D. Same as in C, but correlating IMC-treated and RS IMR90s.
E. Heatmap showing GO terms/pathways associated with the gene subgroups from panel C (color-coded the same way). The number of genes in each subgroup (*N*) is indicated.
F. Dot blot detecting the intracellular levels of HMGB1 and HMGB2 and levels of secreted HMGB1 across passages (left panel) and across days of ICM treatment. Histone H4 serves as a control.
G. Venn diagram (left) showing up- and down-regulated factors from whole-cell proteome data crossed with data from SASP atlas. Box-whisker plot on the right shows the changes in SASP-related proteins (log_2-fold change).

ICM induces genome reorganization similar to RS

It has been shown, that upon senescence entry there is extended chromatin reorganization [88–90]. Lastly, we asked whether ICM treatment could induce similar alterations. For that purpose, proliferating and ICM-treated IMR90s were subjected to Micro-C analysis, which revealed widespread changes across chromosomes (**Fig 2.1.5A**). In both conditions, contact frequencies were decreased with genomic distance. Upon ICM treatment, shorter-range interactions were strengthened, there was a decrease in longer-range ones and at the level of compartments we observed less intermingle and better insulation (**Fig 2.1.5B-C**).

Based on the above observations, we thought to see if these alterations are accompanied by changes in the architectural proteins CTCF and SMC1A, since both are actively participating in shaping nuclear 3D organization [169,242]. To do so, we used proliferating, ICM-treated an senescent IMR90s and applied CUT&Tag-seq. Downstream analysis allowed us to call 4,652 CTCF peaks in proliferating, 6,666 in ICM-treated and 8,440 in senescent cells (top 1%). Similarly, we called 14,884 SMC1A peaks in proliferating, 17,810 in ICM-treated and 12,928 in senescent IMR90s (top 1%) (**Fig 2.1.5D-E**). Additionally, we were able to observe that, on average, in all three conditions many CTCF peaks were co-occupied by SMC1A [243] and that ICM, despite having its unique profile for both CTCF and SMC1A, was sharing a bigger fraction of CTCF peaks with RS than with proliferating cells (**Fig 2.1.5D**,

F). Interestingly, in ICM condition apart from calling unique CTCF peaks, we could also see that there was an increase in signal of peaks that were shared between proliferating and ICM-treated cells.

Having local information about CTCF upon ICM treatment, we went on to see if changes occurring in 2D (signal strength and distribution) would have any impact on 3D chromatin organization. Taking the aggregate signal from all CTCF peaks from proliferating and all CTCF peaks from ICM-treated IMR90s we saw that around them, on average, insulation was decreased, maybe due to the newly emerged CTF peaks on ICM and their impact on insulation strength (**Fig 2.1.5G**). We also stratified loops based on whether they were found to anchor CTCF or not (**Fig 2.1.5H-I**). Out of 22,871 loops in proliferating IMR90s 2,970 were CTCF loops and 19,901 nonCTCF ones. In ICM-treated IMR90s we called 14,996 loops with 1,801 of them to be CTCF loops and 13,194 nonCTCF ones. From the ICM CTCF loops, 613 were unique and from nonCTCF loops, 4,303 were unique. Interestingly, we observed that these unique CTCF loops (**Fig 2.1.5H**, unique to ICM) presented a stronger signal compared to nonCTCF ones (**Fig 2.1.5I**, unique to ICM) despite their smaller absolute number, pointing to a potentially more significant role in the reestablishment of 3D chromatin structure upon ICM treatment. Taken together, the above data are in agreement with previously described chromatin alteration occurring upon senescence entry[6,86,89,90] and indicative of ICM ability to provoke, apart from gene expression senescent-like changes, senescent-like genome reorganization.

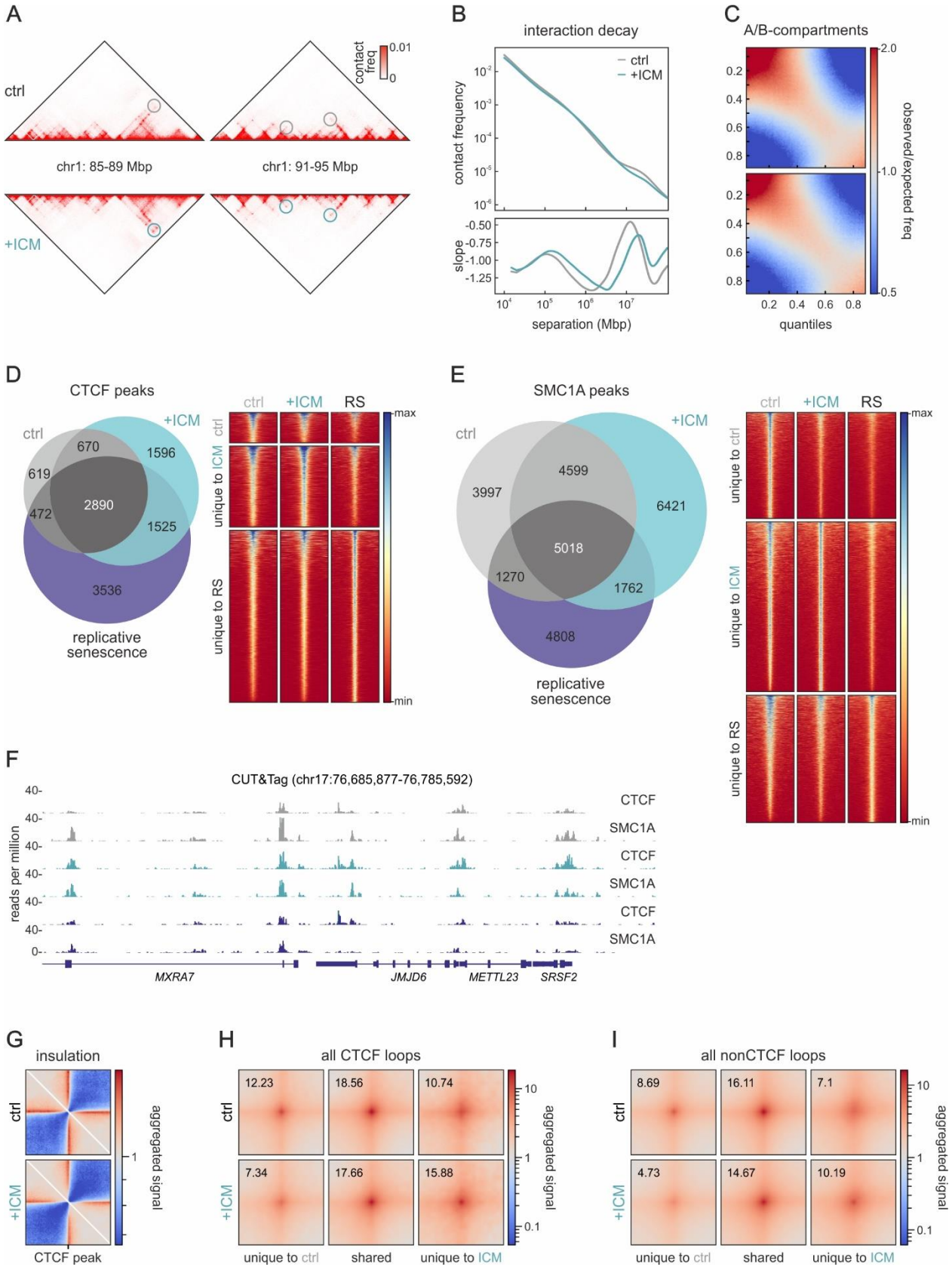
A
ctrl
+ICM
contact freq
0.01
0
chr1: 85-89 Mbp
chr1: 91-95 Mbp
B
interaction decay
ctrl
+ICM
contact frequency
slope
separation (Mbp)
C
A/B-compartments
observed/expected freq
quantiles
D
CTCF peaks
ctrl
+ICM
670
1596
619
2890
472
1525
3536
replicative senescence
RS
unique to ctrl
unique to ICM
unique to RS
max
min
E
SMC1A peaks
4599
3997
6421
5018
1270
1762
4808
F
CUT&Tag (chr17:76,685,877-76,785,592)
reads per million
CTCF
SMC1A
MXRA7
JMJD6
METTL23
SRSF2
G
insulation
aggregated signal
CTCF peak
H
all CTCF loops
12.23
18.56
10.74
7.34
17.66
15.88
unique to ctrl
shared
unique to ICM
I
all nonCTCF loops
8.69
16.11
7.1
4.73
14.67
10.19

Figure 2.1.5. ICM treatment affects 3D chromatin organization.

A. 10kbp resolution Micro-C maps along a chr1 loci from proliferating (upper triangles) and ICM-treated (lower triangles) IMR90s. Differences between the two are depicted in circles.
B. Decay plots showing Micro-C interaction frequency as a function of genomic distance at 5kbp resolution. Proliferating IMR90s are depicted in grey and ICM-treated in green.
C. Saddle plots corresponding to proliferating (upper panel) and ICM-treated IMR90s (lower panel), showing contact frequencies between inactive (red area in the upper left) and active (red area in the lower right) regions.
D. Left: Venn diagram showing the unique and overlapping CTCF peaks (top 1%) called from CUT&Tag-seq in proliferating, ICM-treated and senescent IMR90s. Right: Heatmaps showing scaled signal distribution of the aforementioned peaks.
E. As in D, but for SMC1A.
F. CTCF and SMC1A CUT&Tag-seq from proliferating (grey), ICM-treated (green) and senescent (purple) IMR90s along a chr17 locus.
G. Insulation plot from Micro-C averaged signal on ±100bp around CTCF summits, with 300kb flanking regions, across proliferating and ICM-treated IMR90s. Top 1% CTCF peaks were used.
H. Aggregate plots showing the averaged Micro-C signal across the 5kb unique and shared CTCF loops, in proliferating and ICM-treated IMR90s, with 50kb padding around the loops.
I. Same as in H, but for nonCTCF loops

Discussion

At this method paper, we have introduced a novel and robust way of inducing cell cycle arrest in culture. Despite its original characterization [235], prolonged ICM treatment has the capability to evict HMGBs out of the nucleus, leading to a similar phenotype with the one of replicative senescence [84]. In this way, we are now able to overcome many of the cavities when studying senescence *in vitro.*

The impact that senescent cells have in normal human aging, but also in the abnormal conditions mentioned earlier on, make them a highly appealing pharmacological target, too. A lot of research is focusing nowadays on how to modulate the action, the impact, but also the removal of senescent cells from an organism. The relatively new, but rather active, field of senolytic drugs [244,245] hopes to give answers to all or some of these questions. ICM, being a chemical compound itself, could be proven such a potent candidate and its unique feature of modulating the cellular localization of HMGBs points to this direction.

Already from its early characterization ICM was perceived as a therapeutic candidate and there are now studies testing its pharmacokinetics [235,246]. Later studies, showed that ICM could block the secretion of HMGB1 and HMGB2 from macrophages, leading to reduced production of pro-inflammatory cytokines from these cells and proved to be an efficient compound for sepsis treatment [247]. ICM was used in the transplantation field, as well, since it was shown to significantly decrease the levels of HMGB1 secreted from pancreatic cells post-surgical in patients with type 1 diabetes, thus reducing the possibilities of transplant rejection [248]. Data from our lab, using pancreatic cancer cell lines with either high or low levels of HMGBs (high levels of HMGBs is a bad-prognosis marker) have shown promising early results after treatment with ICM. Taken together, inflachromene is a remarkable tool both in for *in vitro* cell culture and as a pharmacological target *in vivo* and with our study, we aim to accelerate its utilization.

Materials and Methods

Cell culture and senescent assays

Single IMR90 isolates (I90-83, passage 5; Coriell Biorepository) were continuously passaged at 37°C under 5% CO2 in Minimal Essential Medium L-Glutamine without HEPES (MEM 1X) (Gibco™ Life Technologies GmbH, 31095052) supplemented with 10 % FBS (Life Technologies, 10500064), 1X (1%) MEM Non-essential Amino Acid Solution without L-glutamine (Sigma-Aldrich, M7145-100ML) and 1% Penicillin/Streptomycin (Gibco™ Life Technologies, 15140122). The senescent state of the cells was addressed by senescence-associated β-galactosidase assay (Cell Signaling) according to the manufacturer's instructions. Cells were driven into senescence either by continuously passaging them to replicative exhaustion or by using Inflachromene (concentration and period of treatment is depicted on individuals experiments). Cell proliferation was monitored using the Sartorius IncuCyte S3 Live-Cell Analysis System and acquiring a picture every 8h for a total of 11 days. Finally, DNA methylation at six selected CpG islands [238] was measured by isolating genomic DNA at the different cell states and performing targeted pyrosequencing (Cygenia GmbH)

Protein extraction and western blot

Proliferating and ICM-treated IMR90s (approx. $2x10^6$ per condition) were gently scraped off 15-cm dishes. Cells were then pelleted for 5min at 1,200rpm. The supernatant was discarded and pellets were lysed in 150u of RIPA lysis buffer (20 mM Tris- HCl pH 7.5, 150 mM NaCl, 1 mM EDTA pH 8.0, 1 mM EGTA pH 8.0, 1% NP-40, 1% sodium deoxycholate) containing 1x protease inhibitor cocktail (Roche) for 30min on ice. Sample were then sonicated in low input for 3 cycles (30sec on/30sec off) and centrifuged for 15min at >15,000g. Then the supernatant was collected and the protein concentration was measured using the Pierce BCA Protein Assay Kit (Thermo Fisher Scientific). Rabbit polyclonal anti-HMGB2 (1:1,000; Abcam ab67282); rabbit polyclonal anti-CTCF (1:500; Active motif 61311); rabbit polyclonal anti-EZH2 (1:500; Active motif 39901); rabbit polyclonal anti-H3 (1:500; Abcam ab1791); mouse monoclonal anti-a tubulin (1:1000, Abcam ab7291) were used for blotting.

Immunofluorescence and image analysis

Cells treated with ICM-610CP were cultured in coverslips for 3 days and DNA was subsequently stained with 5-SiR-Hoechst [249] and fixed via incubation with 4% paraformaldehyde (PFA) in Dulbecco's Phosphate-Buffered Saline (DPBS). For every other staining, cells grown on coverslips were fixed via incubation with 4% PFA in DPBS at RT for 10min and then permeabilized with 0,5% Triton-X in PBS for 10min. Blocking was performed with 1% Bovine Serum Albumin (BSA) in PBS at RT for 1h. Cells were then incubated with the primary antibody (diluted in 0.5% BSA/PBS) at RT for 1h at the indicated dilution: mouse monoclonal anti-HMGB1 (1:1,000; Abcam ab190377-1F3); rabbit polyclonal anti-HMGB2 (1:1,000; Abcam ab67282); rabbit polyclonal anti-CTCF (1:500; Active motif 61311); rabbit polyclonal anti-H3K27me3 (1:1,000; Diagenode C15410069); rabbit polyclonal anti-p21 (1:500; Abcam EPR362 - ab109520). The primary antibody was washed with PBS twice for 5min per wash. Cells were incubated with the secondary antibody (diluted in 0.5% BSA/PBS) at RT, in the dark for 1h at the indicated dilution: anti-rabbit Alexa488 (1:1,000, Abcam ab150077); anti-mouse Cy3 (1:1,000, Abcam ab97035). Cells were then washed with PBS twice for 5min per wash. ProLongTM Gold antifade reagent with DAPI (#P36931) was added to the cells. For visualizing nascent transcripts, cells were pre-incubated with 2.5mM 5-ethynyl uridine (EU) for 40min at 37°C in their growth medium, fixed and processed with the Click-iT EdU chemistry kit (Thermo Fiscer). For image acquisition, a widefield Leica DMI8 with an HCX PL APO 63x/1.40 (Oil) objective was used. The acquired images were subsequently analysed with the FIJI software [250]. Measurements of nuclear immunofluorescence signal were generated using a mask drawn on DAPI staining to define nuclear bounds. Background subtractions were then implemented to precisely determine the mean intensity per area of each immune-detected protein.

RNA isolation, sequencing and analysis

Proliferating, senescent and ICM-treated IMR90s were harvested in TRIzol LS (Life Technologies) and total RNA was isolated and DNase I-treated using the DirectZol RNA miniprep kit (Zymo Research). Following selection on poly(dT) beads, barcoded cDNA libraries were generated using the TruSeq RNA library Kit (Illumina) and were paired-end sequenced to >50 million read pairs on a HiSeq4000 platform (Illumina). Default settings of STAR aligner [251] were used to map the raw reads to human reference genome (hg19) and quantification of unique quants was done with *featureCounts* [252]. RUVs function of RUVseq [253] was used to further normalize the counts, prior to differential gene expression estimation using DESeq2 [254]. Genes with an FDR < 0.01 and an absolute (log_2) fold change of > 0.6 were deemed as differentially expressed. Plots were generated using GO term enrichment bar plots from Metascape (http://metascape.org/gp/index.html) [255]. For RNA that was later used for qPCR the isolation procedure was the same as the one described above. cDNA was synthesized with SuperScript™ II Reverse Transcriptase (Invitrogen™ Life Technologies, 18064071) and random primers (Sigma-Aldrich, 11034731001) according to the manufacturer's First-Strand cDNA Synthesis Using SuperScript™ II RT protocol. Full list of primers used for qPCR is at Table 1. Finally, for analysis of nascent RNA in IMR90 the ''factory RNA-seq'' approach was applied on 5mil ICM-treated cells [239], RNA was isolated and sequenced as above, and intronic read counts were obtained and differentially analyzed for the two conditions using the iRNAseq package [256]. GO term/pathway enrichment analyses was performed using Metascape (http://metascape.org/gp/index.html).

ChIP and ChIP-qPCR

Proliferated and ICM-treated IMRO90s were cultured to 80% confluence in 15-cm plates and they were crosslinked in 15mM EGS/PBS (ethylene glycol bis(succinimidyl succinate); Thermo) for 20min at room temperature, followed by fixation for 40min at 4°C in 1% PFA. Cells were then processed with the ChIP-IT High Sensitivity kit (Active motif) according to the manufacturer's instructions. Chromatin was sheared to 200-500bp fragments via sonication using a Bioruptor Plus (25 cycles, 30sec on/30sec off, high input), immunoprecipitation was done using 4ug of anti-HMGB2 antibody (Abcam ab67282) to approx. 30ug of chromatin and the samples were incubated overnight in a rotor at 4°C. DNA was precipitated using protein A/G agarose beads and purified using the ChIP DNA Clean & Concentrator kit (Zymo Research). Clean DNA was later used for qPCR. Oligos used for qPCR are listed in Table 2.

Ribo-seq and analysis

High-throughput ribosome profiling (Ribo-seq) on proliferating, senescent and ICM-treated IMR90s was performed in collaboration with Ribomaps Ltd (https://ribomaps.com) according to an established protocol [257]. Three independent replicas of proliferating, senescent or ICM-treated IMR90s were grown, harvested in ice-cold polysome isolation buffer supplemented with cycloheximide, and shipped to Ribomaps for further processing and library preparation. Roughly 15% of each lysate was kept for RNA isolation and used for RNA-seq of poly(A)-enriched fractions on a HiSeq2500 platform (Illumina). After sequencing of both Ribo- and mRNA-seq libraries, the per base sequencing quality of each replicate passed the quality threshold, raw read counts were assigned to each protein-coding open reading frame (CDS) for Ribo-seq and to each transcript for mRNA-seq, and replicate correlations were tested. Read length distribution for Ribo-seq datasets fell within the expected range (25–35nt), showing strong periodic signals and an enrichment in annotated CDSs. For mRNA-seq, read lengths ranged between 47 and 51 nt and distributed uniformly across transcripts. For differential gene expression analysis, anota2seq [258] was used. Changes in Ribo-seq data depict changes in the ribosome occupancy of the annotated protein-coding CDS, and thus, only ribosome-protected fragments that map to the CDS were used in the analysis.

VST normalized counts outputted using DESeq2 [254] and inputted into anota2seq were used for all subsequent downstream analysis. Differences in genes that pass a default false discovery rate (FDR) threshold of 15% were considered regulated. Such significant differences are then categorized into one of the following three modes: (i) translational: Changes in Ribo-seq that are not explained by changes in RNA-seq and imply changes at the protein level are due to changes at the translational level; (ii) mRNA abundance: Matching changes in RNA-Seq and Ribo-Seq that infer changes at the protein level are predominantly induced by changes at the transcriptional level; (iii) buffering: changes in RNA-seq that are not explained by changes in Ribo-seq and suggest maintenance of constant protein levels induced by changes at the transcriptional level or *vice versa*.

Cleavage Under Targets and tagmentation

0.5 million cells were lifted from plates using accutase, fixed with 0.3% PFA/PBS for 2min at RT and then quenched with 0.125M ice cold glycine for 5min at RT. Samples were then processed according to manufacturer's instructions (Active Motif). Samples were paired-end sequenced to obtain more than 10^7 reads. Reads were processed according to the standard CUT&Tag pipeline (https://yezhengstat.github.io/CUTTag_tutorial/). Briefly, paired-end reads were trimmed for adapter removal and mapped to human (hg38) and E. coli reference genomes (ASM584v2) using Bowtie 2 [259]. E. coli mapped reads were then quantified and used for calibrating human-mapped reads. Peak calling was performed using a multi-FDR-tryout method (FDR <0.01 to <0.1). For CTCF and SMC1, an FDR <0.01 was selected and only peaks with a canonical CTCF motif were considered [260]. Motif search was conducted by utilizing Fimo 5.4.1 of the MEME suite (https://meme-suite.org/meme/doc/fimo.html) against a random markov background model which was created by running the fasta-get-markov command of the aforementioned suite, on random sequences that corresponded to the length and the chromosome of the query CTCF peaks, for each sample.Heat-maps were generated using deepTools [261].

Micro-C and data analysis

Micro-C was performed using the Micro-C v1.0 kit in collaboration with Dovetail Genomics as per manufacturer's instructions. Micro-C libraries (at least 3 per each biological replicate) that passed QC criteria were pooled and paired-end sequenced on a NovaSeq6000 platform (Illumina) to >600 million read pairs per replicate. Micro-C contact matrices were produced using Dovetail Genomics pipeline (https://micro-c.readthedocs.io/en/latest/fastq_to_bam.html). In brief, read pairs were mapped to human reference genome hg38 using BWA, after which low mapping quality (<40) reads and PCR duplicates were filtered out using the *MarkDuplicates* function in Picard tools (v2.20.7), and read coverage tracks (BigWig) were generated and normalized with the RPCG parameter using the *bamCoverage* function of deepTools2 v3.5.1; [261]. Subcompartment analysis was performed by CALDER (Liu et al., 2021b) at 50 kbp-resolution Micro-C data. Compartment switched bins were found by comparing the corresponding resulting CALDER compartments considering the same coordinates across the different samples. The compartment boundaries for each sample corresponded to the 1bp of adjacent bins on which compartment changed from A to B or from B to A. The interaction decay plot was created by using cooltools 0.5.1 and is based on interactions at the chromosomal arms across the two samples indicating the contact probability as a function of separation (described here: https://cooltools.readthedocs.io/en/latest/notebooks/contacts_vs_distance.html). The eigenvalues, needed for the saddle plots, were computed with the cooltools call-compartments command at 10kb resolution and the expected interactions were computed with cooltools compute-expected command at the same resolution. The saddle plot was created with cooltools compute-saddle using 100 digitized bins. The procedure followed is similar to the one described here: https://cooltools.readthedocs.io/en/latest/notebooks/compartments_and_saddles.html Finally, we used coolpuppy 0.9.5 (https://coolpuppy.readthedocs.io/en/latest/) to generate all the aggregate plots. For loop calling, we used a multi-tool (HiCCUPS, SIP, and mustache) and a multi-resolution (5- and 10-kbp) approach as previously described [145,262]. Loop lists coming from each of the three different tools and across the two resolutions were merged using the pgltools intersect command (Greenwald et al., 2017) with a distance tolerance of 1bp. This procedure results in considering loops that were called in adjacent bins across different resolutions or tools as being shared, while unique loops are considered those that exhibit a distance corresponding to at least one bin size (5kb or 10kb) across the different loop-calling approaches. In cases of shared loops across the two resolutions, the 5kb resolution coordinates were kept for further analysis.

In order to find condition-specific loops we furtherly annotated them with ICM-specific CTCF peaks. To detect ICM enriched CTCF peaks, we furtherly filtered peaks based on the control and ICM CUT&TAG signal enclosed in regions around the summits of the ICM CTCF peaks. In more detail, we extracted the control and ICM depth-normalized CUT&TAG signal of regions 100bp around the summits of the ICM peaks by utilizing the multiBigwigSummary command of the Deeptools suite. The CTCF peaks that we considered in the downstream analysis were those that exhibited less than the mean control CUT&TAG signal with higher or equal to 1 fold difference compared to the corresponding ICM signal. 2628 ICM CTCF peaks fulfilled these criteria and were furtherly used to annotate both control and ICM loops. All intersections were performed using pgltools intersect1D without any distance tolerance for CTCF anchors. We considered loops as CTCF associated when at least one of the two anchors overlapped with a CTCF peak of the subset described above. The rest of the loops were annotated as non-CTCF. We furtherly divided the loops into condition-specific and shared loops. Condition-specific loops had at least one unique anchor. This analysis was done, as described before, by utilizing the pgltools intersect command with 1bp tolerance distance for both the shared and the unique loops.

scRNA-seq

In brief proliferating, ICM-treated and senescent IMR90s ($8x10^5$ cells/condition) were grown at 80% confluency, harvested with trypsin and froze at -80ºC. Single cell RNA-seq was performed using the 10X Genomics kit in collaboration with Active Motif. Libraries that passed QC criteria were paired-end sequenced to at least 250mil reads per library. The downstream analysis was performed by Active Motif.

Statistical tests

P-values associated with Student's *t*-tests, Fischer's exact tests and with the Wilcoxon–Mann–Whitney tests were calculated using GraphPad (https://graphpad.com/). Unless otherwise stated, *P*-values < 0.01 were deemed as statistically significant.

Table 1: List of qPCR primers used in this study.

Primer Name	Forward Seq 5‘-3‘	Reverse Seq 5‘-3‘
HSC70	TTA TTG GAG CCA GGC CTA CAC	GCG ACA TAG CTT GGA GTG GT
LMNB1	CTG GCC AAG ATG TGA AGG TTA	TCC TCT TCT TCA GGT ATG GTT GTT
HMGB1	TGA GCT CCA TAG AGA CGC G	GAT GAC ATT TTG CCT CTC GG
HMGB2	CCA ATG CTC CTA AAA GGC CAC C	CCA ATG GAT AGG CCA GGG TGT T
HMGA1	GAAAAGGACGGCACTGAGAA	CCCCGAGGTCTCTTAGGTGT
HDAC9	CATGAGAACTTGACACGGCA	TGCTCCAGTTTCTGCTCCTT
CCND2	TGGCCTCCAAACTCAAAGAG	CACTTCAACTTCCCCAGCAC
CDKN1A	TGGAGACTCTCAGGGTCGAA	GGATTAGGGCTTCCTCTTGG
SMC1	GGGGAGAAGACAGTGGCAG	TTGGTGTTATCCAAGGCAGC
CTCF	CAG AGG TTA ATG CAG AGA AAG TG	AAT GCC ATG CCA CAG AGATG
RBL1	GTATTCCAAGAGAAGTTGTGGCA	GGTCCACTGGAACAGTCAGG

Table 2: List of primers used in HMGB2 ChIP-qPCR experiment.

Location (hg19)	Primer pair ID	Forward Seq 5‘-3‘	Reverse Seq 5‘-3‘
chr10: 92671441-92671590	#a	ATGCGGGTTTACCATGCAGA	GGCCGAGAGCCATAAAGACA
chr1: 205091401-205091550	#b	TCAGACTCCGCAGGAAAGGT	AAGTACGCGCCTTGGTGAG
chr15: 39890983-39891451	#c	CATACAATAAAGGTGGTGCCAG	TTCAGGAGCTTAATACTGGAGGC
chr20: 43229526-43229628	#d	GACACGCTCAATAGGCTGAGT	GGGCTCTTATCCTTTCCCGA
chr10: 12085032-12085261	#e	TGAGTGCCATTCACTTAACAGC	GCTGGTAGTGGCTACCTTACG
chr3: 197676616-197677150	#f	TCAGTGCGAAGCCGATTTCC	AACATCTTTCGACTCCGCCC

Supplements

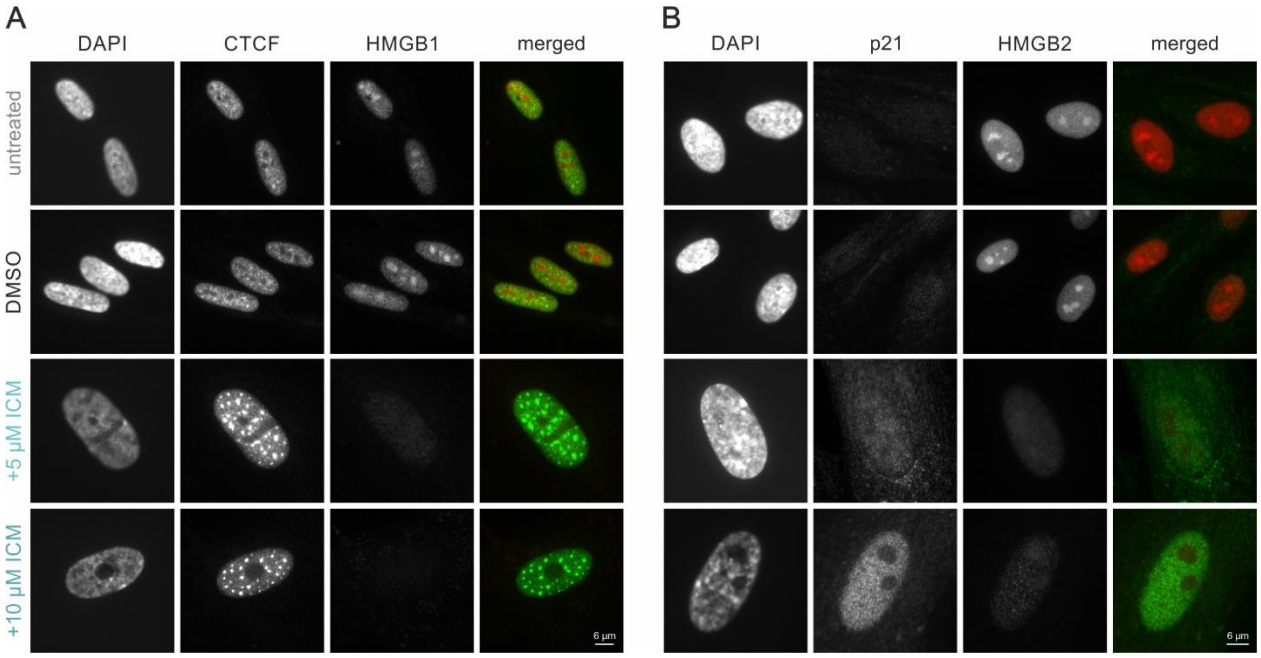

Figure 2.1.S1. ICM treatment evicts HMGB1 and HMGB2 from the nucleus.

A. Representative widefield images of proliferating, DMSO, 5uM and 10uM ICM-treated IMR90a immunostained for CTCF/HMGB1. DNA is stained with DAPI. Bar: 6um
B. Same as in A, but for p21/HMGB2

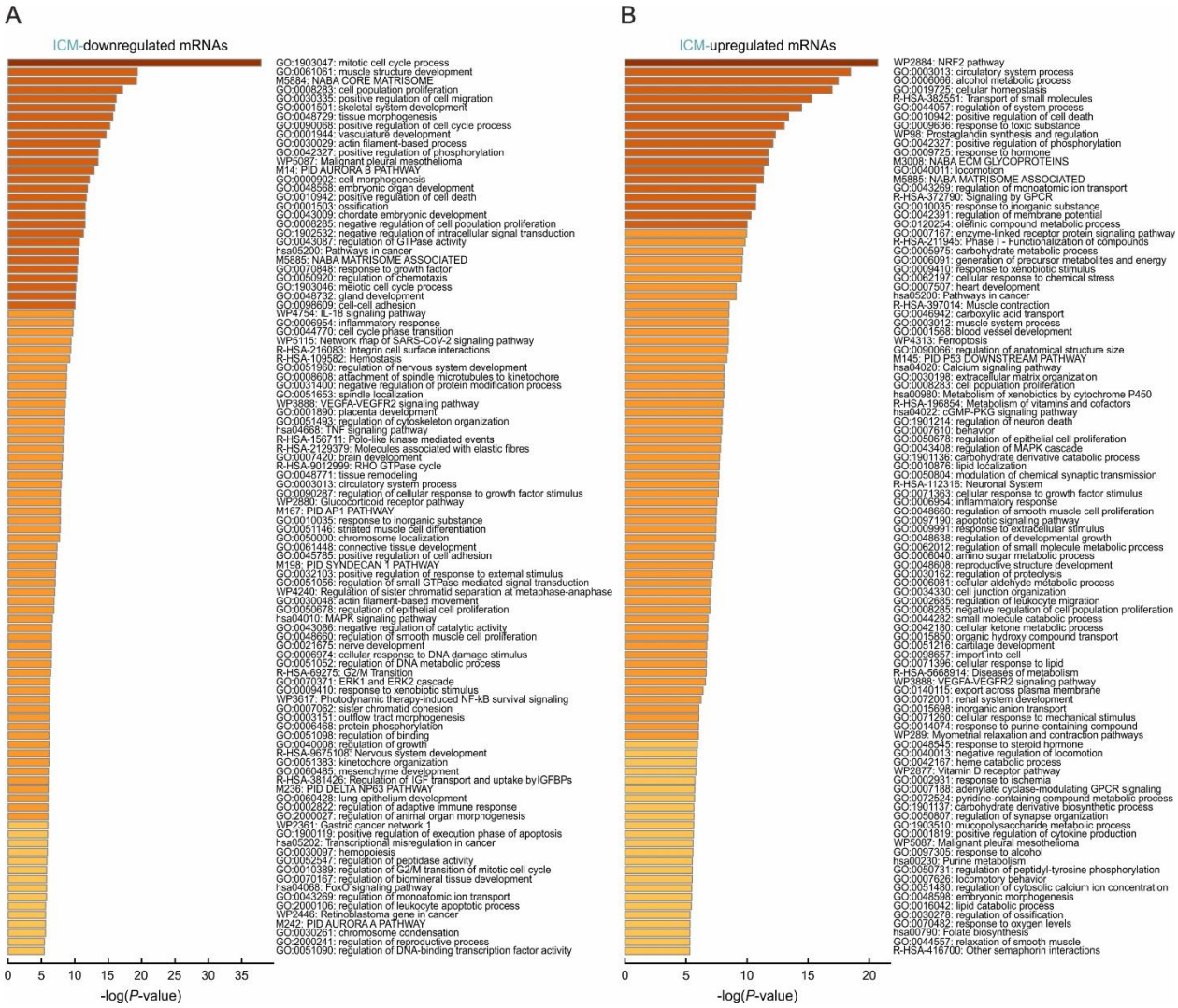

Figure 2.1.S2. ICM treatment mimics RS mRNA changes.

A. GO term/pathway analysis of downregulated genes upon ICM treatment.
B. Same as in A, but for upregulated.

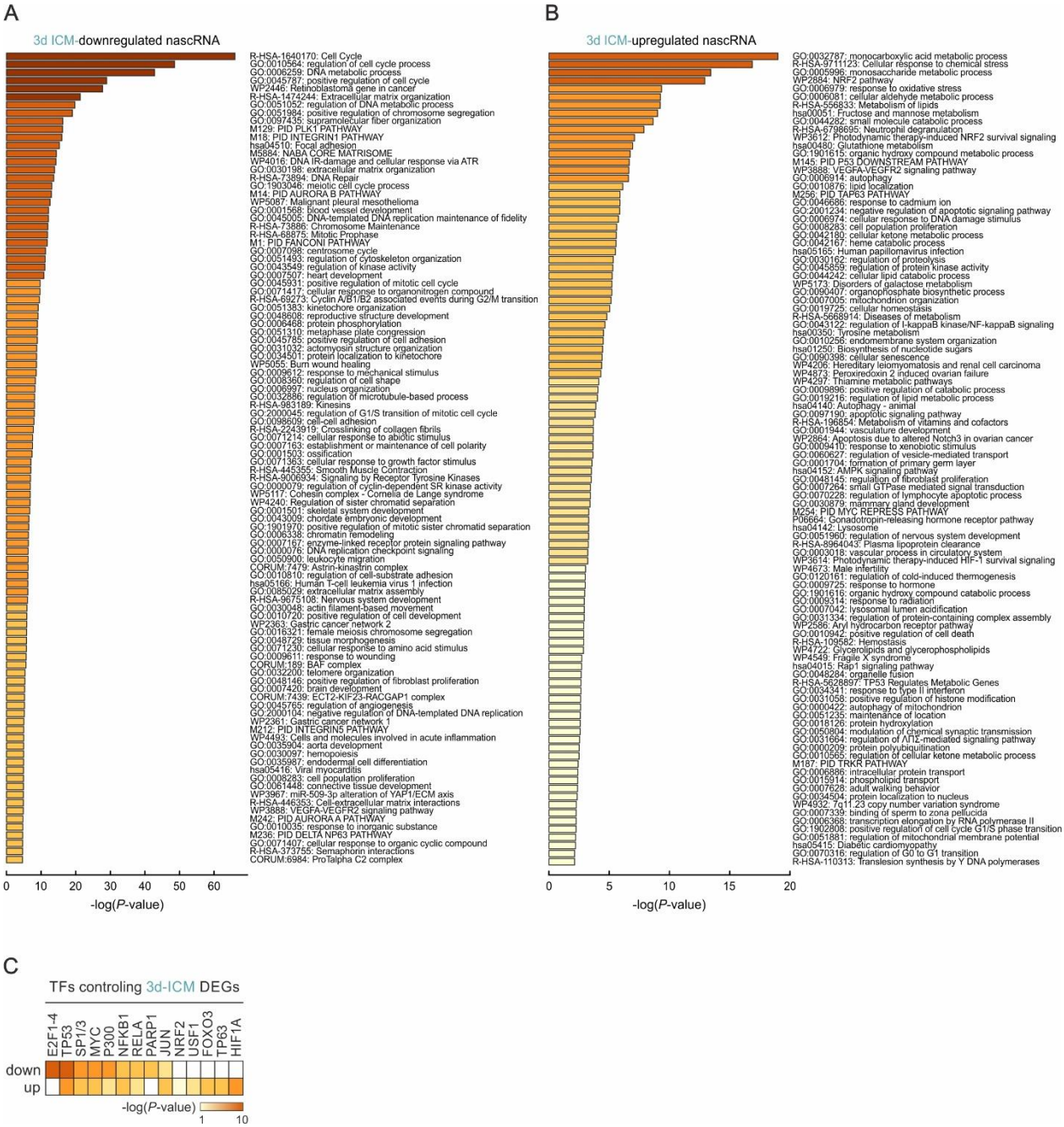

Figure 2.1.S3. 3 days of ICM treatment alters nascent RNA expression.

A. GO term/pathway analysis of downregulated genes upon ICM treatment.
B. Same as in A, but for upregulated.
C. GO term/pathway analysis of transcription factors controlling down- and/or up-regulated genes upon ICM treatment.

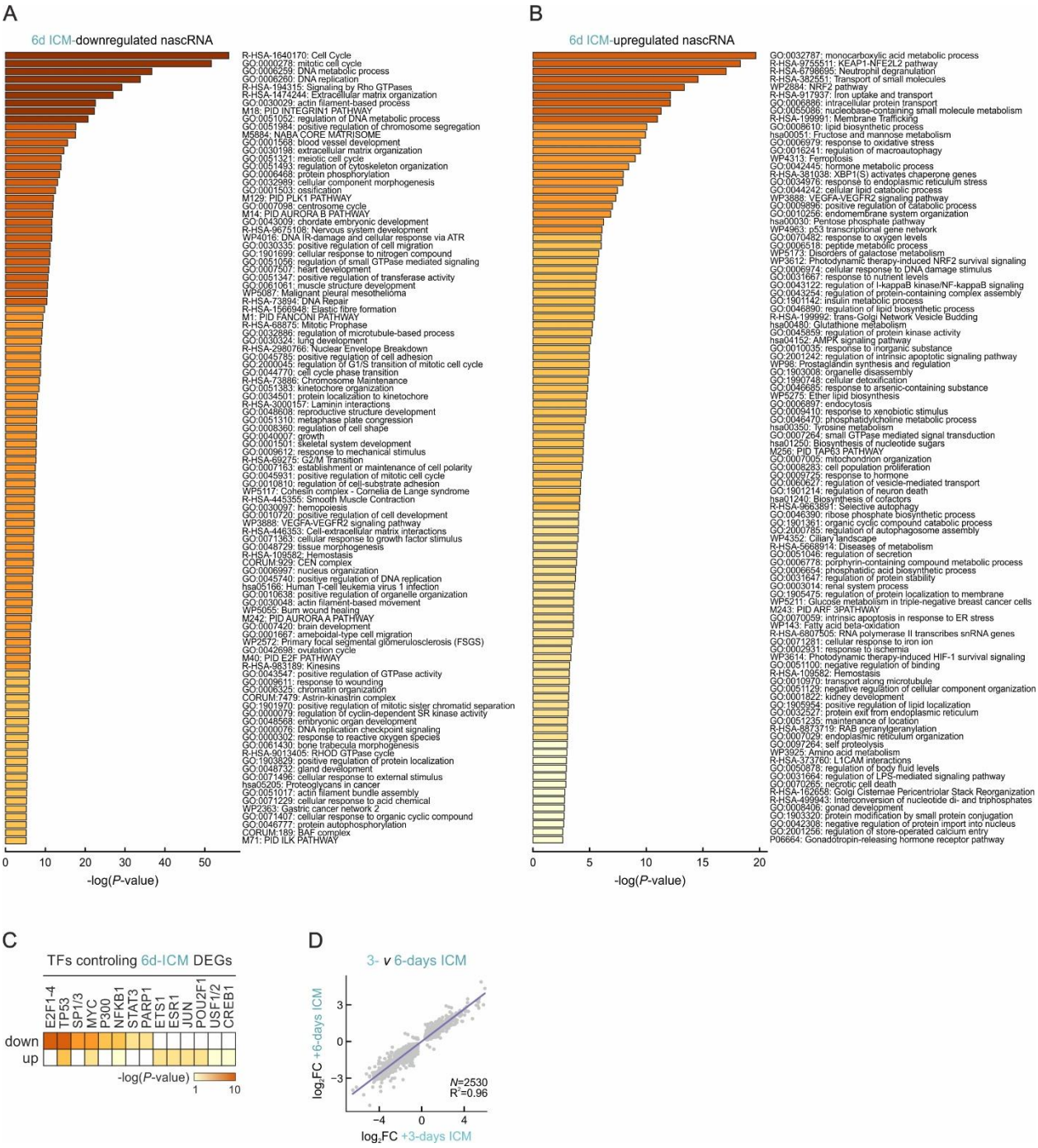

Figure 2.1.S4. 6 days of ICM treatment shares great similarities with 3 days.

A. GO term/pathway analysis of downregulated genes upon ICM treatment.

B. Same as in A, but for upregulated.

C. GO term/pathway analysis of transcription factors controlling down- and/or up-regulated genes upon ICM treatment.

D. Correlation plot showing the similarity (log_2FC) between 3 and 6 days of ICM treatment at the level of nascent RNA. N is the number of the correlated genes and R^2 the coefficient value.

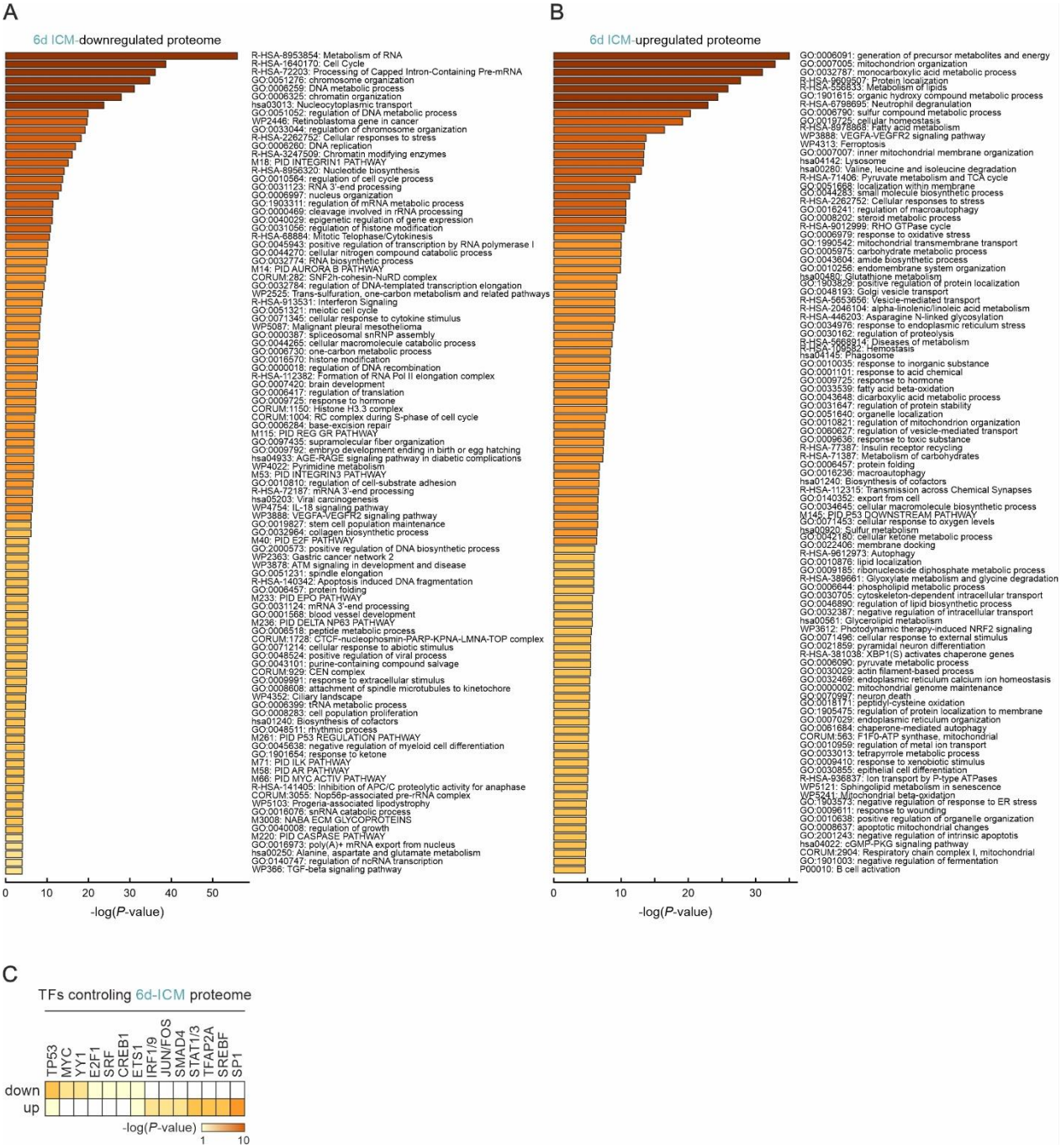

Figure 2.1.S5. Whole proteome analysis upon ICM treatment.

A. GO term/pathway analysis of downregulated genes upon ICM treatment.
B. Same as in A, but for upregulated.
C. GO term/pathway analysis of transcription factors controlling down- and/or up-regulated genes upon ICM treatment.

Chapter II – Repurposing components of the splicing and cell cycle machinery to cluster CTCF in senescence

My contribution is reflected in the following experiments as outlined below:

• Growing and conducting senescent assays and immunostainings to IMR90 cells

• All the experiments related to siRNA-mediated knockdowns and overexpression

• CUT&Tag and CUT&RUN experiments for proliferating, ICM-treated and senescent IMR90 cells

• I generated Micro-C data in collaboration with Dovetail Genomics. Micro-C data analysis was performed by A. Stavropoulou and V. Varamogianni-Mamatsi on the basis of input by me and Dr. Papantonis

The following figure panels were prepared by myself with the data input from experiments prepared and/or analyzed by me or indicated contributor:

• Figure 2.2.1B-D, H. Immunostainings and quantifications in proliferating and ICM-treated IMR90s

• Figure 2.2.1E. IDR prediction for CTCF

• Figure 2.2.1G. qPCR to assess knock-down efficiency

• Figure 2.2.S1. Immunostainings and quantifications in proliferating and ICM-treated IMR90s

• Figure 2.2.2B. Same as in Figure 2.2.1E, but for BANF1

• Figure 2.2.2C. Sample preparation and WB analysis

• Figure 2.2.2D. Same as in Figure 2.2.1G, but for BANF1

• Figure 2.2.2E. Immunostainings and quantifications in proliferating and ICM-treated IMR90s

• Figure 2.2.3B. Same as in Figure 2.2.1E, but for SRRM2

• Figure 2.2.3C,E-G. Immunostainings and quantifications in proliferating and ICM-treated IMR90s

• Figure 2.2.3D. Same as in Figure 2.2.1G, but for SRRM2

• Figure 2.2.3H Analysis and quantification of data provided by I. Liebermann

• Figure 2.2.S2. Drug treatment, immunostainings and quantifications in proliferating and ICM-treated IMR90s

• Figure 2.2.4B. Venn diagram and node for PARP-1, PARP-2, and PARP-3 [263]

• Figure 2.2.4C. Drug treatment, immunostainings and quantifications in proliferating IMR90s

• Figure 2.2.5A. CUT&Tag and CUT&RUN experiments and tracks for CTCF and SON in proliferating and ICM-treated IMR90s

• Figure 2.2.5B. Micro-C heatmaps from data provided by Dovetail Genomics and analyzed by V. Varamogianni-Mamatsi

• Figure 2.2.5E. Micro-C heatmaps from data provided by Dovetail Genomics and analyzed by V. Varamogianni-Mamatsi

Repurposing components of the splicing and cell cycle machinery to cluster CTCF in senescence

Spiros Palikyras[1], Vassiliki Varamogianni-Mamatsi[1], Isabel Liebermann[1], Konstantinos Sofiadis[2], Athanasia Stavropoulou[3,4], Argyris Papantonis[1*]

[1] Institute of Pathology, University Medical Center Göttingen, 37075 Göttingen, Germany

[2] Oncode Institute, Hubrecht Institute-KNAW and University Medical Center Utrecht, 3584 CT Utrecht, the Netherlands

[3] Institute for Bioinnovation, Biomedical Sciences Research Center "Alexander Fleming", Vari, Greece

[4] Institute for Fundamental Biomedical Research, Biomedical Sciences Research Center "Alexander Fleming", Vari, Greece.

[*]Corresponding author: AP

Abstract

Replicative cellular senescence is characterized by complex molecular events. Amongst others, senescence entry alters gene expression patterns and reorganizes chromatin. Upon loss of HMGB2 and senescence entry, CTCF dramatically re-organizes its pattern into distinct senescence-induced CTCF clusters (SICCs). Here we shed light to the nature of these clusters and we aim to characterize the properties that assist in their formation. Using ICM we induced senescence and the emergence of SICCs. Out of the targets that were found to be enriched in the ICM fraction of a CTCF CoIP/MS experiment BANF1 and SRRM2 (component of nuclear speckles) seem to have prominent role in the formation of SICCs. *si-madiated* knockdown of both led to decreased numbers of cells containing CTCF clusters. CTCF CUT&Tag-seq, SON CUT&RUN-seq and Micro-C analysis, revealed genome wide changes in terms of CTCF signal upon ICM treatment and alter interactions with the nuclear speckles machinery. Lastly, Chrom3D simulations allowed for chromatin visualization and demonstrated the spatial proximity between SICCs and nuclear speckles in the context of a senescent nucleus.

Introduction

Aging is an obscure biological process involving a myriad of steps. The most prominent hallmark of this course of events is replicative cellular senescence; an irreversible cell cycle arrest.[17] Replicative senescence (RS) is usually triggered by telomere shortening, due to recurrent cell divisions [25] and involves the activation of p53-mediated DNA damage response (DDR).[264] Alongside with growth arrest, gene expression changes,[6] heterochromatin and lamin reshuffling [44,107,109,133,135] and global chromatin reorganization [87,89,91,92] are occurring, too. Advances in high-throughput chromatin capture techniques [265] have assisted in understanding how chromatin is organized in 3D space, but also how this architecture is influenced upon distinct stimuli, senescence for instance. It is now appreciated, that in Mbp scale chromosomes are divided into active euchromatic A and inactive heterochromatic B compartments and at the sub-Mbp level into topologically associated domains (TADs). Chromatin loops within a given TAD have higher interaction frequency when compared with loops in other TADs.[146]

Senescence is a rather appealing model to study the interplay between chromatin structure and function, due to the alterations that genome undergoes upon initiation of this cascade.[86] Long-range interactions are lost and shorter-range are favored shaping more compacted chromosomes as senescence proceeds.[87,266] Central role in genome architecture is attributed to the CCCTC-binding factor (CTCF). CTCF is a highly conserved zinc-finger transcription factor and has been extensively studied for its extremely pivotal role in genome organization.[150,267–269] It is a general architectural protein as it could act as an insulator of heterochromatic spreading,[164] but also its binding motif is enriched at loop anchors participating actively in TADs formation.[146,147] Its function is not restricted only to proliferating cells, but extends to senescent as well, where its levels are slightly reduced. Decreased levels of CTCF lead to upregulation of the senescent regulator $p16^{INK4a}$, due to loss of insulation [125,180] and upregulation of the *IGF2* region, due to loss of imprinting.[270]

Recently, it has been shown that CTCF could actively participate in DDR and in the course of time, this is what fairly describes senescence on its basis. [271–273] Work from our lab revealed an additional prominent player on forging the senescent landscape; the high-mobility group B2 (HMGB2) protein.[90]

HMGB family of proteins are highly abundant nuclear factors and known chromatin binders; they unwind, bend or loop DNA thanks to their HMG-box DNA-binding domains.[124,183] Zirkel *et al.* showed that eviction of HMGB2 from the nucleus of proliferating cells suffices to induce the replicative senescent cascade and substantial chromatin alterations, due to suppression of genes related to conformation maintenance. This consequence might be driven by the fact that HMGB2 binds, on average, position at TAD boundaries and within TADs, thus its absence generates transcriptional changes. Remarkably, the loss of HMGB2 from the nucleus was shown to dramatically reorganize the pattern of CTCF into senescence-induced CTCF clusters (SICCs).

Similar to SICCs, there are plenty of other membraneless organelles inside the eukaryotic nucleus.[184] The most distinguished of all is the nucleolus which actively participates in the metabolic homeostasis of the cell, both in proliferating state and in senescence.[185,197,274] The nuclear speckles (NS), a significantly smaller in size structure (20-50nm), have recently gained some interest for their role in stress response.[230,275–277] The current understanding about NS is that they function as a repository for pre-mRNA splicing factors and they are involved in plenty cellular processes; from transcription to mRNA nuclear export.[278] Still though their role remains elusive.

Here we present evidence of an interplay between the NS and SICCs in forming the senescent genome. CTCF clusters are capable of immunoprecipitating the speckles machinery in senescence and microscopical proofs validate their spatial proximity. Disruption of the NS abolishes by large the presence of SICCs, but not *vice versa* indicative for their characteristic nature. In addition, genome-wide studies and *in-silico* models pinpoint to a senescent-genome re-conformation around nuclear speckles assisted by CTCF clusters.

Results

Chemically-induced senescence uncovers SICCs state transition

We had previously demonstrated that upon loss of HMGB2 and senescence entry, CTCF dramatically reorganizes its pattern into SICCs (**Figure 2.2.1A**) [90]. In addition, we had antecedently characterized the use of Inflachromene (ICM) as a potent and robust factor to induce a replicative-like senescent phenotype (Palikyras et al. in preparation). Its action consists, among others, of HMGB1/2 nuclear eviction, thus propagating the senescent cascade [84,90] (Palikyras et al. in preperation). Therefore, we first examined if the nuclear loss of HMGBs1/2 through ICM treatment could induce the formation of SICCs. For that purpose, human lung fibroblasts (IMR90) were treated with 10uM of ICM for 3 and 6 days; untreated cells served as controls (from now on this is the main concentration used for ICM treatment, unless otherwise stated). Following immunostaining, we were able to observe the complete loss of HMGB1/2 from the nucleus already after 3 days, but also after 6 days, of treatment and the simultaneous emergence of CTCF clusters in both cases (**Figure 2.2.1A-B**). In line with former observations [90], ICM-mediated loss of HMGB2 from the nucleus had as a result decreased levels of nascent RNA transcription, which became apparent after applying 5-EU to ICM treated cells (**Figure 2.2.1C**).

The appearance of these clusters, a reminiscent of liquid droplets, made us to hypothesize that they might be held together via phase separation. Phase separation has been proposed to organize complex biological processes through accumulation of factors and creation of membraneless organelles (MLOs) in a concentration-dependent manner [279–281]. To address this hypothesis we took advantage of 1,6-hexanediol (1,6-HD), an aliphatic compound which is widely used to disrupt such formations and it is suggested to act via interaction with the intrinsically disordered regions (IDRs) of the proteins which participate in phase separated droplets [282]. To that extend, 3 and 6 days ICM-treated IMR90s were added 6% of 1,6-HD for 1min, before fixing the cells. Interestingly, 1,6-HD was able to completely disrupt SICCs formed after 3 days of ICM treatment (*pvalue* <0.01), but not the ones formed after 6 days (**Figure 2.2.1D**), hinting to the direction that prolonged ICM treatment might lead cells to what is known as ‘deep senescence’ [283] and modulating the nature of CTCF clusters.

Additionally, using the IUPred2A tool [284,285] it was predicted that parts of the N- and C- termini of CTCF could be disordered (**Figure 2.2.1E**, IDR score >0.5), thus holding some potentials to be phase separated.

SICCs co-immunoprecipitate with a wide range of factors

Trying to elucidate the nature of SICCs, we wanted to identify any possible interaction partners that would hint towards a functional direction, as well. To do so, we used two sets of IMR90s, untreated and 6 days ICM-treated, and we performed a co-immunoprecipitation coupled with mass spectrometry assay (Co-IP/MS). After comparative analysis of these results, we ended up with a list of a dozen of proteins that were enriched in the ICM fraction and covered the given criteria (Table 1). Proteins with a wide spectrum of biological processes were identified, such as the sequestosome protein 1 (SQSTM1, or p62), ataxin-2 (ATXN2) and the fragile X mental retardation protein 1 (FMR1) (**Figure 2.2.1F**), to mention only a few. Having our candidate interaction partners, we began to examine any potential contribution of any of these in the formation and maintenance of SICCs by siRNA-mediated knock-down. In **Figure 2.2.1G**, ATAXN2, FMR1 and SQSTM1 RT-qPCR results are shown after 48h of knock-down depicting the successful silencing of the respective genes, both in control and ICM-treated IMR90s. Despite showing a very high silencing efficiency (more than 75%, **Figure 2.2.1G**) at the RNA level, when fraction of these cells was stained for CTCF and either p62, ATAXN2 or FMR1 the impact in the integrity of the clusters was minimal (**Figure 2.2.1H** and **Figure 2.2.S1**).

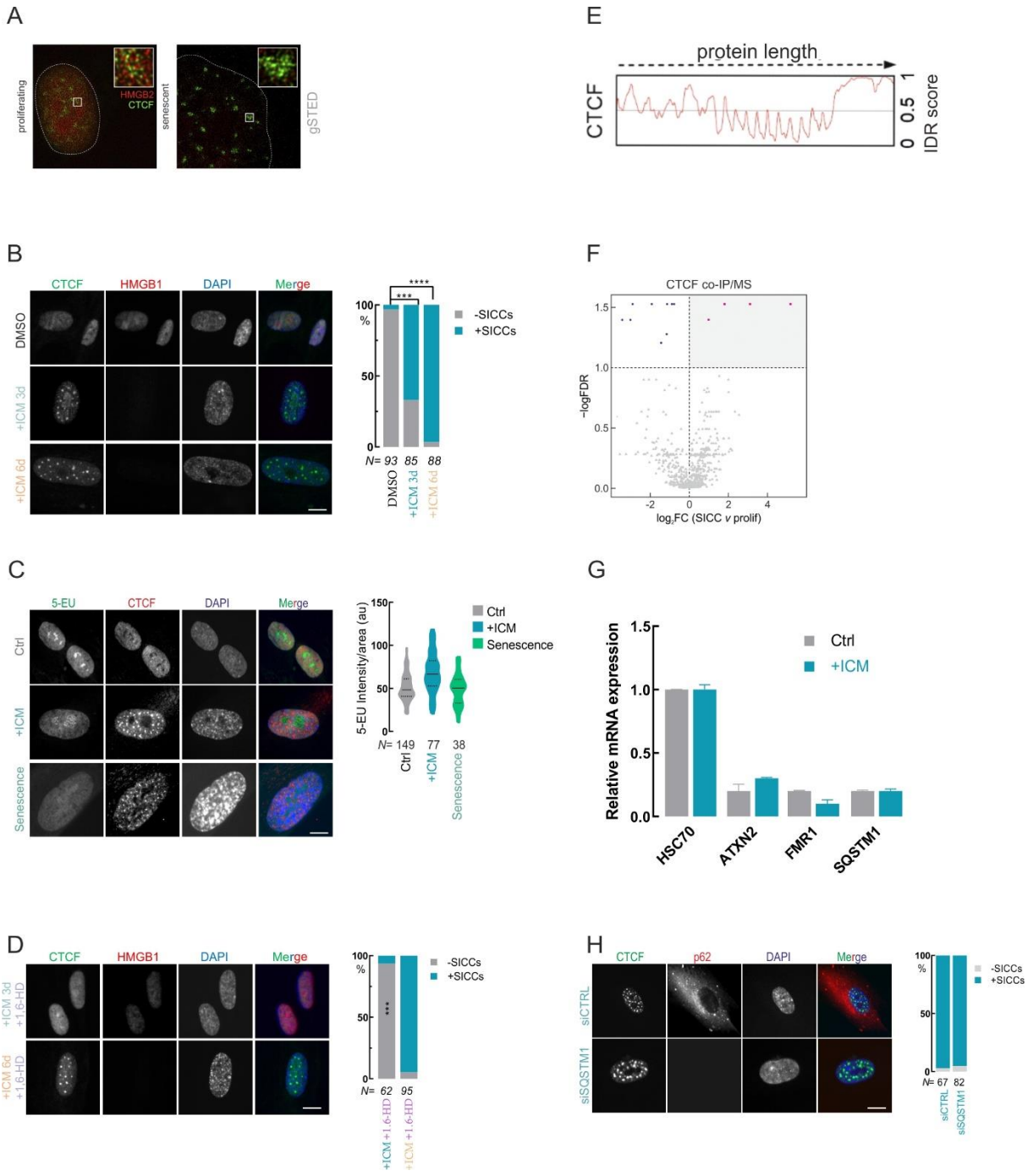

Figure 2.2.1. ICM treatment induces SICCs formation and modulates their state.

A. Super-resolution images of ICM-treated IMR90 immunostained for CTCF/HMGB2. Insets: magnified clusters.

B. Representative immunofluorescence images of IMR90 showing reduced levels of HMGB1 upon ICM treatment for 3 or 6 days and CTCF reorganizing its pattern into SICCs (second and third panel). Bar plots (on the right) quantify the number of cells bearing SICCs per condition (bottom; N is the number of cells analyzed per each condition/cell type). Bar: 5um. P<0.001; Wilcoxon–Mann–Whitney test.

C. 5-EU RNA labeling in proliferating, ICM-treated and senescent IMR90. Cells are immunostained for CTCF and DAPI staining has been used for the DNA. Violin plot on the right depicts the differences in the intensity of EU incorporation in different condition (bottom; N is the number of cells analyzed per each condition/cell type). Bar: 5um

D. Representative immunofluorescence images of 3 or 6 days ICM-treated IMR90 showing the impact of 1,6-HD treatment, respectively. Bar plots (on the right) quantify the number of cells bearing SICCs per condition (bottom; N is the number of cells analyzed per each condition/cell type). Bar: 5um. P<0.001; Wilcoxon–Mann–Whitney test.
E. IUPred2A tool returns IDR predictions for CTCF protein. Fragments of the proteins with IDR score >0.5 are predicted to bear disordered tertiary structures.
F. Volcano plot showing mass-spec data for proteins co-immunoprecipitating with CTCF and are enriched upon ICM treatment ($log_2FC>0.6$).
G. Representative real time qPCR demonstrating the efficiency of *siRNA*-mediated knockdown against *ATXN2*, *FMR1* or *SQSTM1* in proliferating and ICM-treated cells. Error bars represent standard deviation values.
H. Typical widefield images (on the left) of of ICM-treated IMR90 after scr and *SQSTM1* knockdown immunostained for p62/CTCF. Bar plots (on the right) quantify the number of cells bearing SICCs per condition (bottom; N is the number of cells analyzed per each condition/cell type). Bar: 10um.

BANF1 supports the formation of SICCs

Among the diverse factors that were augmented in the ICM fraction of CTCF Co-IP/MS was barrier-to-autointegration factor 1 (BANF1) (**Figure 2.2.2A**). BANF1 has been described to bridge anaphase chromosomes together during mitosis, thus preventing nuclear fragmentation [286]. In addition, it has been shown to actively participate in age-related diseases, as a complex of BANF1 with its two major interactors, Lamin A/C and Emerin (EMD), was reported to be disrupted in autosomal progeroid syndromes [287]. An interesting feature of this protein is that it is executing its purpose without direct interactions with chromatin, but rather by forming a dense network of factors wrapped around chromosomes, thus acting as a 'molecular glue'. Based on that, we wanted to examine if BANF1 has any propensity to carry any disordered domains. IDR prediction with IUPred2A showed us overall it is a structured protein with significantly low probability to bear any disordered regions (IDR score <0.5) (**Figure 2.2.2B**).

BANF1 can be found both in the cytoplasmic and chromatin-bound fraction in proliferating cells. Therefore, we asked if ICM treatment could possibly have any effect on its localization, but also on its relevant amount, since cells undergoing senescence present reduced levels of cell division. To answer this, we did a fractionation WB in control and ICM-treated cells (**Figure 2.2.2C**). CTCF was used as a control for the chromatin fraction and actin as a loading control. Not so unexpected, we observed reduced protein levels of BANF1 upon ICM treatment.

Interestingly, however, the remaining protein was found predominantly in the chromatin fraction indicating that BANF1 might be still needed in the senescent environment.

Next, we asked if BANF1 could assist in the formation and/or maintenance of SICCs. IMR90s were treated with ICM to induce SICCs formation and later expression of BANF1 was silenced using si*RNA* knock down. Upon successful reduction of *BANF1* RNA levels (**Figure 2.2.2D**) a fraction of these cells were stained for CTCF and BANF1. Surprisingly, consequent to BANF1 loss, SICCs were significantly disrupted (Figure 2E, IF panel), as well as the number of cells carrying CTCF clusters (**Figure 2.2.2E**, bar plot) indicating that there is a connection between the two.

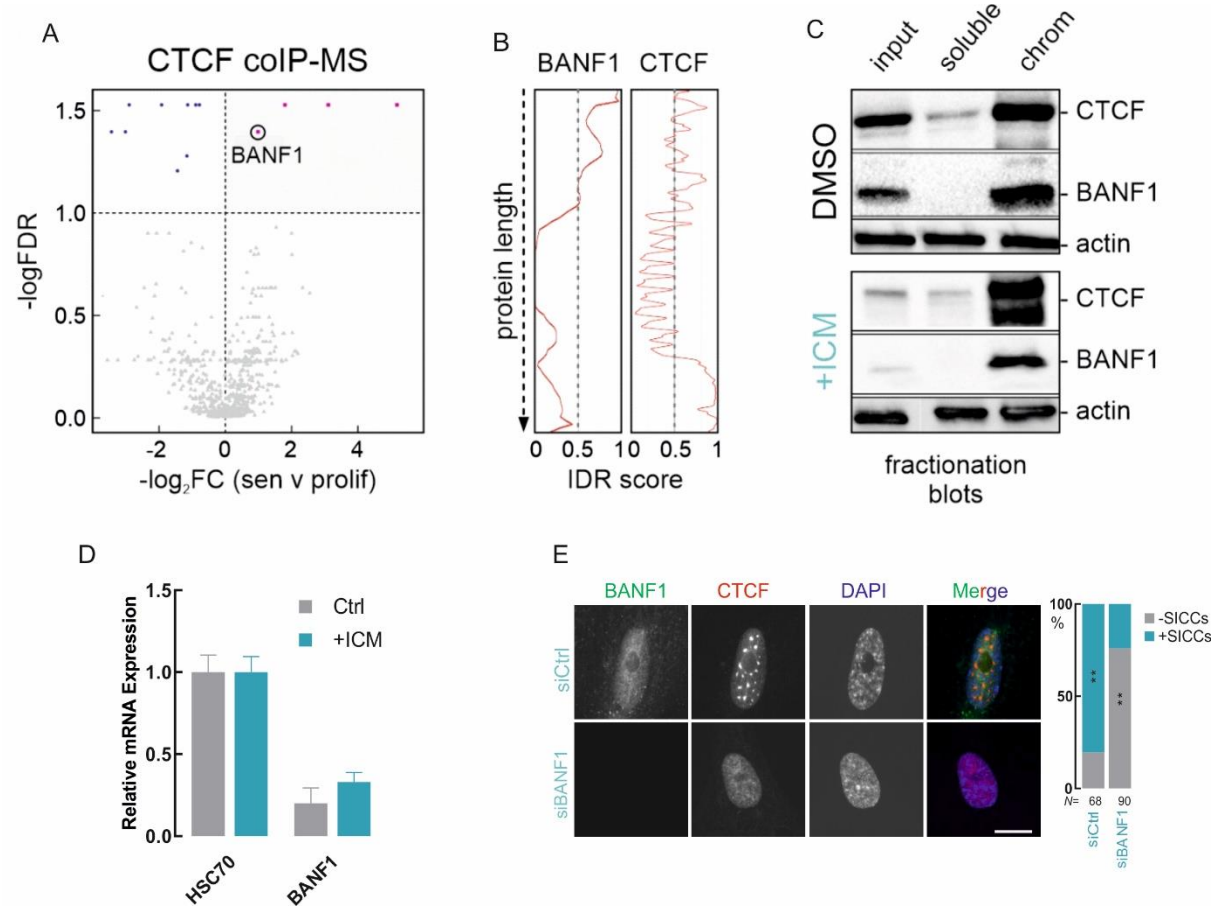

Figure 2.2.2. BANF1 support SICCs' formation.

A. Volcano plot showing BANF1 enrichment in the ICM-treated fraction of mass-spec data for proteins co-immunoprecipitating with CTCF upon ICM treatment.
B. IUPred2A tool returns IDR predictions for CTCF and BANF1 proteins. Fragments of the proteins with IDR score >0.5 are predicted to bear disordered tertiary structures.

C. Fractionation blots showing CTCF and BANF1 in proliferating versus ICM-treated IMR90; actin provides a loading control.
D. Representative real time qPCR demonstrating the efficiency of *siRNA*-mediated knockdown against *BANF1* in proliferating and ICM-treated cells. Error bars represent standard deviation values.
E. Typical widefield images (on the left) of of ICM-treated IMR90 after scr and *BANF1* knockdown immunostained for CTCF/BANF1. Bar plots quantify the number of cells bearing SICCs per condition (bottom; N is the number of cells analyzed per each condition/cell type). P<0.01; Wilcoxon–Mann–Whitney test.

SICCs co-immunoprecipitate the nuclear speckles machinery

Serin/Arginine Repetitive Matrix 2 protein (SRRM2), component of nuclear speckles (NS), was also found to be enriched in the 'senescent' fraction of the CTCF Co-IP/MS (**Figure 2.2.3A**, *pvalue* = 0.002). Nuclear speckles are MLOs in the inter-chromosomal space of the nucleus and they participate mainly in a variety of RNA-related procedures [278]. SRRM2, together with the Ser/Arg rich protein SC-35 and the splicing co-factor SON are core components of the NS [213]. IDR prediction with IUPred2A returns a high probability for SRRM2 bearing disordered domains (IDR score >0.7) (**Figure 2.2.3B**), in line with what is already known (https://www.uniprot.org/uniprotkb/Q9UQ35/entry). SRRM2 proved to be a prime candidate in our effort to understand how SICCs are formed for two main reasons; i) co-staining of CTCF and SC-35 after treating cells with ICM for 6 days revealed that the two structures are co-localized in the senescent nucleus (Figure 3C) and ii) knocking-down *SRRM2* from ICM-treated IMR90s for 6 days was sufficient to completely abolish CTCF clusters (**Figure 2.2.3D-E**, *pvalue* <0.01). In addition to this, modulating the shape of the speckles, as it was previously described [219], with either 3uM tautomycin or 10uM cantharidin, two potent serine/threonine phosphatase inhibitors [288,289], caused the reduction of cells containing CTCF clusters by 40% and 34%, respectively (**Figure 2.2.S2A-B**).

Next, we asked the question if the SICCs are, for some reason, part of the NS machinery or if they consist of two separate entities. Nuclear speckles have been characterized as phase separated entities inside the nucleus [290–292] and, as such, are prone to 1,6-HD's action [293]. To this extend, IMR90 were treated with ICM for 3 days to induce senescence and SICCs and afterwards a fraction of them were treated with 6% 1,6-HD for 1min. Untreated cells were used as control. Interestingly, upon 1,6-HD treatment we observed a significant disruption of CTCF clusters in the majority of cells (>60% decrease, *pvalue* <0.01) without any obvious alterations in the integrity of speckles (**Figure 2.2.3F**).

In addition, STED imaging of CTCF clusters and nuclear speckles reveal their close proximity, but not their overlap (**Figure 2.2.3G**).

Finally, to further investigate the link between SRRM2 and the presence or absence of CTCF clusters, we generated a doxycycline-inducible IMR90 line carrying the RNA-binding domain of SRRM2 coupled to a Venus tag (SRRM2_RBD-Venus), with the assistance of a piggybac-based vector. Overexpression was induced to cells carrying the piggybac vector using doxycycline (dox) for 6h (**Figure 2.2.3H**). Intriguingly, we noticed that overexpression of the RBD was sufficient to localize this truncate form of SRRM2 in the nuclear speckles, as the Venus signal co-localized with the SC-35 one. On top of that, in the same cells we observed that CTCF clusters started to appear, thus indicating that this domain is ample for SICCs formation.

CTCF PARylation levels might drive SICCs formation

Poly(ADP-ribosylation), or PARylation, is lately acknowledged as an important process in the overall organization of cellular architecture [294]. The post-translational modification (PTM) of covalently attaching ADP-ribose(s) to proteins using PAR polymerase (PARP) enzymes has been shown to assist in multiple biological procedures, such as DNA repair responses [295], stress granules maintenance [296] and liquid-droplets formation [297–299]. In the context of senescence, RNA-seq data from our lab and others [240] have shown an overall downregulation in the majority of PARP enzymes and ICM-induced senescence seems to follow a similar pattern as well (**Figure 2.2.4A**).

It has already been described [300] that CTCF could be found in three different PARylation states, thus migrating differently on a western blot assay: at 180kDa the highly-PARylated form and at 130kDa the hypo- and non-PARylated one. In our effort to elucidate the nature of SICCS, we observed that upon ICM treatment, CTCF changes its PARylation status and there was a gain for the hypo- and non-PARylated CTCF form (**Figure 2.2.2C**). This finding became more intriguing when we compared publicly available mass spectrometry data from HeLa cells for the three main representatives of the PARP-enzymes family; PARP1, PARP2 and PARP3 [263]. There, we saw that CTCF and SRRM2 were common targets for all three PARPs (**Figure 2.2.4B**, Venn diagram), while BANF1 for PARP1 and PARP3. Conforming to what was mentioned above, the 851 common targets for all three enzymes have prominent roles in key cellular processes like cell cycle, RNA metabolism and chromatin organization (**Figure 2.2.4B**, right node).

In addition, treatment with 2uM of the PARP1/2 inhibitor Olaparib for 24h in proliferating IMR90 was sufficient to cause the formation of CTCF clusters (**Figure 2.2.4C**). Taken together, the above observations seem to favor a hypothesis where PARylation status of CTCF might be crucial for the shaping of these entities.

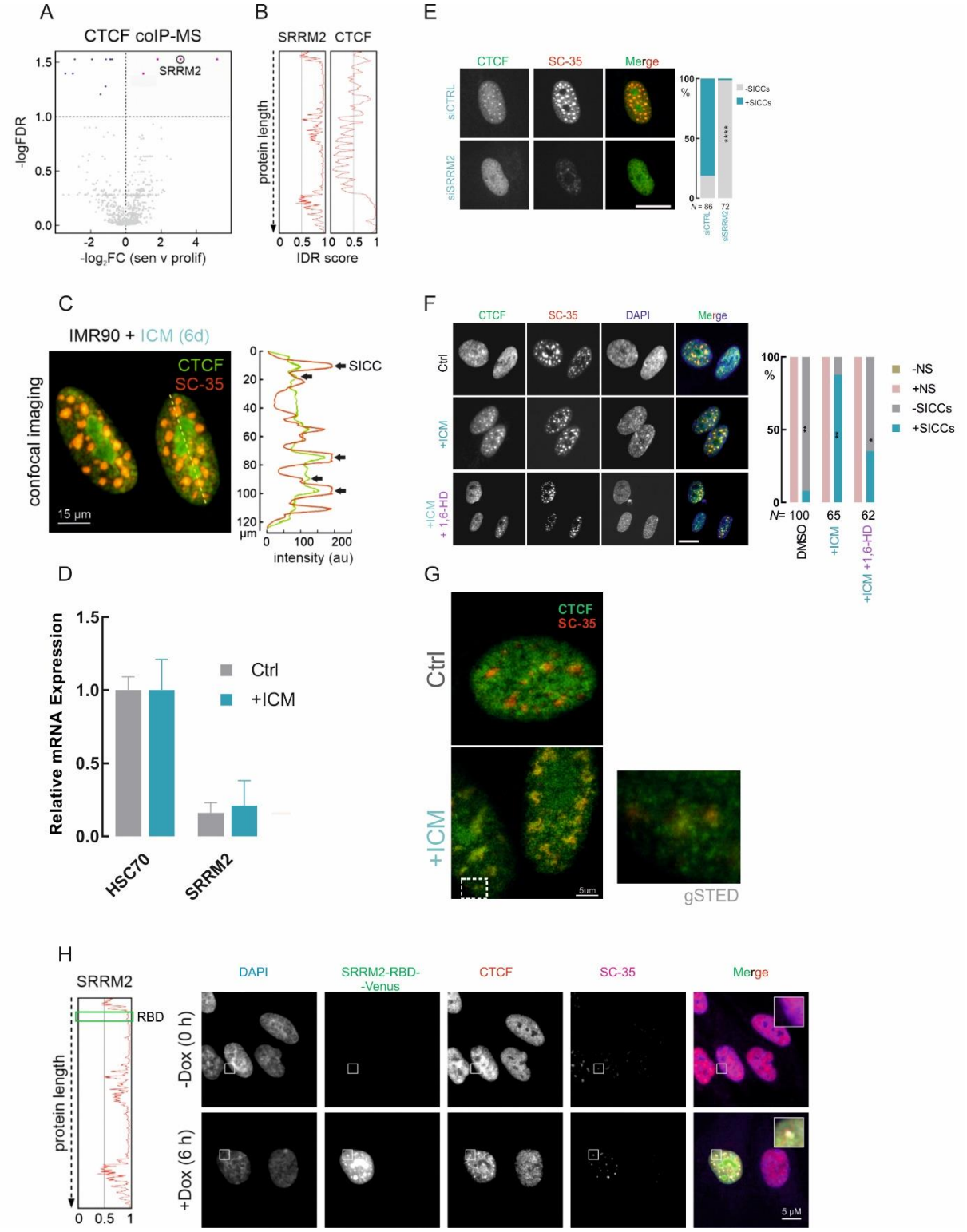

Figure 2.2.3. SICCs interaction with nuclear speckles modulates their integrity.

A. Volcano plot showing SRRM2 enrichment in the ICM-treated fraction of mass-spec data for proteins co-immunoprecipitating with CTCF upon ICM treatment.
B. IUPred2A tool returns IDR predictions for CTCF and SRRM2 proteins. Fragments of the proteins with IDR score >0.5 are predicted to bear disordered tertiary structures.
C. Typical image of ICM-treated IMR90 immunostained for CTCF/SC-35. Fluorescence levels were used to produce lineplot depicted the overlap between the two proteins. Bar: 15um
D. Representative real time qPCR demonstrating the efficiency of *siRNA*-mediated knockdown against *SRRM2* in proliferating and ICM-treated cells. Error bars represent standard deviation values.
E. Typical widefield images (on the left) of of ICM-treated IMR90 after scr and *SRRM2* knockdown immunostained for CTCF/SC-35. Bar plots (on the right) quantify the number of cells bearing SICCs per condition (bottom; N is the number of cells analyzed per each condition/cell type). P<0.01; Wilcoxon–Mann–Whitney test.
F. Representative immunofluorescence images of control, ICM-treated and ICM-treated plus 1,6-HD IMR90 immunostained for CTCF/SC-35 (on the left). Bar plots quantify the number of cells bearing SICCs and/or nuclear speckles per condition (bottom; N is the number of cells analyzed per each condition/cell type). P<0.01; Wilcoxon–Mann–Whitney test.
G. Super-resolution images of ICM-treated IMR90 immunostained for CTCF/SC-35. Insets: magnified clusters.
H. Right: linear representation of SRRM2 domains. Left: typical images of Dox-induced IMR90s expressing either an empty vector or Venus-SRRM2-RBD and immunostained for CTCF/SC-35. Insets: magnified clusters. Bar: 5um

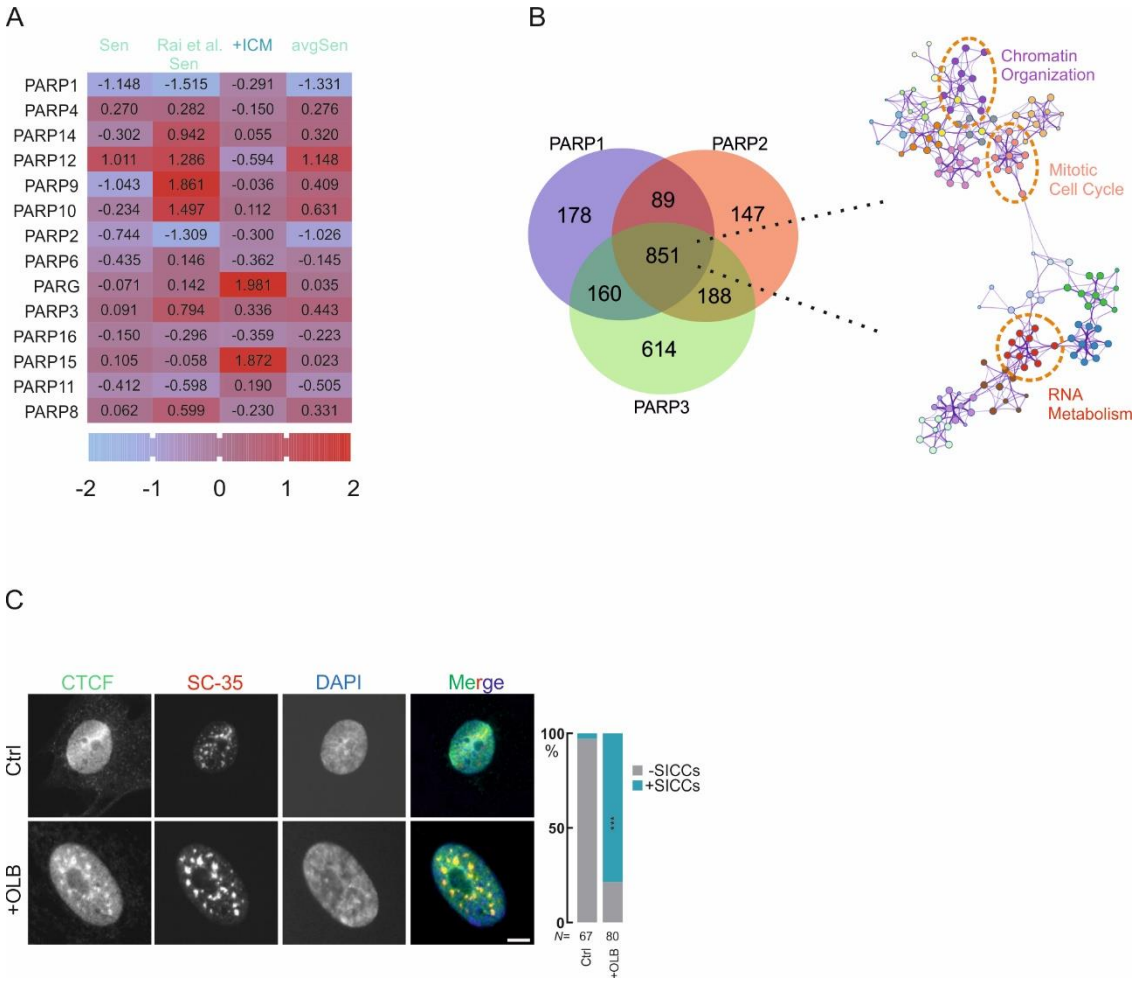

Figure 2.2.4. Inhibition of PARP1/2 leads to the formation of CTCF clusters.

A. Heat-map showing differences in the expression levels of PARP enzymes in senescence and upon ICM-treatment. As a comparison, publicly available senescent RNA-seq data have been used [240]. The last column depict the average differences between our and publicly available data.
B. Venn diagram showing the overlap of mass spectrometry results from experiments using the NAD+ analog-sensitive approach for PARP-1, PARP-2, and PARP-3 [263]. Highlighted in the interaction node on the right are the most prominent GO term/pathways.
C. Typical widefield images (on the left) of proliferating IMR90 with or without 2uM olabarib treatment for 24h, immunostained for CTCF/SC-35. Bar plots (on the right) quantify the number of cells bearing SICCs per condition (bottom; N is the number of cells analyzed per each condition/cell type). P<0.01; Wilcoxon–Mann–Whitney test.

ICM treatment alters CTCF signal and NS chromatin association

Having, so far, microscopic evidences of an interplay between SICCs and NS, we asked if we could reflect these into changes in the chromatin landscape. Using CUT&Tag-seq [301] we identified 5321 peaks for CTCF in proliferating IMR90s and 6681 peaks in ICM-treated. Out of these, 1569 peaks were unique for the ICM, but overall we observed an increase in CTCF signal even among shared peaks, pointing to a possible accumulation of CTCF in the corresponding loci (**Figure 2.2.5A**, CTCF tracks). To identify chromatin regions interacting with nuclear speckles we used SON CUT&RUN-seq [302] and we were able to call 1785 SON domains in proliferating cells and 1463 domains in ICM-treated. Interestingly, 922 chromatin loci were found to be in close proximity with NS upon ICM treatment, whereas in proliferating IMR90 these interactions were completely absent, hinting towards a switch in chromatin association with NS upon ICM treatment (**Figure 2.2.5A**, SON tracks).

Next, and in order to get a genome-wide view of possible changes upon ICM treatment that could 'recapitulate' CTCF clustering, we took advantage of Micro-C [145] (see methods for details). Comparing the heat-maps between proliferating and ICM-treated IMR90s two features were immediately emerging: first, on average, there was a preference for stronger longer-range interactions upon ICM treatment, and, second, there was stronger insulation between higher-order domains in ICM induced senescence, in agreement with what we had observed in replicative senescence (**Figure 2.2.5B**) [90] (Palikyras et al. in preparation). Additionally, interaction decay plots uncovered extensive alterations in both longer- and shorter-interactions upon ICM treatment (Palikyras et al. in preparation). In contrast, when looking into A/B compartments, we observed no differences between conditions (**Figure 2.2.S3**). Taken together, the Micro-C allowed us to identify genome-wide changes upon ICM treatment with a tendency in sub-Mbps scale.

Chrom3D folds the genome around SICCs and NS in an unbiased manner

In an effort to visualize the aforementioned changes in relationship with the emergence of SICCs upon ICM treatment, we exploited the abilities of Chrom3D tool [303]. Using this tool we were able to simulate the spatial position of chromosomes relative to each other and to nuclear periphery taking as input TAD-TAD interaction data from our Micro-C matrices (see methods for details). Next, we supplemented the model with information about the relative position of CTCF and SON in proliferating and ICM-induced IMR90, from the respective CUT&Tag and CUT&RUN experiments. The output of this simulation could be seen in **Figure 2.2.5C**, where it could be appreciated that the nucleus could be divided into three interaction categories: i) genomic regions (in grey) where CTCF and SON do not interact, ii) genomic regions (non-TADs, in red) with CTCF and SON interactions and iii) TADs (in pink) with CTCF and SON interactions. When the distances of red and pink beads were calculated, it was shown that in ICM-treated IMR90s they tended to be in closer spatial proximity than in proliferating cells (**Figure 2.2.5D**, left side, *pvalue*<0.01). Trying to eliminate any possible bias from our model we went on and 'swapped' the data as follow: we took the information from ICM-treated cells of CTCF CUT&Tag and SON CUT&RUN experiments and applied these coordinates to a 'proliferating' nucleus (proliferate Micro-C matrix) and *vice versa*. The results showed that the distribution of the CTCF/SON beads was random in these 'swapped' conditions, thus reinforcing our trust to Chrom3D's output (**Figure 2.2.5D**, right side, *pvalue*<0.01).

Lastly, we asked whether genomic regions with specific characteristics might be the ones which come in close proximity and assist in the formation of SICCs. To that end, we simulated all individual chromosomes in the two different conditions (proliferating and ICM-treated) and we superimposed them with the corresponding Micro-C matrix (in **Figure 2.2.5E** chr10 is shown as an example). Surprisingly, we observed that the interaction between CTCF and SON and the following formation of SICCs is largely random and it did not seem to follow a certain pattern, where for example junks of chromatin from neighbouring TADs would preferentially be engaged in giving rise to such structures. However, SICCs showed a preference for regions that are predominantly in A compartments and there was a slight preference for promoter-bound CTCF to be represented there, at the expense of loop-anchored CTCF (**Figure 2.2.S3**).

Figure 2.2.5. Chrom3D simulation visualizes SICCs and NS interactions.

A. CTCF CUT&Tag-seq and SON CUT&RUN-seq from proliferating and ICM-treated IMR90 along a chr10 locus. Proliferating tracks are depicted in grey and ICM tracks in dark green.
B. 10kbp resolution Micro-C maps along a chr6 and chr13 locus from proliferating (upper triangles) and ICM-treated (lower triangles) IMR90. Black arrows are pointing o differences between the two conditions
C. Chrom3D representation of the whole genome in proliferating and ICM-treated cells (top bubbles), as well as an overview of SON/CTCF interaction regions (enlarged bubbles). Each sphere represents one TAD. TADs with SON/CTCF interactions are depicted in salmon pink, other genomic regions with SON/CTCF interactions in red and in grey genomic regions without SON/CTCF interactions are shown. Bar plot on the right depicts the percentage of each of the three different distributions.
D. Middle-left part: Chrom3D representation of the relative distribution between SON and CTCF along chr10 in proliferating (up) and ICM-treated (bottom) IMR90. Violin plot on the left depicts the distances calculated between SON/CTCF beads. $P<0.01$; Wilcoxon–Mann–Whitney test. Middle-right part: Chrom3D representation of the relative distribution between SON and CTCF along chr10 in swapped conditions (ICM CTCF peaks in proliferating cells; up and Control CTCF peaks in ICM-treated cells; bottom). Swapped genomic regions are depicted in purple. Violin plots on the left depict the distances calculated between different SON/CTCF beads. $P<0.01$; Wilcoxon–Mann–Whitney test.
E. Left part: 10kbp resolution Micro-C maps along chr10 in proliferating versus ICM-treated IMR90. The small black triangles represent chromatin loci that are coming together on ICM to form a 'cluster'. Middle part: Chrom3D simulation of chr10 depicts these exact loci. Right part: Violin plot represents the distances calculated between different SON/CTCF beads. $P<0.01$; Wilcoxon–Mann–Whitney test.

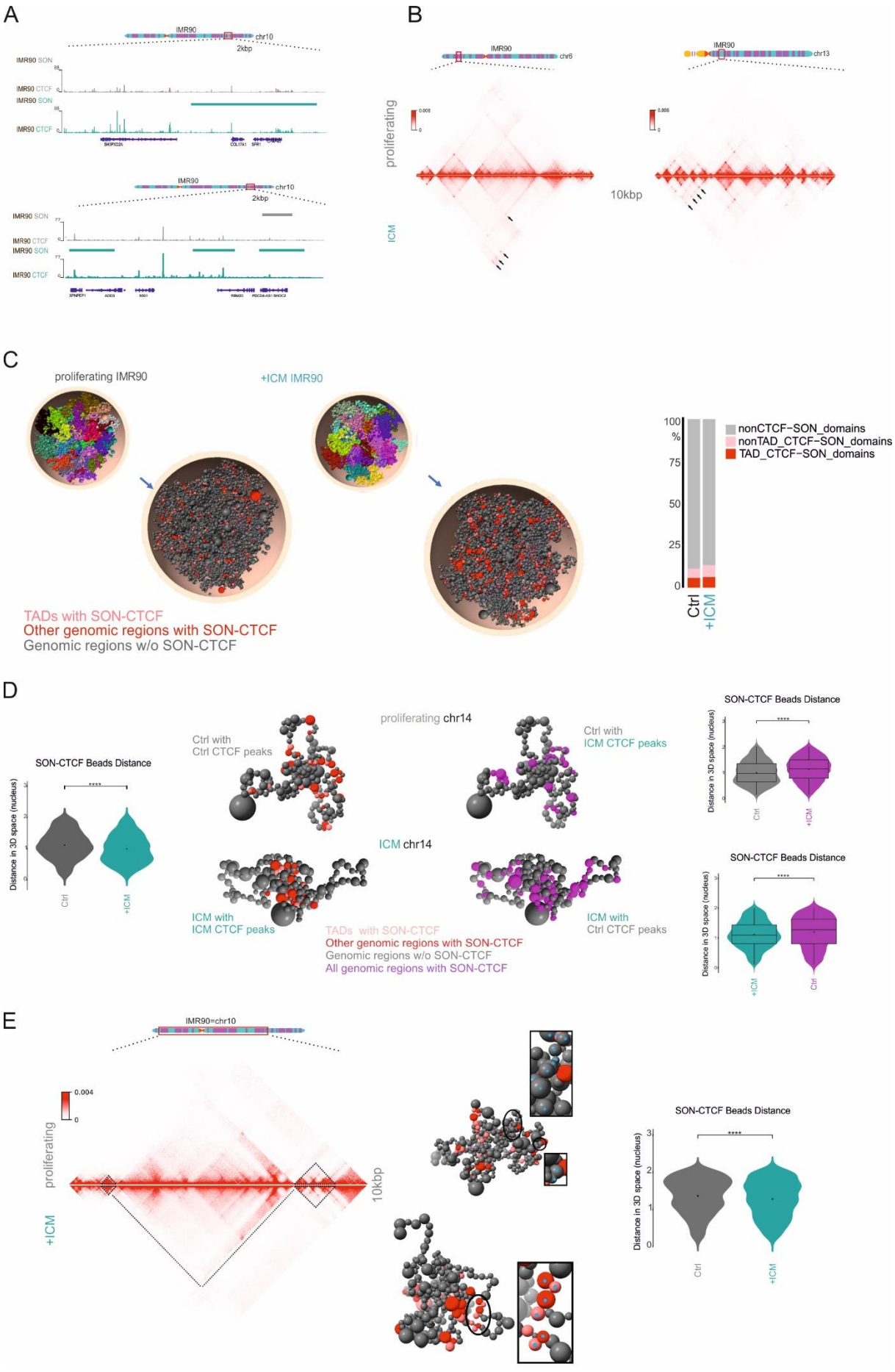
A
IMR90
chr10
2kbp
IMR90 SON
IMR90 CTCF
B
IMR90
chr6
chr13
proliferating
ICM
10kbp
C
proliferating IMR90
+ICM IMR90
TADs with SON-CTCF
Other genomic regions with SON-CTCF
Genomic regions w/o SON-CTCF
nonCTCF−SON_domains
nonTAD_CTCF−SON_domains
TAD_CTCF−SON_domains
Ctrl
+ICM
D
SON-CTCF Beads Distance
Distance in 3D space (nucleus)
Ctrl with
Ctrl CTCF peaks
proliferating chr14
Ctrl with
ICM CTCF peaks
ICM chr14
ICM with
ICM CTCF peaks
ICM with
Ctrl CTCF peaks
TADs with SON-CTCF
Other genomic regions with SON-CTCF
Genomic regions w/o SON-CTCF
All genomic regions with SON-CTCF
E
IMR90=chr10
0.004
proliferating
+ICM
10kbp

Discussion

There are many cellular hallmarks in existence to characterize the senescent state of a cell [17]. Many of them are describing the extended changes occurring at the level of higher-order chromatin and how this polymer is altering its architecture to adapt to the new environment [86,88,89]. Work from our lab had successfully managed to characterize HMGB2 as a key regulator for senescence entry and the subsequent chromatin re-organization [90]. Among other observations we had noticed the dramatic re-localization of CTCF into very distinct clusters, the SICCs.

In our effort to characterize and elucidate the role of these membraneless clusters we have uncovered their tight relationship with another entity, this of nuclear speckles (NS). We demonstrated that disruption of NS assists in the abolishment of SICCs to varying degrees. It is worth to mention that this is not the first time that CTCF was shown to interact with NS. A recent study showed that upon stress, unbound CTCF protein forms complexes that are localized in NS, without obvious changes at the chromatin-bound fraction [275]. However, in our case we have evidences to believe that SICCs are bound to chromatin and in close proximity with NS. By applying a harsher treatment prior to immunostaining, that leaves intact only the strongly chromatin-bound proteins and significantly reduces the noise, we were able to still detect perfectly formed SICCs (data not shown). At the same time STED imaging and 1,6-HD treatment pointing towards the stand-alone nature of these two entities. However, the reason why these two structures are in such close proximity is still puzzling. It has been demonstrated that genomic loci proximal to NS have a transcriptional advantage, under certain stress conditions, as they are capable of enhanced gene expression [228,304,305]. Moreover, it was described that p53 drives NS association of a group of its targets, thus boosting their RNA expression [230]. Hence, it is tempting to hypothesize that something similar might occur in our system, as well. In an environment where the majority of metabolic processes are lowered, the decreased level of transcripts produced should have access to the splicing and nuclear exportation machinery with the least consumption of energy. Therefore, if there is active transcription taking place inside or in the periphery of SICCs (which remains to be investigated) it might be beneficial to neighbour with the main nuclear provider of such factors.

Another open question that stems from our observations is whether RNAs are actively participating in the formation and maintenance of SICCs. Following the notion that SICCs might be held together via phase separation-like forces, it is not unreasonable to assume this. In fact, it was recently shown that the DNA-binding domain (DBD) of CTCF has the ability to phase separate [306], and it was proposed that via these interactions CTCF could, at least in part, fulfil its insulation properties as it would offer endogenous CTCF the possibility to form clusters at chromatin loci with low abundance of transcription activators. In our case, SICCs where found to be sensitive to 1,6-HD treatment early after their emergence, a feature that was progressively lost following continuous ICM treatment. This indicates a potential transition of SICCs from a more liquid to a more solid state. Additionally, overexpression of the RNA-binding domain of SRRM2 proved sufficient in promoting CTCF clustering, while preliminary CTCF eCLIP data revealed significant enrichment in RNA being pulled down upon ICM treatment compared to the control state. All the above serve as substantial evidence in support of the concept of phase separation acting in the formation and maintenance of SICCs. And as phase separation may be pharmacologically targeted, once could envisage interventions that prevent or slow down SICC formation, and perhaps even senescence entry, in the near future.

Methods

Cell Culture

Primary lung fibroblasts (IMR90) isolates (I79 and I83, passage 5; Coriell Biorepository) were continuously passaged in MEM (M4655, Sigma-Aldrich) supplemented with 1x non-essential amino acids and 10% FBS under 5% CO2. Senescence was induced after treating the cells for 3 or 6 days with 10µM Inflachromene (Cayman Chemicals). Wherever is indicated 6% 1,6-hexanediol was used for 1min.

Co-immunoprecipitation coupled to mass spectrometry

Approximately 6 × 10^6 proliferating and an equal number of ICM-treated IMR90s were gently scraped and pelleted for 5min at 700 *g* and then resuspended in 500µl of ice-cold lysis buffer (20mM Tris–HCl pH 8.0, 1% NP-40, 150mM NaCl, 2mM EDTA pH 8.0) supplemented with 1× protease inhibitor cocktail (Roche). This mixture was then incubated for 30min on ice, followed by three cycles of sonication (30sec on, 30sec off, low input) and RNase A treatment, before centrifugation for 15min at > 20,000*g* to pellet cell debris and collect the supernatant. While lysates were precleared, 30µl protein-G magnetic beads (Active Motif) and 10µg of CTCF antibody (Active motif, 61311) were incubated for 2h at 4°C under rotation. Subsequently, the beads were captured on a magnetic rack (Active Motif) and added to the lysates for incubation at 4°C overnight under rotation. The following day, the beads were captured, washed four times with 900µl ice-cold wash buffer I (50mM Tris, 0,05% NP-40, and 50mM NaCl), two times with 500µl of wash buffer II (150mM NaCl, 50Mm Tris), recaptured, supernatant discarded, and purified proteins were predigested in 50µl elution buffer (2M urea, 50mM Tris pH 7.5, 1mM DTT, 50ng trypsin) for 30min at room temperature with gentle agitation. Following addition of 50µl digestion buffer (2M Urea dissolved in 50mM Tris pH 7.5 and 5mM chloroacetamide) and incubation for 30min, another 50µl of elution buffer supplemented with 50ng of LysC and 100ng of trypsin were added to each tube. Proteins were digested overnight at room temperature, the digestion was stopped by adding 1µl trifluoroacetic acid, and peptides of each experiment were split in half, purified on two C18 stage tips, and all three replicates were analyzed by the CECAD proteomic core facility as above (Table 1)

Immunofluorescence & image quantification

IMR90 cells grown on coverslips were fixed in 4% PFA/PBS for 10min at room temperature. After washing once in PBS, cells were permeabilized with 0.5% Triton-X/PBS for 5min at room temperature, blocked using 1% BSA for 1h, and incubated with the appropriate primary antibody for 1h at room temperature (anti-CTCF: 1:500, 61331, Active Motif; anti-SRRM2: 1:500, PA5=59559, Thermo Fischer; anti-SC35: 1:500, NB100-1774, Novus; anti-HMGB1: 1:500, ab190377-1F3, Abcam,). The primary antibody was washed with PBS twice for 5min per wash. Cells were incubated with the secondary antibody (diluted in 0.5% BSA/PBS) at RT, in the dark for 1h at the indicated dilution: anti-rabbit Alexa488 (1:1,000, Abcam ab150077); anti-mouse Cy3 (1:1,000, Abcam ab97035). Cells were then washed with PBS twice for 5min per wash. ProLongTM Gold antifade reagent with DAPI (#P36931) was added to the cells.For visualizing nascent transcripts, cells were pre-incubated with 2.5mM 5-ethynyl uridine (EU) for 40min at 37°C in their growth medium, fixed and processed with the Click-iT EdU chemistry kit (Thermo Fiscer). Images were acquired on a Leica DMI8 microscope with an HCX PL APO 63x/1.40 (Oil) objective using the LASX software. Super-resolution images were acquired on an Abberior STEDYCON microscope with a 100x Plan SuperApochromat 1.4 Oil objective. Quantification of nuclear fluorescence were performed by drawing a mask based on DAPI staining, and then calculating the mean intensity per area falling under this mask. Co-localization was assessed using the FIJI plugin, RGB Profiler (https://imagej.nih.gov/ij/plugins/rgb-profiler.html).

RNA isolation & RT-qPCR analysis

RNA isolation was performed by removing and washing out the growth medium IMR90s, using 1x PBS, then harvesting the cells in Trizol (TRIzol™ Reagent, Invitrogen™, 15596018). Later, the RNA was isolated and DNAseI-treated using the Direct-zol™ RNA MiniPrep Kit (ZYMO RESEARCH™, R2052: 1074069). cDNA was synthesized using the SuperScript™ First-Strand Synthesis System for RT-PCR (Invitrogen™, 11904018), according to manufacturer instructions. For the qPCR, the qPCRBIO SyGreen Mix (PCR Biosystems, PB20.14-51) was used. The reactions were mixed in the 384 Well Skirted PCR Plate (FrameStar, 4ti-0385), and the measurement was performed with the qTOWER3 84 G real time PCR thermocycler (Analytik Jena GmbH). 2ng of cDNA were used in total for each reaction (full list of qPCR primers used on Table 2).

siRNA-mediated knockdown

IMR90s were seeded at ~35,000 cells/cm2 the day of transfection. Lipofectamine RNAiMAX (Lipofectamine™ RNAiMAX Transfection Reagent, Invitrogen™, 13778075) was used for delivering the siRNAs (Table 3) to the cells and the mixture was prepared as instructed by the manufacturer. Knockdown efficiency was assessed 48h after transfection using RT-qPCR and immunostaining.

SICC overexpression experiments

Doxicycline-inducible overexpression IMR90 cells were generated using PiggyBac transposition. The SRRM2 RNA binding-domain was amplified and cloned from cDNA. Following validation by Sanger sequencing, it was subcloned into the DOX-inducible KA0717 expression vector to generate an SRRM2/RBD-Venus fusion. The construct was co-transfected into IMR90 together with transactivator and transposase-encoding vectors (KA0637 and SBI Biosciences #PB200PA-1, respectively) at a DNA mass ratio of 10:1:3 using the Lipofectamine® LTX DNA Transfection Reagents (InvitrogenTM, #56532) as per manufacturer's instructions. Stable, transgene-positive, proliferating IMR90 were selected using 350 µg/ml G418 (Sigma Aldrich). SRRM2/RBD-Venus expression was induced using doxycycline for 24h, and IMR90 carrying the empty Venus vector served as a control (for more details see Rao et al., 2016).

Chromatin-immunoprecipitation and western blot

Protocol adapted from [307]. In brief, cells were scraped, washed once with 1X ice/cold PBS and then lysed with ice/cold lysis buffer (20mM Tris-Hcl ph=8, 1% NP-40, 150mM NaCl, 1X PIC, water) for 20min on ice. Then, samples were sonicated (3 cycles, 30sec on, 30sec off), spun down at full speed for 15min and the supernatant was transferred to new tubes. 20µl were kept as input control. 30µl of protein G magnetic beads (IP ChIP-IT® Protein G Magnetic Beads, Active Motif) were used per sample, after washing them 2X with ice/cold lysis buffer and resuspended in 250µl of lysis buffer. Samples were placed in a rotor and pre-cleaned with 50µl of the beads for 2h, at 4^{o}C. Whenever is indicated Rnase, Benzonase and/or DNaseI (100µg/ml) treatment was performed at this step. In the rest of the beads 5µg of the respective antibody was added and incubated using the same conditions as above.

The pre-cleaned lysates were then transferred to the antibody-bound beads and they were left to rotate overnight at 4°C. The next day, samples were washed once with lysis buffer, 3X with wash buffer I (50mM Tris-Hcl ph=7.5, 0.05% NP-40, 150mM NaCl, water) and once with wash buffer II (50mM Tris-Hcl, 150mM NaCl, water). After the last wash, beads were resuspended in 20µl 1X Laemmli buffer and boiled at 95°C for 10min to elute the proteins. The eluted samples were then used for western blot analysis.

Cleavage under targets and release using nuclease (CUT&RUN)

150,000 cells were lifted from plates using trypsin and were then processed according to manufacturer's instructions (Cell Signaling). Samples were paired-end sequenced to obtain more than 10^7 reads. Read pairs were aligned to the human reference genome GRCh38 using *Bowtie2* (v2.3.4.1), PCR duplicates were removed using the *MarkDuplicates* function in Picard tools (v2.20.7), and read coverage tracks (BigWig) were generated and normalized with the RPCG parameter using the *bamCoverage* function of deepTools2, v3.5.1 [261]. For SON, domains were called using epic with 16kb window sizes and differential peaks were called using epic2-df [308].

Micro-C and data analysis

Micro-C was performed using the Micro-C v1.0 kit in collaboration with Dovetail Genomics as per manufacturer's instructions. Micro-C libraries (at least 3 per each biological replicate) that passed QC criteria were pooled and paired-end sequenced on a NovaSeq6000 platform (Illumina) to >600 million read pairs per replicate. Micro-C contact matrices were produced using Dovetail Genomics pipeline (https://micro-c.readthedocs.io/en/latest/fastq_to_bam.html). In brief, read pairs were mapped to human reference genome hg38 using BWA, after which low mapping quality (<40) reads and PCR duplicates were filtered out using the *MarkDuplicates* function in Picard tools (v2.20.7), and read coverage tracks (BigWig) were generated and normalized with the RPCG parameter using the *bamCoverage* function of deepTools2 v3.5.1; [261]. For Lamin and SON, peaks were called using epic with 16kb window sizes and differential peaks were called using epic2-df [308]. For others, peaks were called using SEACR (1.3) with an FDR cutoff of <0.01 [309].

Chrom3D

For simulating 3D chromosome model of IMR90 Micro-C data, the Chrom3D tool was used [303]. For all chromosomes, intra-TAD interactions were specified according to Micro-C output. Association with LADs was added as described in the Chrom3D manual for the whole genome and then distributed for each chromosome (https://github.com/Chrom3D). LADs for proliferating and ICM-treated IMR90 cells were inferred from LAD Atlas (https://osf.io/dk8pm/wiki/home/). In the end, a *.gtrack* file (Chrom3D input) for chromosome visualization was produced using Chrom3D scripts (https://github.com/Chrom3D/preprocess_scripts). Next, a *.BED* file specifying the genomic positions of the TADs (1 TAD = 1 bead) was created, and any gaps between them were filled as described in the Chrom3D manual. Finally, *.gtrack* files corresponding to each cluster were merged and inputted in Chrom3D, using 1,000,000 iterations (-n), a nuclear radius of 5 (-r), and a scale total volume of the beads relative to the volume of the nucleus set to 0.15 (-y). For whole genome visualizations that take into account interchromosomal interactions, Micro-C data were analyzed via HiCPro v2.11.4 at 10-kbp and 1-Mbp resolution, before LADs, TADs, and Micro-C matrices were used for the production of a diploid *.gtrack* file using default parameters; chromosomes Y and M were removed. IDs of beads containing CTCF and SON peaks were identified and colored using the script *processing_scripts/color_beads.py* and the *blend* keyword to maintain coloring. The statistical significance of the 3D distances was estimated by applying the Wilcoxon–Mann–Whitney test in R. All 3D models were visualized in Chimera-X v1.3.

Statistical tests

P-values associated with Student's *t*-tests, Fischer's exact tests and with the Wilcoxon–Mann–Whitney tests were calculated using GraphPad (https://graphpad.com/). Unless otherwise stated, *P*-values < 0.01 were deemed as statistically significant.

Table 1: ICM CTCF CoIP/MS enriched targets

Protein Name	Pvalue Treated vs ctrl	Log2FC
Sequestosome-1	0	0.9423
Alpha-2-macroglobulin	0.003	4.6331
Microtubule-associated protein 1A;MAP1A heavy chain;MAP1 light chain LC2	0.002	0.3083
BTB/POZ domain-containing protein KCTD3	0.002	-0.4176
Chloride channel CLIC-like protein 1	0.001	0.5215
Ataxin-2	0.001	0.1208
Src substrate cortactin	0.005	0.1212
Thioredoxin	0.042	0.1580
Barrier-to-autointegration factor;Barrier-to-autointegration factor, N-terminally processed	0.01	-0.7542
Plectin	0.02	0.7231
Ubiquitin-like protein ISG15	0.024	-0.4944
Serine/arginine repetitive matrix protein 2	0.002	0.1666
Cytoskeleton-associated protein 4	0.003	0.3924
Myosin light chain 3	0.001	N/A
Microtubule-associated protein 1B;MAP1B heavy chain;MAP1 light chain LC1	0.006	-0.1864
Eukaryotic translation initiation factor 3 subunit A	0.01	0.0624
Fragile X mental retardation protein 1	0.015	-0.4974

Table 2: List of qPCR primers used in this study

Primer Name	Forward Seq 5‘-3‘	Reverse Seq 5‘-3‘
HSC70	TTA TTG GAG CCA GGC CTA CAC	GCG ACA TAG CTT GGA GTG GT
ATXN2	CCC TTC AGT ACA AGC CCA CC	GCA GTA GAA GGG AGG AGG GA
FMR1	TGT CTC TGG GAC TTT CTG CAA	TCC TGA ATC AGC TTT CCA TTT T
SRRM2	TAC GAA ACA GCC TAG CAG CC	GGC TAG GTC GAG TTG CAG ATT
BANF1	TCC CAA AAG CAC CGA GAC TTC	ACT GGC CAA GGA CAA CAT AGG
SQSTM1	CTGCACAAGAACCTGGCTTT	CACTGGAAAAGGCAACCAAG

Table 3: List of siRNAs used in this study

siRNA	Company	Cat. No
Accell BANF1	Dharmacon	E-011536-00-0050
Accell Non-targeting Control Pool	Dharmacon	D-001910-10-50
Universal Negative Control	Sigma	SIC001
SRRM2 siRNA (SASI_Hs01_00014413, SASI_Hs01_00014414)	Sigma	NM_016333
ATXN2 siRNA (SASI_Hs01_00159982, SASI_Hs01_00159984)	Sigma	NM_002973
FMR1 siRNA (SASI_Hs01_00139633,SASI_Hs01_00139634)	Sigma	NM_002024
SQSTM1 siRNA (SASI_Hs01_00118616, SASI_Hs01_00118618)	Sigma	NM_003900

Supplements

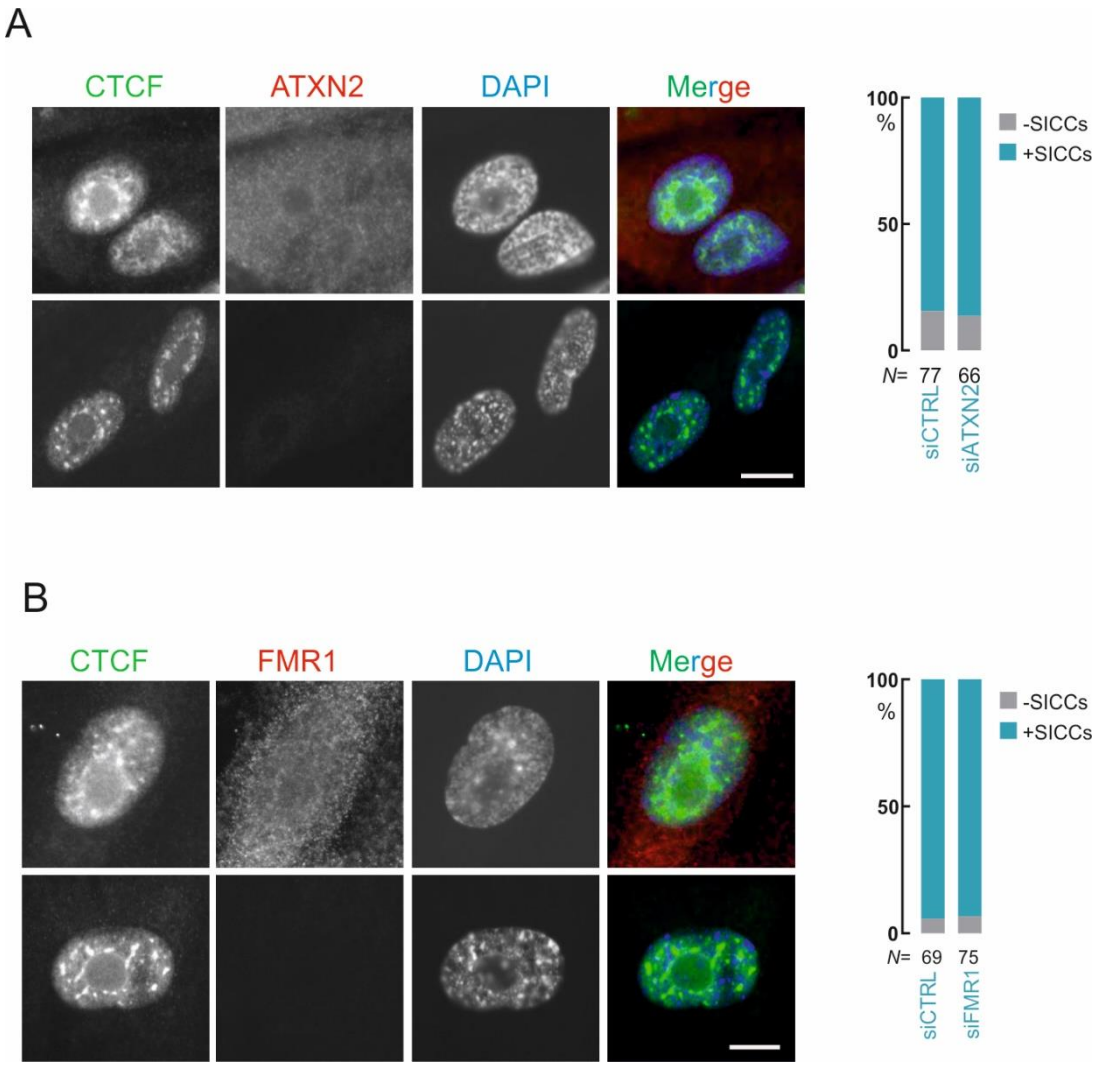

Figure 2.2.S1. Knock-down of *ATXN2* & *FMR1* does not disrupt SICCsICM treatment induces SICCs formation and modulates their state.

A. Typical widefield images (on the left) of of ICM-treated IMR90 after scr and *SQSTM1* knockdown immunostained for ATXN2/CTCF. Bar plots (on the right) quantify the number of cells bearing SICCs per condition (bottom; N is the number of cells analyzed per each condition/cell type). DAPI was used to satin the nucleus. Bar: 10um.

B. Same as above, but for FMR1

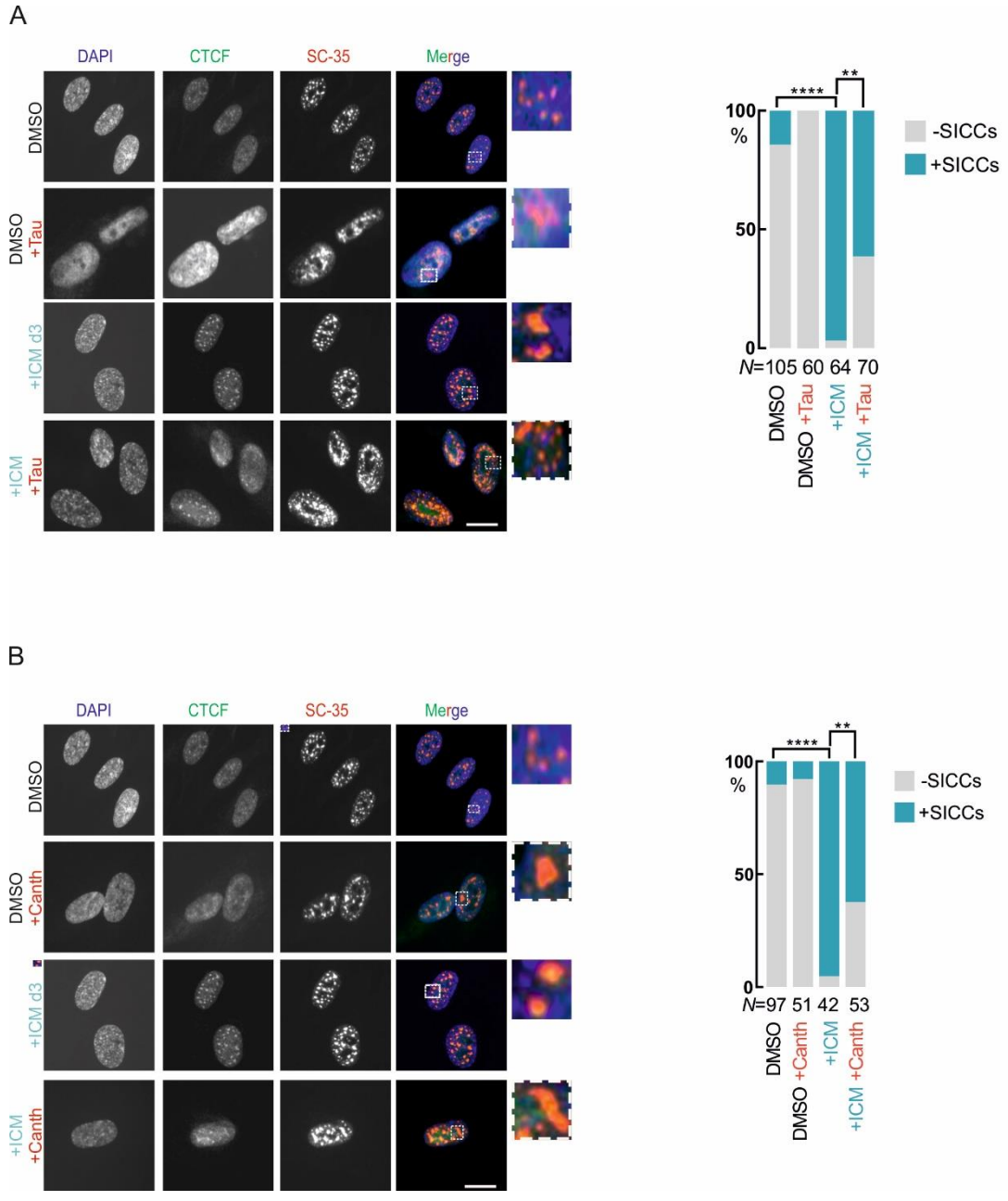

Figure 2.2.S2. NS chemical modulation affects SICCs' integrity.

A. Typical widefield images (on the left) of proliferating and ICM-treated IMR90 with and without treatment with 3uM tautomycin for 1h, immunostained for CTCF/SC-35. Bar plots (on the right) quantify the number of cells bearing SICCs per condition (bottom; N is the number of cells analyzed per each condition/cell type). P<0.01; Wilcoxon–Mann–Whitney test.

B. As above, but cells where either treated or not with 10uM cantharidin for 1h.

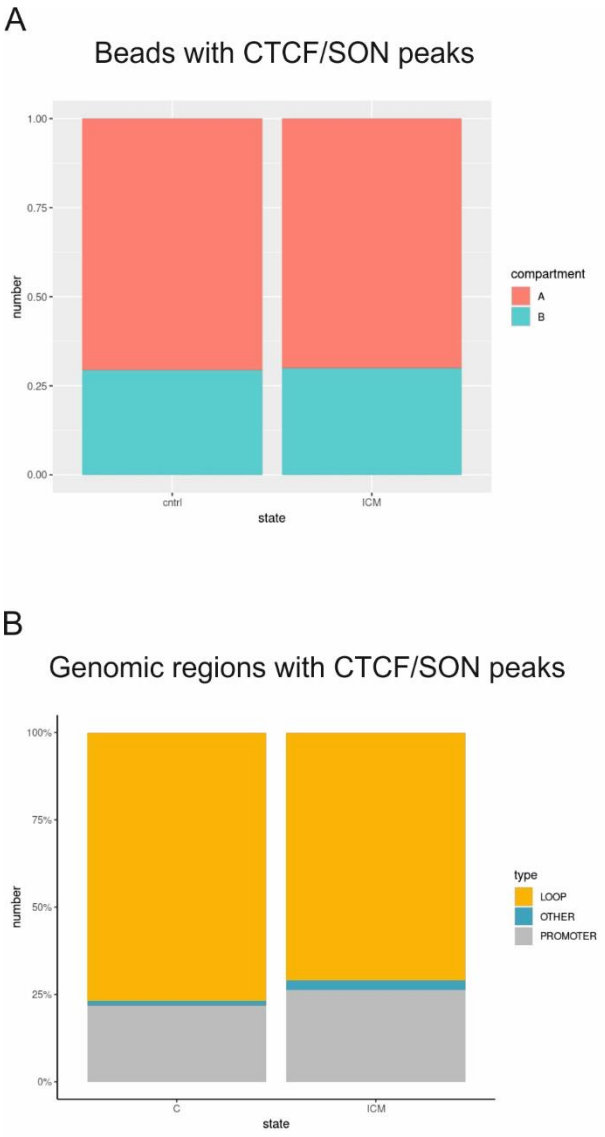

Figure 2.2.S3. NS chemical modulation affects SICCs' integrity.

A. Bar plots showing the percentage of CTCF and SON peaks correlated with either A or B compartment in control and ICM-treated IMR90s.
B. Bar plots showing the distribution of CTCF and SON peaks across genome in control and ICM-treated IMR90s. Loop sites are shown in orange, promoter sites in grey and everything else in dark green.

3. Discussion

Proliferating cells utilize inherent mechanisms that ensure the controlled expansion of their population through coordinated DNA replication and cell division. As a consequence, the normal homeostasis of these cells is preserved and characteristic features and functions are re-established. During mitosis, chromatin loops, topologically associating domains, and A/B compartments of higher-order chromatin are temporarily disrupted [310,311]. However, upon transition from mitosis to G1 phase, there is a rapid 'bottom-up' genomic re-organization – first, sub-TADs are formed, giving rise to multi-domain TADs and sequentially to A/B compartments [312]. Critical role during this process is played by partially-bound CTCF on mitotic chromosomes. During ana/telophase CTCF is fully bound on chromosomes and together with cohesin they start re-establishing the structural loops [312].

In contrast, upon senescence entry cell division is abated and genome organization is significantly altered [86–88]. Changes in chromatin composition, loss of LADs interactions, redistribution of heterochromatin (SAHF) and loss of long range chromatin interactions are among the genomic hallmarks of this growth arrest. Howbeit, many steps in this complicated cascade of events are still elusive. In an effort to understand as many of them, it has been already demonstrated that a number of factors acquire a novel role in senescence and usually the proteins that are repurposed are related with architectural changes [84,90,131,313,314]. Work from our lab has already demonstrated the crucial role that HMGB proteins have in senescence initiation and their impact on shaping the senescent genome [84,90]. Perhaps, the most striking of these observations is related to the massive reorganization that CTCF undergoes upon HMGB2 eviction from the nucleus and senescence entry [90]. The notice of the emergence of senescence-induced CTCF clusters (SICCs) after replicative growth arrest was what gave the sparkle for the creation of this dissertation. Thereby, the main focus was to understand how SICCs are formed and maintained in the nuclear space and what might be their function and purpose in cell's life.

3.1 *Developing a robust system to study senescence*

In our attempt to study SICCs we developed a novel way to chemically induce a replicative senescence-like phenotype. Inflachromene (ICM) was described as an inhibitor of HMGB1/2 nuclear eviction [235]. In our hands, however, we observed that extended periods of treatment (3 and 6 days) of IMR90s with ICM cause the exact opposite effect, resulting in the initiation of the senescent cascade. In that way, this system allowed us to deal with a variety of issues arising when studying senescence in vitro. Treating the cells with ICM essentially generates a largely homogeneous population of senescent cells within a few days. Additionally, it does so in a robust way. However, it remains elusive what is the exact mechanism rendering ICM association with HMGBs.

Autophagy has an essential role for cellular homeostasis as it mediates the well-timed degradation of damaged organelles and proteins. It is tightly regulated and constitutively active at basal levels. Cytoplasmic HMGB1 (cHMGB1) has been reported to hold a prominent place in some of these processes, mainly acting as an autophagy inducer [315–317]. For example, blockage of HMGB1 translocation to the cytoplasm by the pleiotropic telomeric protein TERF2/TRF2 has as a result reduced levels of starvation-mediated autophagy, a phenomenon which could be mimicked by the usage of ICM [317]. In a similar manner, absence of cHMGB1 from stressed pancreatic beta cells leads to decreased autophagic response and increased apoptosis [316]. In a recent study, it was shown that cHMGB1 accomplishes its 'autophagic' purposes through direct interaction with Beclin 1, a major regulator of autophagy [315]. There, they showed that upon treating HEK cells with ICM and blocking HMGB1 migration to the cytoplasm autophagy was suppressed. At the same time ICM was able to cause ubiquitylation-dependent degradation of Beclin 1 and, thus, indirectly suppressing autophagy. Data from our very own Ribo-seq showed that autophagic pathways were upregulated at the levels of RNA upon ICM treatment, but the protein synthesis levels remained effectively unchanged between conditions (proliferating Vs IMC-treated IMR90), pointing in the direction of an autophagy-related mechanism for our system, as well.

Another interesting observation and a benefit of the ICM system was the induction of cell-autonomous senescence independent of any inflammatory side effects. One of the main hallmarks in senescence as was discussed in the introduction part is the secretion of a variety of pro-inflammatory factors and cytokines, the SASP. HMGB1, and to a lesser extent HMGB2, is a master regulator of the availability of SASP-related transcripts [84]. Antibody-blocked HMGB1 impairs the production and secretion of SASP [241]. Moreover, even though the majority of HMGB2 is lost from the nucleus upon senescence entry, it has been reported that any remaining protein is preferentially associated with SASP-related gene promoters and induces their expression [124]. However, going back to our Ribo-seq results, after ICM treatment SASP genes were upregulated, but the protein synthesis remained unchanged. Furthermore, using culture medium from cells treated with ICM and subjected it to either cytokine arrays or HMGB1/2 ELISA did not return any detectable levels of any proinflammatory factors (data not shown). Hence, it could be claimed, with a certain degree of confidence, that ICM induces a SASP-less form of senescence. Having said that, there is still plenty of work left to be done to fully understand this system and its mechanism of action.

3.2 *CTCF reorganization in light of senescence entry*

When discussing about genome organization, more than often, CTCF coincides with other factors about its importance on establishing and maintaining higher-order chromatin structure [318]. Its repertoire regarding multiple biological processes has been updated since its discovery and gradually, but steadily, shifted our perception of CTCF true capabilities [159,174,242,267,319]. However, what was relatively constant so far was the localization pattern of this master regulator; an almost uniform, carpet-like, nuclear distribution. Therefore, and almost inevitably, our striking observation about senescence-induced CTCF clusters (SICCs) triggered our curiosity regarding their nature and role. Having developed a functional system to chemically induce senescence, allowed us for some freedom and flexibility regarding things we could try to investigate SICCs.

3.2.1 *Is SICC formation driven via phase separation?*

From very early on, the structure and the appearance of these clusters made it greatly appealing to hypothesize that the driving forces assisting on their formation were via phase separation. A long-standing phenomenon in physics, has gained great interest over the last decade also in the biological field [280]. Nowadays, many membraneless organelles (MLOs) inside the cell are characterized as phase-separated entities. The nucleolus, the nuclear speckles and the paraspeckles in the nucleus and the stress granules and the centriole in the cytoplasm are only a few examples of this increasing blossom [320]. Although the field is still in its infancy and certain discoveries should be taken with a grain of salt, there are already some tools available that assist to the elucidation and characterization of phase-separated droplets. One of these, is the use of the aliphatic compound 1,6-hexanediol (1,6-HD) [282]. It has been demonstrated that hexanediol can disrupt liquid-like droplets, by interacting with the intrinsically disordered domains of the proteins participating there. Moreover, it was shown that it can differentiate between liquid- and solid-like structures [282]. Something similar was observed in the case of SICCs, as well. After short treatment of ICM (3 days) the newly emerged CTCF clusters were susceptible to 1,6-HD action and they were almost completely disrupted, implying a liquid-like droplet, while after more extended periods of ICM treatment this ability was compromised, maybe due to a phase transition into a more solid state.

The notion that SICCs might be held together via phase separation gains some ground when taking a closer look to the two proteins that seem to facilitate their formation. BANF1 is a small and well-structured protein, around 10kDa; not a typical candidate to be found in MLOs. Nonetheless, the way that this protein fulfills its role gathers some interest. Its action as a ‘molecular glue’ holding other factors wrapped around mitotic chromosomes attributes it a ‘structural’ characteristic. Furthermore, it has been recently shown that the reformation of sealed nuclei is partially mediated via phase separation of the inner nuclear membrane protein 2 (LEM2) [321]. LEM2 accomplishes its role via interaction with BANF1, which offers the necessary chromatin affinity. The above, demonstrates that BANF1 has the ability to, at least indirectly, participate in the formation of liquid droplets. Hence, it is not unreasonable to speculate that something similar might happen in the case of SICCs, too. On the other hand, SRRM2 is a highly disordered protein and part of the nuclear speckles, a structure already characterized to be phase-separated [290]. The association of SICCs with nuclear speckles (NS) brings along another feature in the equation; the possible use of RNAs in the maintenance of CTCF clusters.

It is known, that apart from the proteins that can participate in the creation of liquid-like droplets, RNA can also assist to this direction [219,322,323] and NS is a huge repository of such molecules inside the nucleus. Apart from its ability to bind to DNA using its zinc-finger domain, CTCF has been shown to be capable of direct RNA interactions, too [160,163,324,325]. In our hands, when we overexpressed the RNA-binding domain (RBD) of SRRM2 we observed that it was sufficient to induce the formation of CTCF clusters, maybe because it offers a scaffold where more and more CTCF could bind. Taken together all the above, the hypothesis that phase separation is the driving force that keeps SICCs in place might not be unrealistic, but it definitely needs more thorough investigation.

3.2.2 *Post-translational modifications (PTMs) & SICCs*

During our study, we collected converged data supporting that PTMs might assist either directly, or indirectly, in the formation and maintenance of SICCs. It is known, that CTCF holds great capacity for multiple post-translational modifications, each contributing to certain functions of the protein [326]. Phosphorylation of CTCF, at different sites of its 11 zinc-fingers domain, can regulate its DNA biding capacity and it is highly dynamic during cell differentiation [327]. Noteworthily, disruption of CTCF phosphorylation in just one amino acid (S224) is sufficient to cause dysregulation in multiple target genes, including p53 and p21, two major senescence modulators [328].

In our case, and in an effort to decode the interplay between SICCs and NS, we used two phosphatase inhibitors, cantharidin and tautomycin, targeting the serine/threonine (Ser/Thr) protein phosphatases 1 and 2A (PP1 and PP2A) [219,288,289]. PP1 and PP2A are the most abundant Ser/Thr phosphatases in eukaryotic cells and they participate in the regulation of cell cycle [329–332]. It was also shown, that PP1 could partially contribute to higher order chromatin establishment by regulating the formation of heterochromatin in interphase [333].

Additionally to these roles, modulation of PP1 and/or PP2A can perturb the structure of nuclear speckles by affecting the sub-nuclear distribution of pre-mRNA splicing factors [219,334]. Most of the factors located in NS are serine/arginine-rich (SR) proteins, thus prone to regulation by Ser/Thr phosphatases. Once they have fulfilled their role in a given RNA process, they are subjected to dephosphorylation by PP1 and/or PP2A and either returning to NS until they are needed again or they are used in the cytoplasm as RNA chaperons [335].

In the concentration we used here, cantharidin inhibited PP2A, leading NS to fuse into larger structures, indicating that hyperphosphorylation might promote NS aggregation. In contrast, inhibition of PP1 with tautomycin (in the concentration used in the study), led to NS fragmentation. Both of these modulations had the same impact at the number of cells carrying SICCs; their decrease. This observation might suggest that global phosphorylation levels carried out by Ser/Thr phosphatases and the subsequent integrity of NS is potentially important for SICCs integrity, as well.

Another PTM with increasing importance is poly(ADP-ribosyl)ation (PARylation). It is predominantly taking place on the N-terminus of CTCF and influences its insulation abilities [327]. Decreased CTCF PARylation levels have been linked with breast tumor progression and cell proliferation [336]. That being said, CTCF is found to exist in different PARylation statuses in healthy cells; highly-, hypo- and non-PARylated [300]. Upon senescence entry and on, the majority of PARP enzymes are found to be downregulated, something that holds true also upon ICM treatment. Reduced levels of PARP enzymes might have been the cause of the increased we observed in the hypo-PARylated form of CTCF. This finding, however, triggered more questions, primarily, *which form of CTCF participates and gives rise to SICCs?* A premature answer to this comes from the next observation we did after the use of olaparib, a potent PARP1/2 inhibitor. There, we saw that upon inhibition of the two most abundant PARPs we were able to recapitulate the presence of CTCF clusters, in a 'non-senescent environment'. Collectively, the above data might point to a direction where hypo-PARylated CTCF actively forms clusters, but there is still a considerable amount of work that needs to be done, before drawing any conclusions.

3.2.3 *Towards a biological relevance of SICCs*

No matter how much effort we devote on describing the SICCs, the ultimate question remains: what might be the biological relevance of these entities? Upon senescence entry, many things are changing and many processes are altered. From its secretome, all the way up to its higher-order chromatin organization a cell has to adapt to a restructured surrounding in order to survive long enough to be marked as apoptotic. In a constantly variable and dynamic environment, what might have been the first thing that someone would explore in order to attribute a function to these clusters? A rather perplexed, but, at the same time, much-studied biological process, tightly connected to senescence, is DNA damage response (DDR).

There are accumulating evidences over the past few years that CTCF actively participates in DDR [337]. It has been mostly associated with DNA double-strand breaks (DSBs) repair and homologous recombination (HR). It was shown to execute this task via interactions with the DNA repair protein Rad51 (propagating the formation of Rad51 foci) and the retinoblastoma-binding protein 8 (RBBP8), both participating in HR [338–340]. Furthermore, the recruitment of CTCF on the site of lesion seems to be an early event since it occurs roughly within the first 30sec upon damage [272]. This time frame coincides with another major event of DDR, the phosphorylation of histone H2A variant H2AX, at Ser139 (γH2AX) [341]. γH2AX domains are adjoined by CTCF, both before and during DDR, but upon DNA damage more CTCF is recruited on site [342]. There, CTCF is hypothesized to act by confining γH2AX foci and not allowing them to expand further than the site of damage. The above idea is supported by data showing that γH2AX foci are increased in the absence of CTCF [272].

Moreover, it has been shown that CTCF is recruited in sites of DSBs via PARylation. This last observation is still under debate, since there are studies claiming that PARylation is needed in order for CTCF to be recruited on the site of lesion, while others suggest that part of its zinc-finger domain is sufficient for recruitment and subsequent PARylation is only used to amplify the effect [272,339]. Regardless, once more the PARylation status of CTCF seems to raise particular significance. Besides this, BANF1 has also been shown to participate in DDR via regulation of PARP1 activity upon oxidative DNA damage, through direct interaction and inhibition of PARP1 auto-PARylation[343].

From the above, it seems that many pieces from our puzzle could potentially come together to explain the existence of SICCs. Preliminary results from our lab are pointing to the direction of a possible connection between these clusters and DNA damage. When CTCF was co-stained with γH2AX we could observe a complete segregation between the two entities, with γH2AX foci flanking SICCs, but never co-localizing. Treatment of ICM-treated cells with known DNA damage inducers (e.g. olabarib and etoposide) revealed that there was an overall decrease in the extend of DNA damage (compared with proliferating cells treated with the same drugs) and this was quantified either by the reduced existence of γH2AX foci per cell or reduced amount of cells bearing detectable signal for γH2AX (data not shown). Thus, it is appealing to hypothesize that SICCs might act as a protective mechanism against excessive DNA damage in senescent cells, a notion that needs further investigation.

Collectively, all the observations been made throughout this dissertation suggest that CTCF might have a previously uncharacterized role upon senescence entry. The hypothesis that SICCs might act as a prevention mechanism against excessive DNA damage is rather tempting. Furthermore, recent studies involving phase separation as a mechanism of 'isolating' sites of lesion so that the DDR machinery could act seamlessly and focally [344–347], come only to increase our curiosity and set the framework for future approaches.

4. References

1. Hayflick L, Moorhead PS. 1961 The serial cultivation of human diploid cell strains. *Exp. Cell Res.* **25**, 585–621. (doi:10.1016/0014-4827(61)90192-6)

2. Hayflick L. 1965 THE LIMITED IN VITRO LIFETIME OF HUMAN DIPLOID CELL STRAINS. *Exp. Cell Res.* **37**, 614–636. (doi:10.1016/0014-4827(65)90211-9)

3. Kuilman T, Michaloglou C, Mooi WJ, Peeper DS. 2010 The essence of senescence. *Genes Dev.* **26**, 2463–2479. (doi:10.1101/gad.1971610)

4. Mikuła-Pietrasik J, Niklas A, Uruski P, Tykarski A, Książek K. 2020 Mechanisms and significance of therapy-induced and spontaneous senescence of cancer cells. *Cell. Mol. Life Sci.* **77**, 213–229. (doi:10.1007/S00018-019-03261-8/FIGURES/2)

5. Pazolli E, Alspach E, Milczarek A, Prior J, Piwnica-Worms D, Stewart SA. 2012 Chromatin remodeling underlies the senescence- associated secretory phenotype of tumor stromal fibroblasts that supports cancer progression. *Cancer Res.* **72**, 2251–2261. (doi:10.1158/0008-5472.CAN-11-3386/650143/AM/CHROMATIN-REMODELING-UNDERLIES-THE-SENESCENCE)

6. Rai TS, Adams PD. 2012 Lessons from senescence: Chromatin maintenance in non-proliferating cells. *Biochim. Biophys. Acta* **1819**, 322–331. (doi:10.1016/j.bbagrm.2011.07.014)

7. Galanos P *et al.* 2016 Chronic p53-independent p21 expression causes genomic instability by deregulating replication licensing. *Nat. Cell Biol. 2016 187* **18**, 777–789. (doi:10.1038/ncb3378)

8. Saleh T, Tyutyunyk-Massey L, Gewirtz DA. 2019 Tumor cell escape from therapy-induced senescence as a model of disease recurrence after dormancy. *Cancer Res.* **79**, 1044–1046. (doi:10.1158/0008-5472.CAN-18-3437/661365/P/TUMOR-CELL-ESCAPE-FROM-THERAPY-INDUCED-SENESCENCE)

9. Zampetidis CP *et al.* 2021 A recurrent chromosomal inversion suffices for driving escape from oncogene-induced senescence via subTAD reorganization. *Mol. Cell* **81**, 4907-4923.e8. (doi:10.1016/J.MOLCEL.2021.10.017)

10. Campisi J. 2013 Aging, Cellular Senescence, and Cancer. *https://doi.org/10.1146/annurev-physiol-030212-183653* **75**, 685–705. (doi:10.1146/ANNUREV-PHYSIOL-030212-183653)

11. Van Deursen JM. 2014 The role of senescent cells in ageing. *Nat. 2014 5097501* **509**, 439–446. (doi:10.1038/nature13193)

12. Coppé JP, Patil CK, Rodier F, Sun Y, Muñoz DP, Goldstein J, Nelson PS, Desprez PY, Campisi J. 2008 Senescence-Associated Secretory Phenotypes Reveal Cell-Nonautonomous Functions of Oncogenic RAS and the p53 Tumor Suppressor. *PLOS Biol.* **6**, e301. (doi:10.1371/JOURNAL.PBIO.0060301)

13. Campisi J, D'Adda Di Fagagna F. 2007 Cellular senescence: when bad things happen to good cells. *Nat. Rev. Mol. Cell Biol. 2007 89* **8**, 729–740. (doi:10.1038/nrm2233)

14. Rodier F *et al.* 2009 Persistent DNA damage signalling triggers senescence-associated inflammatory cytokine secretion. *Nat. Cell Biol. 2009 118* **11**, 973–979. (doi:10.1038/ncb1909)

15. Sulli G, Di Micco R, Di Fagagna FDA. 2012 Crosstalk between chromatin state and DNA damage response in cellular senescence and cancer. *Nat. Rev. Cancer 2012 1210* **12**, 709–720. (doi:10.1038/nrc3344)

16. Chandra T *et al.* 2015 Global reorganization of the nuclear landscape in senescent cells. *Cell Rep.* **10**, 471–483. (doi:10.1016/j.celrep.2014.12.055)

17. López-Otín C, Blasco MA, Partridge L, Serrano M, Kroemer G. 2013 The Hallmarks of Aging. *Cell* **153**, 1194–1217. (doi:10.1016/J.CELL.2013.05.039)

18. Di Leonardo A, Linke SP, Clarkin K, Wahl GM. 1994 DNA damage triggers a prolonged p53-dependent G1 arrest and long-term induction of Cip1 in normal human fibroblasts. *Genes Dev.* **8**, 2540–2551. (doi:10.1101/GAD.8.21.2540)

19. Zetterberg A, Larsson O. 1985 Kinetic analysis of regulatory events in G1 leading to proliferation or quiescence of Swiss 3T3 cells. *Proc. Natl. Acad. Sci. U. S. A.* **82**, 5365–5369. (doi:10.1073/PNAS.82.16.5365)

20. Gorgoulis V *et al.* 2019 Cellular Senescence: Defining a Path Forward. *Cell* **179**, 813–827. (doi:10.1016/J.CELL.2019.10.005/ATTACHMENT/84B2BABE-BEB1-4FB7-838C-E264EDC7473E/MMC3.PDF)

21. Laplante M, Sabatini DM. 2012 mTOR signaling in growth control and disease. *Cell* **149**, 274–293. (doi:10.1016/J.CELL.2012.03.017)

22. Korotchkina LG, Leontieva O V., Bukreeva EI, Demidenko ZN, Gudkov A V., Blagosklonny M V. 2010 The choice between p53-induced senescence and quiescence is determined in part by the mTOR pathway. *Aging (Albany. NY).* **2**, 344–352. (doi:10.18632/AGING.100160)

23. Blagosklonny M V. 2012 Cell cycle arrest is not yet senescence, which is not just cell cycle arrest: terminology for TOR-driven aging. *Aging (Albany. NY).* **4**, 159–165. (doi:10.18632/AGING.100443)

24. Johnson SC, Rabinovitch PS, Kaeberlein M. 2013 mTOR is a key modulator of ageing and age-related disease. *Nat. 2013 4937432* **493**, 338–345. (doi:10.1038/nature11861)

25. Harley CB, Futcher AB, Greider CW. 1990 Telomeres shorten during ageing of human fibroblasts. *Nature* **345**, 458–460. (doi:10.1038/345458A0)

26. Bodnar AG *et al.* 1998 Extension of life-span by introduction of telomerase into normal human cells. *Science* **279**, 349–352. (doi:10.1126/SCIENCE.279.5349.349)

27. Rossiello F, Jurk D, Passos JF, d'Adda di Fagagna F. 2022 Telomere dysfunction in ageing and age-related diseases. *Nat. Cell Biol. 2022 242* **24**, 135–147. (doi:10.1038/s41556-022-00842-x)

28. Takai H, Smogorzewska A, De Lange T. 2003 DNA damage foci at dysfunctional telomeres. *Curr. Biol.* **13**, 1549–1556. (doi:10.1016/S0960-9822(03)00542-6)

29. Shay JW, Pereira-Smith OM, Wright WE. 1991 A role for both RB and p53 in the regulation of human cellular senescence. *Exp. Cell Res.* **196**, 33–39. (doi:10.1016/0014-4827(91)90453-2)

30. Rovillain E, Mansfield L, Lord CJ, Ashworth A, Jat PS. 2011 An RNA interference screen for identifying downstream effectors of the p53 and pRB tumour suppressor pathways involved in senescence. *BMC Genomics* **12**, 1–12. (doi:10.1186/1471-2164-12-355/FIGURES/4)

31. Hafner A, Bulyk ML, Jambhekar A, Lahav G. 2019 The multiple mechanisms that regulate p53 activity and cell fate. *Nat. Rev. Mol. Cell Biol. 2019 204* **20**, 199–210. (doi:10.1038/s41580-019-0110-x)

32. Kastenhuber ER, Lowe SW. 2017 Putting p53 in Context. *Cell* **170**, 1062–1078. (doi:10.1016/J.CELL.2017.08.028)

33. Bourgeois B, Madl T. 2018 Regulation of cellular senescence via the FOXO4-p53 axis. *Febs Lett.* **592**, 2083. (doi:10.1002/1873-3468.13057)

34. Labaer J, Garrett MD, Stevenson LF, Slingerland JM, Sandhu C, Chou HS, Fattaey A, Harlow E. 1997 New functional activities for the p21 family of CDK inhibitors. *Genes Dev.* **11**, 847–862. (doi:10.1101/GAD.11.7.847)

35. Chen J, Saha P, Kornbluth S, Dynlacht BD, Dutta A. 1996 Cyclin-binding motifs are essential for the function of p21CIP1. *Mol. Cell. Biol.* **16**, 4673–4682. (doi:10.1128/MCB.16.9.4673)

36. Wiedemeyer WR. 2018 Resistance Mechanisms to Cyclin-Dependent Kinase Inhibitors. , 181–210. (doi:10.1007/978-3-319-67932-7_8)

37. Fischer M, Müller GA. 2017 Cell cycle transcription control: DREAM/MuvB and RB-E2F complexes. *https://doi.org/10.1080/10409238.2017.1360836* **52**, 638–662. (doi:10.1080/10409238.2017.1360836)

38. Benhamed M, Herbig U, Ye T, Dejean A, Bischof O. 2012 Senescence is an endogenous trigger for microRNA-directed transcriptional gene silencing in human cells. *Nat. Cell Biol. 2012 143* **14**, 266–275. (doi:10.1038/ncb2443)

39. Serrano M, Hannon GJ, Beach D. 1993 A new regulatory motif in cell-cycle control causing specific inhibition of cyclin D/CDK4. *Nat. 1993 3666456* **366**, 704–707. (doi:10.1038/366704a0)

40. Petrova N V., Velichko AK, Razin S V., Kantidze OL. 2016 Small molecule compounds that induce cellular senescence. *Aging Cell* **15**, 999–1017. (doi:10.1111/ACEL.12518)

41. Krishnamurthy J, Torrice C, Ramsey MR, Kovalev GI, Al-Regaiey K, Su L, Sharpless NE. 2004 Ink4a/Arf expression is a biomarker of aging. *J. Clin. Invest.* **114**, 1299–1307. (doi:10.1172/JCI22475)

42. Bracken AP *et al.* 2007 The Polycomb group proteins bind throughout the INK4A-ARF locus and are disassociated in senescent cells. *Genes Dev.* **21**, 525. (doi:10.1101/GAD.415507)

43. Gould A. 1997 Functions of mammalian Polycomb group and trithorax group related genes. *Curr. Opin. Genet. Dev.* **7**, 488–494. (doi:10.1016/S0959-437X(97)80075-5)

44. Bracken AP, Pasini D, Capra M, Prosperini E, Colli E, Helin K. 2003 EZH2 is downstream of the pRB-E2F pathway, essential for proliferation and amplified in cancer. *EMBO J.* **22**, 5323–5335. (doi:10.1093/EMBOJ/CDG542)

45. Campisi J. 2005 Senescent cells, tumor suppression, and organismal aging: good citizens, bad

neighbors. *Cell* **120**, 513–522. (doi:10.1016/J.CELL.2005.02.003)

46. Kumari R, Jat P. 2021 Mechanisms of Cellular Senescence: Cell Cycle Arrest and Senescence Associated Secretory Phenotype. *Front. Cell Dev. Biol.* **9**, 485. (doi:10.3389/FCELL.2021.645593/BIBTEX)

47. Sun Y, Coppé JP, Lam EWF. 2018 Cellular Senescence: The Sought or the Unwanted? *Trends Mol. Med.* **24**, 871–885. (doi:10.1016/J.MOLMED.2018.08.002)

48. Lopes-Paciencia S, Saint-Germain E, Rowell MC, Ruiz AF, Kalegari P, Ferbeyre G. 2019 The senescence-associated secretory phenotype and its regulation. *Cytokine* **117**, 15–22. (doi:10.1016/J.CYTO.2019.01.013)

49. Wajapeyee N, Serra RW, Zhu X, Mahalingam M, Green MR. 2008 Oncogenic BRAF Induces Senescence and Apoptosis through Pathways Mediated by the Secreted Protein IGFBP7. *Cell* **132**, 363–374. (doi:10.1016/j.cell.2007.12.032)

50. Severino V, Alessio N, Farina A, Sandomenico A, Cipollaro M, Peluso G, Galderisi U, Chambery A. 2013 Insulin-like growth factor binding proteins 4 and 7 released by senescent cells promote premature senescence in mesenchymal stem cells. *Cell Death Dis. 2013 411* **4**, e911–e911. (doi:10.1038/cddis.2013.445)

51. Özcan S, Alessio N, Acar MB, Mert E, Omerli F, Peluso G, Galderisi U. 2016 Unbiased analysis of senescence associated secretory phenotype (SASP) to identify common components following different genotoxic stresses. *Aging (Albany. NY).* **8**, 1316–1327. (doi:10.18632/AGING.100971)

52. Kortlever RM, Higgins PJ, Bernards R. 2006 Plasminogen activator inhibitor-1 is a critical downstream target of p53 in the induction of replicative senescence. *Nat. Cell Biol. 2006 88* **8**, 877–884. (doi:10.1038/ncb1448)

53. Elzi DJ, Lai Y, Song M, Hakala K, Weintraub ST, Shiio Y. 2012 Plasminogen activator inhibitor 1 - Insulin-like growth factor binding protein 3 cascade regulates stress-induced senescence. *Proc. Natl. Acad. Sci. U. S. A.* **109**, 12052–12057. (doi:10.1073/PNAS.1120437109/SUPPL_FILE/SD02.XLS)

54. Freund A, Orjalo A V., Desprez P-Y, Campisi J. 2010 Inflammatory networks during cellular

senescence: causes and consequences. *Trends Mol. Med.* **16**, 238–246. (doi:10.1016/J.MOLMED.2010.03.003)

55. Acosta JC *et al.* 2008 Chemokine Signaling via the CXCR2 Receptor Reinforces Senescence. *Cell* **133**, 1006–1018. (doi:10.1016/j.cell.2008.03.038)

56. Kuilman T, Michaloglou C, Vredeveld LCW, Douma S, van Doorn R, Desmet CJ, Aarden LA, Mooi WJ, Peeper DS. 2008 Oncogene-Induced Senescence Relayed by an Interleukin-Dependent Inflammatory Network. *Cell* **133**, 1019–1031. (doi:10.1016/j.cell.2008.03.039)

57. Orjalo A V., Bhaumik D, Gengler BK, Scott GK, Campisi J. 2009 Cell surface-bound IL-1α is an upstream regulator of the senescence-associated IL-6/IL-8 cytokine network. *Proc. Natl. Acad. Sci. U. S. A.* **106**, 17031–17036. (doi:10.1073/PNAS.0905299106/SUPPL_FILE/0905299106SI.PDF)

58. Acosta JC *et al.* 2013 A complex secretory program orchestrated by the inflammasome controls paracrine senescence. *Nat. Cell Biol. 2013 158* **15**, 978–990. (doi:10.1038/ncb2784)

59. Nelson G, Wordsworth J, Wang C, Jurk D, Lawless C, Martin-Ruiz C, von Zglinicki T. 2012 A senescent cell bystander effect: senescence-induced senescence. *Aging Cell* **11**, 345–349. (doi:10.1111/J.1474-9726.2012.00795.X)

60. Nelson G, Kucheryavenko O, Wordsworth J, von Zglinicki T. 2018 The senescent bystander effect is caused by ROS-activated NF-κB signalling. *Mech. Ageing Dev.* **170**, 30–36. (doi:10.1016/J.MAD.2017.08.005)

61. Takasugi M, Okada R, Takahashi A, Virya Chen D, Watanabe S, Hara E. 2017 Small extracellular vesicles secreted from senescent cells promote cancer cell proliferation through EphA2. *Nat. Commun. 2017 81* **8**, 1–11. (doi:10.1038/ncomms15728)

62. Schroder K, Tschopp J. 2010 The Inflammasomes. *Cell* **140**, 821–832. (doi:10.1016/J.CELL.2010.01.040)

63. Dou Z *et al.* 2017 Cytoplasmic chromatin triggers inflammation in senescence and cancer. *Nat. 2017 5507676* **550**, 402–406. (doi:10.1038/nature24050)

64. Glück S *et al.* 2017 Innate immune sensing of cytosolic chromatin fragments through cGAS promotes senescence. *Nat. Cell Biol. 2017 199* **19**, 1061–1070. (doi:10.1038/ncb3586)

65. Yang H, Wang H, Ren U, Chen Q, Chena ZJ. 2017 CGAS is essential for cellular senescence. *Proc. Natl. Acad. Sci. U. S. A.* **114**, E4612–E4620. (doi:10.1073/PNAS.1705499114/SUPPL_FILE/PNAS.1705499114.SM01.AVI)

66. Takahashi A *et al.* 2018 Downregulation of cytoplasmic DNases is implicated in cytoplasmic DNA accumulation and SASP in senescent cells. *Nat. Commun. 2018 91* **9**, 1–12. (doi:10.1038/s41467-018-03555-8)

67. De Cecco M *et al.* 2019 L1 drives IFN in senescent cells and promotes age-associated inflammation. *Nat. 2019 5667742* **566**, 73–78. (doi:10.1038/s41586-018-0784-9)

68. Takahashi A *et al.* 2012 DNA Damage Signaling Triggers Degradation of Histone Methyltransferases through APC/CCdh1 in Senescent Cells. *Mol. Cell* **45**, 123–131. (doi:10.1016/J.MOLCEL.2011.10.018)

69. Kang C *et al.* 2015 The DNA damage response induces inflammation and senescence by inhibiting autophagy of GATA4. *Science (80-.).* **349**. (doi:10.1126/SCIENCE.AAA5612/SUPPL_FILE/KANG.SM.PDF)

70. Calcinotto A, Kohli J, Zagato E, Pellegrini L, Demaria M, Alimonti A. 2019 Cellular Senescence: Aging, Cancer, and Injury. *Physiol. Rev.* **99**, 1047–1078. (doi:10.1152/physrev.00020.2018)

71. Gorgoulis VG, Halazonetis TD. 2010 Oncogene-induced senescence: the bright and dark side of the response. *Curr. Opin. Cell Biol.* **22**, 816–827. (doi:10.1016/J.CEB.2010.07.013)

72. Michaloglou C *et al.* 2005 BRAFE600-associated senescence-like cell cycle arrest of human naevi. *Nature* **436**, 720–724. (doi:10.1038/NATURE03890)

73. Braig M *et al.* 2005 Oncogene-induced senescence as an initial barrier in lymphoma development. *Nat. 2005 4367051* **436**, 660–665. (doi:10.1038/nature03841)

74. Lujambio A *et al.* 2013 Non-Cell-Autonomous Tumor Suppression by p53. *Cell* **153**, 449–460. (doi:10.1016/J.CELL.2013.03.020)

75. Jun J Il, Lau LF. 2010 The matricellular protein CCN1 induces fibroblast senescence and restricts fibrosis in cutaneous wound healing. *Nat. Cell Biol. 2010 127* **12**, 676–685. (doi:10.1038/ncb2070)

76. Demaria M *et al.* 2014 An Essential Role for Senescent Cells in Optimal Wound Healing through

Secretion of PDGF-AA. *Dev. Cell* **31**, 722–733. (doi:10.1016/J.DEVCEL.2014.11.012)

77. Besancenot R, Chaligné R, Tonetti C, Pasquier F, Marty C, Lécluse Y, Vainchenker W, Constantinescu SN, Giraudier S. 2010 A senescence-like cell-cycle arrest occurs during megakaryocytic maturation: implications for physiological and pathological megakaryocytic proliferation. *PLoS Biol.* **8**. (doi:10.1371/JOURNAL.PBIO.1000476)

78. Coppe JP, Kauser K, Campisi J, Beauséjour CM. 2006 Secretion of Vascular Endothelial Growth Factor by Primary Human Fibroblasts at Senescence. *J. Biol. Chem.* **281**, 29568–29574. (doi:10.1074/JBC.M603307200)

79. Di Mitri D *et al.* 2014 Tumour-infiltrating Gr-1+ myeloid cells antagonize senescence in cancer. *Nat. 2014 5157525* **515**, 134–137. (doi:10.1038/nature13638)

80. Demaria M *et al.* 2017 Cellular senescence promotes adverse effects of chemotherapy and cancer relapse. *Cancer Discov.* **7**, 165–176. (doi:10.1158/2159-8290.CD-16-0241/333293/AM/CELLULAR-SENESCENCE-PROMOTES-ADVERSE-EFFECTS-OF)

81. Chen F *et al.* 2018 Targeting SPINK1 in the damaged tumour microenvironment alleviates therapeutic resistance. *Nat. Commun. 2018 91* **9**, 1–19. (doi:10.1038/s41467-018-06860-4)

82. Eggert T *et al.* 2016 Distinct Functions of Senescence-Associated Immune Responses in Liver Tumor Surveillance and Tumor Progression. *Cancer Cell* **30**, 533–547. (doi:10.1016/J.CCELL.2016.09.003)

83. Zhang W, Qu J, Liu G-H, Belmonte JCI. 2020 The ageing epigenome and its rejuvenation. *Nat. Rev. Mol. Cell Biol.* **21**, 137–150. (doi:10.1038/s41580-019-0204-5)

84. Sofiadis K *et al.* 2021 HMGB1 coordinates SASP-related chromatin folding and RNA homeostasis on the path to senescence. *Mol. Syst. Biol.* **17**. (doi:10.15252/MSB.20209760)

85. Pal S, Tyler JK. 2016 Epigenetics and aging. *Sci. Adv.* **2**, e1600584–e1600584. (doi:10.1126/sciadv.1600584)

86. Parry AJ, Narita M. 2016 Old cells, new tricks: chromatin structure in senescence. *Mamm. Genome* **27**, 320–331. (doi:10.1007/s00335-016-9628-9)

87. Criscione SW, Cecco M De, Siranosian B, Zhang Y, Kreiling JA, Sedivy JM, Neretti N. 2016 Reorganization of chromosome architecture in replicative cellular senescence. *Sci. Adv.* **2**.

(doi:10.1126/sciadv.1500882)

88. Criscione SW, Teo YV, Neretti N. 2016 The Chromatin Landscape of Cellular Senescence. *Trends Genet.* **32**, 751–761. (doi:10.1016/j.tig.2016.09.005)

89. Sun L, Yu R, Dang W. 2018 Chromatin Architectural Changes during Cellular Senescence and Aging. *Genes (Basel).* **9**. (doi:10.3390/genes9040211)

90. Zirkel A *et al.* 2018 HMGB2 Loss upon Senescence Entry Disrupts Genomic Organization and Induces CTCF Clustering across Cell Types. *Mol. Cell* **70**, 730-744.e6. (doi:10.1016/j.molcel.2018.03.030)

91. Evans SA, Horrell J, Neretti N. 2019 The three-dimensional organization of the genome in cellular senescence and age-associated diseases. *Semin. Cell Dev. Biol.* **90**, 154. (doi:10.1016/J.SEMCDB.2018.07.022)

92. Sati S *et al.* 2020 4D Genome Rewiring during Oncogene-Induced and Replicative Senescence. *Mol. Cell* **78**, 522-538.e9. (doi:10.1016/J.MOLCEL.2020.03.007)

93. Luger K, Dechassa ML, Tremethick DJ. 2012 New insights into nucleosome and chromatin structure: an ordered state or a disordered affair? *Nat. Rev. Mol. Cell Biol. 2012 137* **13**, 436–447. (doi:10.1038/nrm3382)

94. Dang W, Steffen KK, Perry R, Dorsey JA, Johnson FB, Shilatifard A, Kaeberlein M, Kennedy BK, Berger SL. 2009 Histone H4 lysine 16 acetylation regulates cellular lifespan. *Nature* **459**, 802–807. (doi:10.1038/NATURE08085)

95. Feser J, Truong D, Das C, Carson JJ, Kieft J, Harkness T, Tyler JK. 2010 Elevated histone expression promotes life span extension. *Mol. Cell* **39**, 724–735. (doi:10.1016/J.MOLCEL.2010.08.015)

96. McCormick MA *et al.* 2015 A Comprehensive Analysis of Replicative Lifespan in 4,698 Single-Gene Deletion Strains Uncovers Conserved Mechanisms of Aging. *Cell Metab.* **22**, 895–906. (doi:10.1016/J.CMET.2015.09.008)

97. Liu L, Cheung TH, Charville GW, Hurgo BMC, Leavitt T, Shih J, Brunet A, Rando TA. 2013 Chromatin modifications as determinants of muscle stem cell quiescence and chronological aging. *Cell Rep.* **4**, 189–204. (doi:10.1016/J.CELREP.2013.05.043)

98. Adams PD *et al.* 2013 Lysosome-mediated processing of chromatin in senescence. *J. Cell Biol.* **202**, 129–143. (doi:10.1083/JCB.201212110/VIDEO-1)

99. Tsuchiya M, Dang N, Kerr EO, Hu D, Steffen KK, Oakes JA, Kennedy BK, Kaeberlein M. 2006 Sirtuin-independent effects of nicotinamide on lifespan extension from calorie restriction in yeast. *Aging Cell* **5**, 505–514. (doi:10.1111/J.1474-9726.2006.00240.X)

100. Xu F, Zhang K, Grunstein M. 2005 Acetylation in histone H3 globular domain regulates gene expression in yeast. *Cell* **121**, 375–385. (doi:10.1016/J.CELL.2005.03.011)

101. Liu WH, Churchill MEA. 2012 Histone Transfer Among Chaperones. *Biochem. Soc. Trans.* **40**, 357. (doi:10.1042/BST20110737)

102. Kaeberlein M, McVey M, Guarente L. 1999 The SIR2/3/4 complex and SIR2 alone promote longevity in Saccharomyces cerevisiae by two different mechanisms. *Genes Dev.* **13**, 2570–2580. (doi:10.1101/GAD.13.19.2570)

103. Larson K, Yan SJ, Tsurumi A, Liu J, Zhou J, Gaur K, Guo D, Eickbush TH, Li WX. 2012 Heterochromatin Formation Promotes Longevity and Represses Ribosomal RNA Synthesis. *PLOS Genet.* **8**, e1002473. (doi:10.1371/JOURNAL.PGEN.1002473)

104. Han S, Brunet A. 2012 Histone methylation makes its mark on longevity. *Trends Cell Biol.* **22**, 42–49. (doi:10.1016/J.TCB.2011.11.001)

105. Jin C *et al.* 2011 Histone Demethylase UTX-1 Regulates C. elegans Life Span by Targeting the Insulin/IGF-1 Signaling Pathway. *Cell Metab.* **14**, 161–172. (doi:10.1016/J.CMET.2011.07.001)

106. Zhang W *et al.* 2015 Aging stem cells. A Werner syndrome stem cell model unveils heterochromatin alterations as a driver of human aging. *Science* **348**, 1160–1163. (doi:10.1126/SCIENCE.AAA1356)

107. Scaffidi P, Misteli T. 2006 Lamin A-dependent nuclear defects in human aging. *Science* **312**, 1059–1063. (doi:10.1126/SCIENCE.1127168)

108. Shumaker DK *et al.* 2006 Mutant nuclear lamin A leads to progressive alterations of epigenetic control in premature aging. *Proc. Natl. Acad. Sci. U. S. A.* **103**, 8703–8708. (doi:10.1073/PNAS.0602569103)

109. Dechat T, Pfleghaar K, Sengupta K, Shimi T, Shumaker DK, Solimando L, Goldman RD. 2008

Nuclear lamins: major factors in the structural organization and function of the nucleus and chromatin. *Genes Dev.* **22**, 832–853. (doi:10.1101/GAD.1652708)

110. Kamakaka RT, Biggins S. 2005 Histone variants: deviants? *Genes Dev.* **19**, 295–316. (doi:10.1101/GAD.1272805)

111. Skene PJ, Henikoff S. 2013 Histone variants in pluripotency and disease. *Development* **140**, 2513–2524. (doi:10.1242/DEV.091439)

112. Filipescu D, Müller S, Almouzni G. 2014 Histone H3 variants and their chaperones during development and disease: contributing to epigenetic control. *Annu. Rev. Cell Dev. Biol.* **30**, 615–646. (doi:10.1146/ANNUREV-CELLBIO-100913-013311)

113. Duarte LF *et al.* 2014 Histone H3.3 and its proteolytically processed form drive a cellular senescence programme. *Nat. Commun. 2014 51* **5**, 1–12. (doi:10.1038/ncomms6210)

114. Maze I *et al.* 2015 Critical Role of Histone Turnover in Neuronal Transcription and Plasticity. *Neuron* **87**, 77–94. (doi:10.1016/J.NEURON.2015.06.014)

115. Zhang R *et al.* 2005 Formation of MacroH2A-containing senescence-associated heterochromatin foci and senescence driven by ASF1a and HIRA. *Dev. Cell* **8**, 19–30. (doi:10.1016/J.DEVCEL.2004.10.019)

116. Gaspar-Maia A *et al.* 2013 MacroH2A histone variants act as a barrier upon reprogramming towards pluripotency. *Nat. Commun.* **4**. (doi:10.1038/NCOMMS2582)

117. Kreiling JA *et al.* 2011 Age-associated increase in heterochromatic marks in murine and primate tissues. *Aging Cell* **10**, 292–304. (doi:10.1111/J.1474-9726.2010.00666.X)

118. Chen H, Ruiz PD, McKimpson WM, Novikov L, Kitsis RN, Gamble MJ. 2015 MacroH2A1 and ATM Play Opposing Roles in Paracrine Senescence and the Senescence-Associated Secretory Phenotype. *Mol. Cell* **59**, 719–731. (doi:10.1016/J.MOLCEL.2015.07.011)

119. Kozlowski M, Ladurner AG. 2015 ATM, MacroH2A.1, and SASP: The Checks and Balances of Cellular Senescence. *Mol. Cell* **59**, 713–715. (doi:10.1016/J.MOLCEL.2015.08.010)

120. Adams PD. 2007 Remodeling of chromatin structure in senescent cells and its potential impact on tumor suppression and aging. *Gene* **397**, 84–93. (doi:10.1016/J.GENE.2007.04.020)

121. Narita M, Nũnez S, Heard E, Narita M, Lin AW, Hearn SA, Spector DL, Hannon GJ, Lowe SW. 2003 Rb-mediated heterochromatin formation and silencing of E2F target genes during cellular senescence. *Cell* **113**, 703–716. (doi:10.1016/S0092-8674(03)00401-X)

122. Di Micco R *et al.* 2011 Interplay between oncogene-induced DNA damage response and heterochromatin in senescence and cancer. *Nat. Cell Biol.* **13**, 292–302. (doi:10.1038/NCB2170)

123. Zhang R, Chen W, Adams PD. 2007 Molecular dissection of formation of senescence-associated heterochromatin foci. *Mol. Cell. Biol.* **27**, 2343–2358. (doi:10.1128/MCB.02019-06)

124. Papantonis A. 2021 HMGs as rheostats of chromosomal structure and cell proliferation. *Trends Genet.* **37**, 986–994. (doi:10.1016/j.tig.2021.07.004)

125. Salama R, Sadaie M, Hoare M, Narita M. 2014 Cellular senescence and its effector programs. *Genes Dev.* **28**, 99–114. (doi:10.1101/GAD.235184.113)

126. Ricketts MD, Frederick B, Hoff H, Tang Y, Schultz DC, Rai TS, Vizioli MG, Adams PD, Marmorstein R. 2015 Ubinuclein-1 confers histone H3.3-specific-binding by the HIRA histone chaperone complex. *Nat. Commun.* **6**. (doi:10.1038/NCOMMS8711)

127. Ferbeyre G, De Stanchina E, Querido E, Baptiste N, Prives C, Lowe SW. 2000 PML is induced by oncogenic ras and promotes premature senescence. *Genes Dev.* **14**, 2015. (doi:10.1101/gad.14.16.2015)

128. Bischof O, Kirsh O, Pearson M, Itahana K, Pelicci PG, Dejean A. 2002 Deconstructing PML-induced premature senescence. *EMBO J.* **21**, 3358. (doi:10.1093/EMBOJ/CDF341)

129. Corpet A, Olbrich T, Gwerder M, Fink D, Stucki M. 2014 Dynamics of histone H3.3 deposition in proliferating and senescent cells reveals a DAXX-dependent targeting to PML-NBs important for pericentromeric heterochromatin organization. *Cell Cycle* **13**, 249–267. (doi:10.4161/CC.26988)

130. Reeves R. 2001 Molecular biology of HMGA proteins: Hubs of nuclear function. *Gene* **277**, 63–81. (doi:10.1016/S0378-1119(01)00689-8)

131. Narita M, Narita M, Krizhanovsky V, Nuñez S, Chicas A, Hearn SA, Myers MP, Lowe SW. 2006 A Novel Role for High-Mobility Group A Proteins in Cellular Senescence and Heterochromatin

Formation. *Cell* **126**, 503–514. (doi:10.1016/j.cell.2006.05.052)

132. Funayama R, Saito M, Tanobe H, Ishikawa F. 2006 Loss of linker histone H1 in cellular senescence. *J. Cell Biol.* **175**, 869–880. (doi:10.1083/JCB.200604005)

133. Chandra T *et al.* 2012 Independence of repressive histone marks and chromatin compaction during senescent heterochromatic layer formation. *Mol. Cell* **47**, 203–214. (doi:10.1016/j.molcel.2012.06.010)

134. Shimi T *et al.* 2011 The role of nuclear lamin B1 in cell proliferation and senescence. *Genes Dev.* **25**, 2579–2593. (doi:10.1101/GAD.179515.111)

135. Shah PP *et al.* 2013 Lamin B1 depletion in senescent cells triggers large-scale changes in gene expression and the chromatin landscape. *Genes Dev.* **27**, 1787–1799. (doi:10.1101/GAD.223834.113)

136. Adams PD *et al.* 2013 Lysosome-mediated processing of chromatin in senescence. *J. Cell Biol.* **202**, 129–143. (doi:10.1083/JCB.201212110)

137. Lenain C, Gusyatiner O, Douma S, van den Broek B, Peeper DS. 2015 Autophagy-mediated degradation of nuclear envelope proteins during oncogene-induced senescence. *Carcinogenesis* **36**, 1263–1274. (doi:10.1093/CARCIN/BGV124)

138. Dou Z *et al.* 2015 Autophagy mediates degradation of nuclear lamina. *Nature* **527**, 105–109. (doi:10.1038/NATURE15548)

139. Guelen L *et al.* 2008 Domain organization of human chromosomes revealed by mapping of nuclear lamina interactions. *Nature* **453**, 948–951. (doi:10.1038/NATURE06947)

140. Sadaie M *et al.* 2013 Redistribution of the Lamin B1 genomic binding profile affects rearrangement of heterochromatic domains and SAHF formation during senescence. *Genes Dev.* **27**, 1800–1808. (doi:10.1101/GAD.217281.113)

141. Dang W *et al.* 2014 Inactivation of yeast Isw2 chromatin remodeling enzyme mimics longevity effect of calorie restriction via induction of genotoxic stress response. *Cell Metab.* **19**, 952–966. (doi:10.1016/J.CMET.2014.04.004)

142. Riedel CG *et al.* 2013 DAF-16 employs the chromatin remodeller SWI/SNF to promote stress resistance and longevity. *Nat. Cell Biol.* **15**, 491–501. (doi:10.1038/NCB2720)

143. Pegoraro G, Kubben N, Wickert U, Göhler H, Hoffmann K, Misteli T. 2009 Ageing-related chromatin defects through loss of the NURD complex. *Nat. Cell Biol.* **11**, 1261–1267. (doi:10.1038/NCB1971)

144. Lieberman-Aiden E. 2009 Comprehensive mapping of long range interactions reveals folding principles of the human genome. *Science (80-.).* **326**, 289–293. (doi:10.1126/science.1181369.Comprehensive)

145. Krietenstein N *et al.* 2020 Ultrastructural details of mammalian chromosome architecture. *Mol. Cell* **78**, 554. (doi:10.1016/J.MOLCEL.2020.03.003)

146. Dixon JR, Selvaraj S, Yue F, Kim A, Li Y, Shen Y, Hu M, Liu JS, Ren B. 2012 Topological domains in mammalian genomes identified by analysis of chromatin interactions. *Nature* **485**, 376–380. (doi:10.1038/nature11082)

147. Nora EP *et al.* 2012 Spatial partitioning of the regulatory landscape of the X-inactivation centre. *Nature* **485**, 381–385. (doi:10.1038/nature11049)

148. McCord RP, Nazario-Toole A, Zhang H, Chines PS, Zhan Y, Erdos MR, Collins FS, Dekker J, Cao K. 2013 Correlated alterations in genome organization, histone methylation, and DNA-lamin A/C interactions in Hutchinson-Gilford progeria syndrome. *Genome Res.* **23**, 260–269. (doi:10.1101/GR.138032.112)

149. Dixon JR *et al.* 2015 Chromatin architecture reorganization during stem cell differentiation. *Nat. 2015 5187539* **518**, 331–336. (doi:10.1038/nature14222)

150. Rada-Iglesias A, Grosveld FG, Papantonis A. 2018 Forces driving the three-dimensional folding of eukaryotic genomes. *Mol. Syst. Biol.* **14**, e8214–e8214. (doi:10.1080/11035890609445553)

151. Rowley MJ, Corces VG. 2018 Organizational principles of 3D genome architecture. *Nat. Rev. Genet.* **13**. (doi:10.1038/s41576-018-0060-8)

152. Beagan JA, Phillips-Cremins JE. 2020 On the existence and functionality of topologically associating domains. *Nat. Genet. 2020 521* **52**, 8–16. (doi:10.1038/s41588-019-0561-1)

153. Holwerda S, Laat W de. 2012 Chromatin loops, gene positioning, and gene expression. *Front. Genet.* **3**, 217. (doi:10.3389/fgene.2012.00217)

154. Rao SSP *et al.* 2014 A 3D map of the human genome at kilobase resolution reveals principles

of chromatin looping. *Cell* **159**, 1665–1680. (doi:10.1016/j.cell.2014.11.021)

155. Mariliis Tark-Dame R van D and DWH. 2011 Chromatin folding – from biology to polymer models and back. *J. Cell Sci.* , 839–845. (doi:10.1242/jcs.077628)

156. Jin F *et al.* 2013 A high-resolution map of the three-dimensional chromatin interactome in human cells. *Nat. 2013 5037475* **503**, 290–294. (doi:10.1038/nature12644)

157. Joshi O *et al.* 2015 Dynamic Reorganization of Extremely Long-Range Promoter-Promoter Interactions between Two States of Pluripotency. *Cell Stem Cell* **17**, 748–757. (doi:10.1016/J.STEM.2015.11.010)

158. Kim TH, Abdullaev ZK, Smith AD, Ching KA, Loukinov DI, Green RDD, Zhang MQ, Lobanenkov V V., Ren B. 2007 Analysis of the vertebrate insulator protein CTCF-binding sites in the human genome. *Cell* **128**, 1231–1245. (doi:10.1016/J.CELL.2006.12.048)

159. Ong CT, Corces VG. 2014 CTCF: an architectural protein bridging genome topology and function. *Nat. Rev. Genet. 2014 154* **15**, 234–246. (doi:10.1038/nrg3663)

160. Hansen AS, Hsieh THS, Cattoglio C, Pustova I, Saldaña-Meyer R, Reinberg D, Darzacq X, Tjian R. 2019 Distinct Classes of Chromatin Loops Revealed by Deletion of an RNA-Binding Region in CTCF. *Mol. Cell* **76**, 395-411.e13. (doi:10.1016/J.MOLCEL.2019.07.039/ATTACHMENT/3E081BCF-2002-40A4-9A92-F3BCA38632AC/MMC5.PDF)

161. Rodriguez-hernaez J, Nishana M, Nora EP, Bruneau BG, Furlan-magaril M, Reinberg D. 2019 RNA interactions with CTCF are essential for its proper function. (doi:10.1101/530014)

162. Saldaña-Meyer R *et al.* 2019 RNA Interactions Are Essential for CTCF-Mediated Genome Organization. *Mol. Cell* **76**, 412-422.e5. (doi:10.1016/J.MOLCEL.2019.08.015)

163. Kuang S, Wang L. 2020 Identification and analysis of consensus RNA motifs binding to the genome regulator CTCF. *NAR Genomics Bioinforma.* **2**. (doi:10.1093/nargab/lqaa031)

164. Kellum R, Schedl P. 1991 A position-effect assay for boundaries of higher order chromosomal domains. *Cell* **64**, 941–950. (doi:10.1016/0092-8674(91)90318-S)

165. Sanborn AL *et al.* 2015 Chromatin extrusion explains key features of loop and domain formation in wild-type and engineered genomes. *PNAS* **112**, E6456-65.

(doi:10.1073/pnas.1518552112)

166. Nuebler J, Fudenberg G, Imakaev M, Abdennur N, Mirny LA. 2018 Chromatin organization by an interplay of loop extrusion and compartmental segregation. *Proc. Natl. Acad. Sci. U. S. A.* **115**, E6697–E6706. (doi:10.1073/pnas.1717730115)

167. Banigan EJ, Mirny LA. 2020 Loop extrusion: theory meets single-molecule experiments. *Curr. Opin. Cell Biol.* **64**, 124–138. (doi:10.1016/j.ceb.2020.04.011)

168. de Wit E, Nora EP. 2022 New insights into genome folding by loop extrusion from inducible degron technologies. *Nat. Rev. Genet. 2022* , 1–13. (doi:10.1038/s41576-022-00530-4)

169. Parelho V *et al.* 2008 Cohesins functionally associate with CTCF on mammalian chromosome arms. *Cell* **132**, 422–433. (doi:10.1016/J.CELL.2008.01.011)

170. Peters JM, Tedeschi A, Schmitz J. 2008 The cohesin complex and its roles in chromosome biology. *Genes Dev.* **22**, 3089–3114. (doi:10.1101/GAD.1724308)

171. Baumann K. 2019 Human cohesin extrudes interphase DNA to make loops. *Nat. Rev. Mol. Cell Biol.* **21**, 3. (doi:10.1038/s41580-019-0198-z)

172. Fu Y, Sinha M, Peterson CL, Weng Z. 2008 The insulator binding protein CTCF positions 20 nucleosomes around its binding sites across the human genome. *PLoS Genet.* **4**. (doi:10.1371/JOURNAL.PGEN.1000138)

173. Mawhinney MT, Liu R, Lu F, Maksimoska J, Damico K, Marmorstein R, Lieberman PM, Urbanc B. 2018 CTCF-Induced Circular DNA Complexes Observed by Atomic Force Microscopy. *J. Mol. Biol.* **430**, 759–776. (doi:10.1016/J.JMB.2018.01.012)

174. Franco MM, Prickett AR, Oakey RJ. 2014 The Role of CCCTC-binding factor (CTCF) in genomic imprinting, development, and reproduction. *Biol. Reprod.* **91**, 1–9. (doi:10.1095/BIOLREPROD.114.122945/2434444)

175. Lewis A, Reik W. 2006 How imprinting centres work. *Cytogenet. Genome Res.* **113**, 81–89. (doi:10.1159/000090818)

176. Li T *et al.* 2005 IVF results in de novo DNA methylation and histone methylation at an Igf2-H19 imprinting epigenetic switch. *Mol. Hum. Reprod.* **11**, 631–640. (doi:10.1093/MOLEHR/GAH230)

177. Li T, Hu J-F, Qiu X, Ling J, Chen H, Wang S, Hou A, Vu TH, Hoffman AR. 2008 CTCF regulates allelic expression of Igf2 by orchestrating a promoter-polycomb repressive complex 2 intrachromosomal loop. *Mol. Cell. Biol.* **28**, 6473–6482. (doi:10.1128/MCB.00204-08)

178. Nativio R *et al.* 2009 Cohesin Is Required for Higher-Order Chromatin Conformation at the Imprinted IGF2-H19 Locus. *PLOS Genet.* **5**, e1000739. (doi:10.1371/JOURNAL.PGEN.1000739)

179. Fu VX, Schwarze SR, Kenowski ML, LeBlanc S, Svaren J, Jarrard DF. 2004 A Loss of Insulin-like Growth Factor-2 Imprinting Is Modulated by CCCTC-binding Factor Down-regulation at Senescence in Human Epithelial Cells. *J. Biol. Chem.* **279**, 52218–52226. (doi:10.1074/JBC.M405015200)

180. Hirosue A *et al.* 2012 Quantitative assessment of higher-order chromatin structure of the INK4/ARF locus in human senescent cells. *Aging Cell* **11**, 553–556. (doi:10.1111/J.1474-9726.2012.00809.X)

181. Hou Y, Song Q, Gao S, Zhang X, Wang Y, Liu J, Fu J, Cao M, Wang P. 2021 CTCF Mediates Replicative Senescence Through POLD1. *Front. Cell Dev. Biol.* **9**, 618586. (doi:10.3389/FCELL.2021.618586/FULL)

182. Lake RJ, Boetefuer EL, Won KJ, Fan HY. 2016 The CSB chromatin remodeler and CTCF architectural protein cooperate in response to oxidative stress. *Nucleic Acids Res.* **44**, 2125. (doi:10.1093/NAR/GKV1219)

183. Štros M. 2010 HMGB proteins: interactions with DNA and chromatin. *Biochim. Biophys. Acta* **1799**, 101–113. (doi:10.1016/J.BBAGRM.2009.09.008)

184. Hirose T, Ninomiya K, Nakagawa S, Yamazaki T. 2022 A guide to membraneless organelles and their various roles in gene regulation. *Nat. Rev. Mol. Cell Biol. 2022* , 1–17. (doi:10.1038/s41580-022-00558-8)

185. Tiku V, Antebi A. 2018 Nucleolar Function in Lifespan Regulation. *Trends Cell Biol.* **28**, 662–672. (doi:10.1016/j.tcb.2018.03.007)

186. Bemiller PM, Lee LH. 1978 Nucleolar changes in senescing WI-38 cells. *Mech. Ageing Dev.* **8**, 417–427. (doi:10.1016/0047-6374(78)90041-6)

187. Boisvert FM, Van Koningsbruggen S, Navascués J, Lamond AI. 2007 The multifunctional

nucleolus. *Nat. Rev. Mol. Cell Biol.* **8**, 574–585. (doi:10.1038/NRM2184)

188. Boulon S, Westman BJ, Hutten S, Boisvert FM, Lamond AI. 2010 The nucleolus under stress. *Mol. Cell* **40**, 216–227. (doi:10.1016/J.MOLCEL.2010.09.024)

189. Yankiwski V, Marciniak RA, Guarente L, Neff NF. 2000 Nuclear structure in normal and Bloom syndrome cells. *Proc. Natl. Acad. Sci. U. S. A.* **97**, 5214–5219. (doi:10.1073/PNAS.090525897)

190. Szekely AM, Chen YH, Zhang C, Oshima J, Weissman SM. 2000 Werner protein recruits DNA polymerase delta to the nucleolus. *Proc. Natl. Acad. Sci. U. S. A.* **97**, 11365–11370. (doi:10.1073/PNAS.97.21.11365)

191. Van Den Boom V, Citterio E, Hoogstraten D, Zotter A, Egly JM, Van Cappellen WA, Hoeijmakers JHJ, Houtsmuller AB, Vermeulen W. 2004 DNA damage stabilizes interaction of CSB with the transcription elongation machinery. *J. Cell Biol.* **166**, 27–36. (doi:10.1083/JCB.200401056)

192. Puzianowska-Kuznicka M, Kuznicki J. 2005 Genetic alterations in accelerated ageing syndromes. Do they play a role in natural ageing? *Int. J. Biochem. Cell Biol.* **37**, 947–960. (doi:10.1016/J.BIOCEL.2004.10.011)

193. Colombo E, Marine JC, Danovi D, Falini B, Pelicci PG. 2002 Nucleophosmin regulates the stability and transcriptional activity of p53. *Nat. Cell Biol.* **4**, 529–533. (doi:10.1038/NCB814)

194. Johnson FB, Marciniak RA, Guarente L. 1998 Telomeres, the nucleolus and aging. *Curr. Opin. Cell Biol.* **10**, 332–338. (doi:10.1016/S0955-0674(98)80008-2)

195. Pestov DG, Strezoska Ž, Lau LF. 2001 Evidence of p53-dependent cross-talk between ribosome biogenesis and the cell cycle: effects of nucleolar protein Bop1 on G(1)/S transition. *Mol. Cell. Biol.* **21**, 4246–4255. (doi:10.1128/MCB.21.13.4246-4255.2001)

196. Yuan X, Zhou Y, Casanova E, Chai M, Kiss E, Gröne HJ, Schütz G, Grummt I. 2005 Genetic inactivation of the transcription factor TIF-IA leads to nucleolar disruption, cell cycle arrest, and p53-mediated apoptosis. *Mol. Cell* **19**, 77–87. (doi:10.1016/J.MOLCEL.2005.05.023)

197. Hein N *et al.* 2012 The Nucleolus and Ribosomal Genes in Aging and Senescence. *Senescence* (doi:10.5772/34581)

198. van Damme E, Laukens K, Dang TH, van Ostade X. 2010 A manually curated network of the PML nuclear body interactome reveals an important role for PML-NBs in SUMOylation

dynamics. *Int. J. Biol. Sci.* **6**, 51–67. (doi:10.7150/IJBS.6.51)

199. Pearson M *et al.* 2000 PML regulates p53 acetylation and premature senescence induced by oncogenic Ras. *Nat. 2000 4066792* **406**, 207–210. (doi:10.1038/35018127)

200. Hsu KS, Kao HY. 2018 PML: Regulation and multifaceted function beyond tumor suppression. *Cell Biosci. 2018 81* **8**, 1–21. (doi:10.1186/S13578-018-0204-8)

201. Lallemand-Breitenbach V, de Thé H. 2018 PML nuclear bodies: from architecture to function. *Curr. Opin. Cell Biol.* **52**, 154–161. (doi:10.1016/j.ceb.2018.03.011)

202. Giaccia AJ, Kastan MB. 1998 The complexity of p53 modulation: emerging patterns from divergent signals. *Genes Dev.* **12**, 2973–2983. (doi:10.1101/GAD.12.19.2973)

203. Corpet A, Kleijwegt C, Roubille S, Juillard F, Jacquet K, Texier P, Lomonte P. 2020 PML nuclear bodies and chromatin dynamics: catch me if you can! *Nucleic Acids Res.* **48**, 11890–11912. (doi:10.1093/NAR/GKAA828)

204. Ye X, Zerlanko B, Zhang R, Somaiah N, Lipinski M, Salomoni P, Adams PD. 2007 Definition of pRB- and p53-dependent and -independent steps in HIRA/ASF1a-mediated formation of senescence-associated heterochromatin foci. *Mol. Cell. Biol.* **27**, 2452–2465. (doi:10.1128/MCB.01592-06)

205. Xue Y *et al.* 2003 The ATRX syndrome protein forms a chromatin-remodeling complex with Daxx and localizes in promyelocytic leukemia nuclear bodies. *Proc. Natl. Acad. Sci. U. S. A.* **100**, 10635–10640. (doi:10.1073/PNAS.1937626100)

206. Drané P, Ouararhni K, Depaux A, Shuaib M, Hamiche A. 2010 The death-associated protein DAXX is a novel histone chaperone involved in the replication-independent deposition of H3.3. *Genes Dev.* **24**, 1253. (doi:10.1101/GAD.566910)

207. Sawatsubashi S *et al.* 2010 A histone chaperone, DEK, transcriptionally coactivates a nuclear receptor. *Genes Dev.* **24**, 159–170. (doi:10.1101/GAD.1857410)

208. Fei J *et al.* 2017 Quantitative analysis of multilayer organization of proteins and RNA in nuclear speckles at super resolution. *J. Cell Sci.* **130**, 4180–4192. (doi:10.1242/JCS.206854)

209. Fazal FM, Han S, Parker KR, Kaewsapsak P, Xu J, Boettiger AN, Chang HY, Ting AY. 2019 Atlas of Subcellular RNA Localization Revealed by APEX-Seq. *Cell* **178**, 473-490.e26.

(doi:10.1016/J.CELL.2019.05.027)

210. Dopie J, Sweredoski MJ, Moradian A, Belmont AS. 2020 Tyramide signal amplification mass spectrometry (TSA-MS) ratio identifies nuclear speckle proteins. *J. Cell Biol.* **219**. (doi:10.1083/jcb.201910207)

211. Fei J *et al.* 2017 Quantitative analysis of multilayer organization of proteins and RNA in nuclear speckles at super resolution. *J. Cell Sci.* **130**, 4180–4192. (doi:10.1242/jcs.206854)

212. Wang K, Wang L, Wang J, Chen S, Shi M, Cheng H. 2018 Intronless mRNAs transit through nuclear speckles to gain export competence. *J. Cell Biol.* **217**, 3912–3929. (doi:10.1083/jcb.201801184)

213. Ilik İA, Malszycki M, Lübke AK, Schade C, Meierhofer D, Aktaş T. 2020 SON and SRRM2 are essential for nuclear speckle formation. *Elife* **9**. (doi:10.7554/eLife.60579)

214. Ishov AM, Gurumurthy A, Bungert J. 2020 Coordination of transcription, processing, and export of highly expressed RNAs by distinct biomolecular condensates. *Emerg. Top. Life Sci.* **4**, 281–291. (doi:10.1042/ETLS20190160)

215. Ha M. 2020 Transcription boosting by nuclear speckles. *Nat. Rev. Mol. Cell Biol.* **21**, 64–65. (doi:10.1038/s41580-019-0203-6)

216. Ilık İA, Aktaş T. 2021 Nuclear speckles: dynamic hubs of gene expression regulation. *FEBS J.* , 1–12. (doi:10.1111/febs.16117)

217. Spector DL, Lamond AI. 2011 Nuclear Speckles. *Cold Spring Harb. Perspect. Biol.* **3**. (doi:10.1101/CSHPERSPECT.A000646)

218. Saitoh N, Spahr CS, Patterson SD, Bubulya P, Neuwald AF, Spector DL. 2004 Proteomic analysis of interchromatin granule clusters. *Mol. Biol. Cell* **15**, 3876–3890. (doi:10.1091/mbc.e04-03-0253)

219. Hall LL, Smith KP, Byron M, Lawrence JB. 2006 Molecular anatomy of a speckle. *Anat Rec A Discov Mol Cell Evol Biol* **288**, 664–675. (doi:10.1002/ar.a.20336)

220. Chen W, Yan Z, Li S, Huang N, Huang X, Zhang J, Zhong S. 2018 RNAs as Proximity-Labeling Media for Identifying Nuclear Speckle Positions Relative to the Genome. *iScience* **4**, 204–215. (doi:10.1016/j.isci.2018.06.005)

221. Chen Y *et al.* 2018 Mapping 3D genome organization relative to nuclear compartments using TSA-Seq as a cytological ruler. *J. Cell Biol.* **217**, 4025–4048. (doi:10.1083/jcb.201807108)

222. Chen Y, Belmont AS. 2019 Genome organization around nuclear speckles. *Curr. Opin. Genet. Dev.* **55**, 91–99. (doi:10.1016/J.GDE.2019.06.008)

223. Zhang L, Zhang Y, Chen Y, Gholamalamdari O, Wang Y, Ma J, Belmont AS. 2021 TSA-seq reveals a largely conserved genome organization relative to nuclear speckles with small position changes tightly correlated with gene expression changes. *Genome Res.* **31**, 251–264. (doi:10.1101/GR.266239.120)

224. Barutcu AR *et al.* 2022 Systematic mapping of nuclear domain-associated transcripts reveals speckles and lamina as hubs of functionally distinct retained introns. *Mol. Cell* **82**, 1035-1052.e9. (doi:10.1016/j.molcel.2021.12.010)

225. Hu S, Lv P, Yan Z, Wen B. 2019 Disruption of nuclear speckles reduces chromatin interactions in active compartments. *Epigenetics Chromatin* **12**, 43. (doi:10.1186/s13072-019-0289-2)

226. Szabo Q, Bantignies F, Cavalli G. 2019 Principles of genome folding into topologically associating domains. *Sci. Adv.* **5**, eaaw1668–eaaw1668. (doi:10.1126/sciadv.aaw1668)

227. Chen Y *et al.* 2018 Mapping 3D genome organization relative to nuclear compartments using TSA-Seq as a cytological ruler. *J. Cell Biol.* **217**, 4025–4048. (doi:10.1083/jcb.201807108)

228. Kim J, Venkata NC, Hernandez Gonzalez GA, Khanna N, Belmont AS. 2019 Gene expression amplification by nuclear speckle association. *J. Cell Biol.* **219**, jcb.201904046-jcb.201904046. (doi:10.1083/jcb.201904046)

229. Vassilev LT *et al.* 2004 In Vivo Activation of the p53 Pathway by Small-Molecule Antagonists of MDM2. *Science (80-.).* **303**, 844–848. (doi:10.1126/SCIENCE.1092472/SUPPL_FILE/VASSILEV.SOM.PDF)

230. Alexander KA *et al.* 2021 p53 mediates target gene association with nuclear speckles for amplified RNA expression. *Mol. Cell* **81**, 1666-1681.e6. (doi:10.1016/J.MOLCEL.2021.03.006/ATTACHMENT/3FFF23EF-5EF4-4D6D-A855-D6E922DF68D1/MMC3.XLSX)

231. Zhang J, Ao Y, Zhang Z, Mo Y, Peng L, Jiang Y, Wang Z, Liu B. 2020 Lamin A safeguards the m6A

methylase METTL14 nuclear speckle reservoir to prevent cellular senescence. *Aging Cell* **19**. (doi:10.1111/ACEL.13215)

232. Zhang Q *et al.* 2021 Nuclear speckle specific hnRNP D-like prevents age- and AD-related cognitive decline by modulating RNA splicing. *Mol. Neurodegener.* **16**, 1–19. (doi:10.1186/S13024-021-00485-W/FIGURES/8)

233. Mazin P *et al.* 2013 Widespread splicing changes in human brain development and aging. *Mol. Syst. Biol.* **9**, 633. (doi:10.1038/MSB.2012.67)

234. Schmeer C, Kretz A, Wengerodt D, Stojiljkovic M, Witte OW. 2019 Dissecting Aging and Senescence—Current Concepts and Open Lessons. *Cells 2019, Vol. 8, Page 1446* **8**, 1446. (doi:10.3390/CELLS8111446)

235. Lee S, Nam Y, Koo JY oun., Lim D, Park J, Ock J, Kim J, Suk K, Park SB u. 2014 A small molecule binding HMGB1 and HMGB2 inhibits microglia-mediated neuroinflammation. *Nat. Chem. Biol.* **10**, 1055–1060. (doi:10.1038/nchembio.1669)

236. Krtolica A, Parrinello S, Lockett S, Desprez PY, Campisi J. 2001 Senescent fibroblasts promote epithelial cell growth and tumorigenesis: a link between cancer and aging. *Proc. Natl. Acad. Sci. U. S. A.* **98**, 12072–12077. (doi:10.1073/PNAS.211053698)

237. Dimri GP *et al.* 1995 A biomarker that identifies senescent human cells in culture and in aging skin in vivo. *Proc. Natl. Acad. Sci. U. S. A.* **92**, 9363–9367. (doi:10.1073/PNAS.92.20.9363)

238. Franzen J, Zirkel A, Blake J, Rath B, Benes V, Papantonis A, Wagner W. 2017 Senescence-associated DNA methylation is stochastically acquired in subpopulations of mesenchymal stem cells. *Aging Cell* **16**, 183–191. (doi:10.1111/ACEL.12544)

239. Melnik S, Caudron-Herger M, Brant L, Carr IM, Rippe K, Cook PR, Papantonis A. 2016 Isolation of the protein and RNA content of active sites of transcription from mammalian cells. *Nat. Protoc. 2016 113* **11**, 553–565. (doi:10.1038/nprot.2016.032)

240. Rai TS *et al.* 2014 HIRA orchestrates a dynamic chromatin landscape in senescence and is required for suppression of neoplasia. *Genes Dev.* **28**, 2712–2725. (doi:10.1101/GAD.247528.114)

241. Coppé JP, Desprez PY, Krtolica A, Campisi J. 2010 The senescence-associated secretory

phenotype: the dark side of tumor suppression. *Annu. Rev. Pathol.* **5**, 99–118. (doi:10.1146/ANNUREV-PATHOL-121808-102144)

242. Hansen AS, Pustova I, Cattoglio C, Tjian R, Darzacq X. 2017 CTCF and cohesin regulate chromatin loop stability with distinct dynamics. *Elife* **6**. (doi:10.7554/ELIFE.25776.001)

243. DeMare LE, Leng J, Cotney J, Reilly SK, Yin J, Sarro R, Noonan JP. 2013 The genomic landscape of cohesin-associated chromatin interactions. *Genome Res.* **23**, 1224. (doi:10.1101/GR.156570.113)

244. Robbins PD *et al.* 2020 Annual Review of Pharmacology and Toxicology Senolytic Drugs: Reducing Senescent Cell Viability to Extend Health Span. (doi:10.1146/annurev-pharmtox-050120)

245. Chaib S, Tchkonia T, Kirkland JL. 2022 Cellular senescence and senolytics: the path to the clinic. *Nat. Med. 2022 288* **28**, 1556–1568. (doi:10.1038/s41591-022-01923-y)

246. Lee HH, Im SH, Ahn S, Bae MA, Park SB, Kim SK, Song JS. 2019 A validated UPLC-MS/MS method for pharmacokinetic study of inflachromene, a novel microglia inhibitor. *J. Pharm. Biomed. Anal.* **166**, 183–188. (doi:10.1016/j.jpba.2019.01.013)

247. Cho W *et al.* 2017 Treatment of Sepsis Pathogenesis with High Mobility Group Box Protein 1-Regulating Anti-inflammatory Agents. *J. Med. Chem.* **60**, 170–179. (doi:10.1021/ACS.JMEDCHEM.6B00954/SUPPL_FILE/JM6B00954_SI_002.CSV)

248. Chung H, Hong SJ, Choi SW, Koo JY, Kim M, Kim HJ, Park SB, Park CG. 2019 High mobility group box 1 secretion blockade results in the reduction of early pancreatic islet graft loss. *Biochem. Biophys. Res. Commun.* **514**, 1081–1086. (doi:10.1016/j.bbrc.2019.05.003)

249. Bucevičius J, Kostiuk G, Gerasimaitė R, Gilat T, Lukinavičius G. 2020 Enhancing the biocompatibility of rhodamine fluorescent probes by a neighbouring group effect. *Chem. Sci.* **11**, 7313–7323. (doi:10.1039/D0SC02154G)

250. Schindelin J *et al.* 2012 Fiji: an open-source platform for biological-image analysis. *Nat. Methods 2012 97* **9**, 676–682. (doi:10.1038/nmeth.2019)

251. Dobin A, Davis CA, Schlesinger F, Drenkow J, Zaleski C, Jha S, Batut P, Chaisson M, Gingeras TR. 2013 STAR: ultrafast universal RNA-seq aligner. *Bioinformatics* **29**, 15–21.

(doi:10.1093/BIOINFORMATICS/BTS635)

252. Liao Y, Smyth GK, Shi W. 2014 featureCounts: an efficient general purpose program for assigning sequence reads to genomic features. *Bioinformatics* **30**, 923–930. (doi:10.1093/BIOINFORMATICS/BTT656)

253. Risso D, Ngai J, Speed TP, Dudoit S. 2014 Normalization of RNA-seq data using factor analysis of control genes or samples. *Nat. Biotechnol.* **32**, 896–902. (doi:10.1038/NBT.2931)

254. Love MI, Huber W, Anders S. 2014 Moderated estimation of fold change and dispersion for RNA-seq data with DESeq2. *Genome Biol.* **15**. (doi:10.1186/S13059-014-0550-8)

255. Zhou Y, Zhou B, Pache L, Chang M, Khodabakhshi AH, Tanaseichuk O, Benner C, Chanda SK. 2019 Metascape provides a biologist-oriented resource for the analysis of systems-level datasets. *Nat. Commun.* **10**. (doi:10.1038/S41467-019-09234-6)

256. Madsen JGS, Schmidt SF, Larsen BD, Loft A, Nielsen R, Mandrup S. 2015 iRNA-seq: computational method for genome-wide assessment of acute transcriptional regulation from total RNA-seq data. *Nucleic Acids Res.* **43**, e40. (doi:10.1093/NAR/GKU1365)

257. Ivanov IP, Shin BS, Loughran G, Tzani I, Young-Baird SK, Cao C, Atkins JF, Dever TE. 2018 Polyamine Control of Translation Elongation Regulates Start Site Selection on Antizyme Inhibitor mRNA via Ribosome Queuing. *Mol. Cell* **70**, 254-264.e6. (doi:10.1016/J.MOLCEL.2018.03.015)

258. Oertlin C, Lorent J, Murie C, Furic L, Topisirovic I, Larsson O. 2019 Generally applicable transcriptome-wide analysis of translation using anota2seq. *Nucleic Acids Res.* **47**, E70. (doi:10.1093/NAR/GKZ223)

259. Langmead B, Salzberg SL. 2012 Fast gapped-read alignment with Bowtie 2. *Nat. Methods 2012 94* **9**, 357–359. (doi:10.1038/nmeth.1923)

260. Grant CE, Bailey TL, Noble WS. 2011 FIMO: scanning for occurrences of a given motif. *Bioinformatics* **27**, 1017–1018. (doi:10.1093/BIOINFORMATICS/BTR064)

261. Ramírez F, Dündar F, Diehl S, Grüning BA, Manke T. 2014 deepTools: a flexible platform for exploring deep-sequencing data. *Nucleic Acids Res.* **42**. (doi:10.1093/NAR/GKU365)

262. Hsieh T-HS, Cattoglio C, Slobodyanyuk E, Hansen AS, Rando OJ, Tjian R, Darzacq X. 2020

Resolving the 3D Landscape of Transcription-Linked Mammalian Chromatin Folding. (doi:10.1016/j.molcel.2020.03.002)

263. Martello R, Leutert M, Jungmichel S, Bilan V, Larsen SC, Young C, Hottiger MO, Nielsen ML. 2016 Proteome-wide identification of the endogenous ADP-ribosylome of mammalian cells and tissue. *Nat. Commun. 2016 71* **7**, 1–13. (doi:10.1038/ncomms12917)

264. Herbig U, Jobling WA, Chen BPC, Chen DJ, Sedivy JM. 2004 Telomere shortening triggers senescence of human cells through a pathway involving ATM, p53, and p21(CIP1), but not p16(INK4a). *Mol. Cell* **14**, 501–513. (doi:10.1016/S1097-2765(04)00256-4)

265. Belton JM, McCord RP, Gibcus JH, Naumova N, Zhan Y, Dekker J. 2012 Hi-C: A comprehensive technique to capture the conformation of genomes. *Methods* **58**, 268–276. (doi:10.1016/J.YMETH.2012.05.001)

266. Chiang M, Michieletto D, Brackley CA, Rattanavirotkul N, Mohammed H, Marenduzzo D, Chandra T. 2019 Polymer Modeling Predicts Chromosome Reorganization in Senescence. *Cell Rep.* **28**, 3212-3223.e6. (doi:10.1016/j.celrep.2019.08.045)

267. Phillips JE, Corces VG. 2009 CTCF: Master Weaver of the Genome. *Cell* **137**, 1194–1211. (doi:10.1016/J.CELL.2009.06.001)

268. Dekker J, Marti-Renom MA, Mirny LA. 2013 Exploring the three-dimensional organization of genomes: interpreting chromatin interaction data. *Nat. Rev. Genet.* **14**, 390–403. (doi:10.1038/nrg3454)

269. Pombo A, Dillon N. 2015 Three-dimensional genome architecture: Players and mechanisms. *Nat. Rev. Mol. Cell Biol.* **16**, 245–257. (doi:10.1038/nrm3965)

270. Fu VX, Schwarze SR, Kenowski ML, LeBlanc S, Svaren J, Jarrard DF. 2004 A loss of insulin-like growth factor-2 imprinting is modulated by CCCTC-binding factor down-regulation at senescence in human epithelial cells. *J. Biol. Chem.* **279**, 52218–52226. (doi:10.1074/JBC.M405015200)

271. Li J *et al.* 2019 An alternative CTCF isoform antagonizes canonical CTCF occupancy and changes chromatin architecture to promote apoptosis. *Nat. Commun.* **10**, 1535. (doi:10.1038/s41467-019-08949-w)

272. Han D, Chen Q, Shi J, Zhang F, Yu X. 2017 CTCF participates in DNA damage response via poly(ADP-ribosyl)ation. *Sci. Rep.* **7**, 43530. (doi:10.1038/srep43530)

273. Caiafa P, Zlatanova J. 2009 CCCTC-binding factor meets poly(ADP-ribose) polymerase-1. *J. Cell. Physiol.* **219**, 265–270. (doi:10.1002/jcp.21691)

274. Tiku V *et al.* 2017 Small nucleoli are a cellular hallmark of longevity. *Nat. Commun.* **8**, 16083. (doi:10.1038/ncomms16083)

275. Lehman BJ, Lopez-Diaz FJ, Santisakultarm TP, Fang L, Shokhirev MN, Diffenderfer KE, Manor U, Emerson BM. 2021 Dynamic regulation of CTCF stability and sub-nuclear localization in response to stress. *PLOS Genet.* **17**, e1009277. (doi:10.1371/journal.pgen.1009277)

276. Dion W *et al.* 2022 Four-dimensional nuclear speckle phase separation dynamics regulate proteostasis. *Sci. Adv.* **8**. (doi:10.1126/SCIADV.ABL4150/SUPPL_FILE/SCIADV.ABL4150_MOVIES_S1_TO_S3.ZIP)

277. Urbanek MO, Jazurek M, Switonski PM, Figura G, Krzyzosiak WJ. 2016 Nuclear speckles are detention centers for transcripts containing expanded CAG repeats. *Biochim. Biophys. Acta - Mol. Basis Dis.* **1862**, 1513–1520. (doi:10.1016/J.BBADIS.2016.05.015)

278. Galganski L, Urbanek MO, Krzyzosiak WJ. 2017 Nuclear speckles: molecular organization, biological function and role in disease. *Nucleic Acids Res.* **45**, 10350–10368. (doi:10.1093/nar/gkx759)

279. Hyman AA, Weber CA, Ulicher FJ¨. 2014 Liquid-Liquid Phase Separation in Biology. *Annu. Rev. Cell Dev. Biol* **30**, 39–58. (doi:10.1146/annurev-cellbio-100913-013325)

280. Alberti S. 2017 Phase separation in biology. *Curr. Biol.* **27**, R1097–R1102. (doi:10.1016/J.CUB.2017.08.069)

281. Wright RHG, Le Dily F, Beato M. 2019 ATP, Mg 2+ , Nuclear Phase Separation, and Genome Accessibility. *Trends Biochem. Sci.* **xx**, 1–10. (doi:10.1016/j.tibs.2019.03.001)

282. Kroschwald S, Maharana S, Simon A. 2017 Hexanediol: a chemical probe to investigate the material properties of membrane-less compartments. *Matters* (doi:10.19185/MATTERS.201702000010)

283. Chen JH, Ozanne SE. 2006 Deep senescent human fibroblasts show diminished DNA damage

foci but retain checkpoint capacity to oxidative stress. *FEBS Lett.* **580**, 6669–6673. (doi:10.1016/J.FEBSLET.2006.11.023)

284. Mészáros B, Simon I, Dosztányi Z. 2009 Prediction of Protein Binding Regions in Disordered Proteins. *PLOS Comput. Biol.* **5**, e1000376. (doi:10.1371/JOURNAL.PCBI.1000376)

285. Dosztányi Z. 2018 Prediction of protein disorder based on IUPred. *Protein Sci.* **27**, 331–340. (doi:10.1002/PRO.3334)

286. Samwer M *et al.* 2017 DNA Cross-Bridging Shapes a Single Nucleus from a Set of Mitotic Chromosomes. *Cell* , 956–972. (doi:10.1016/j.cell.2017.07.038)

287. Samson C *et al.* 2018 Structural analysis of the ternary complex between lamin A/C, BAF and emerin identifies an interface disrupted in autosomal recessive progeroid diseases. *Nucleic Acids Res.* **46**, 10460–10473. (doi:10.1093/nar/gky736)

288. Honkanen RE. 1993 Cantharidin, another natural toxin that inhibits the activity of serine/threonine protein phosphatases types 1 and 2A. *FEBS Lett.* **330**, 283–286. (doi:10.1016/0014-5793(93)80889-3)

289. Mitsuhashi S, Matsuura N, Ubukata M, Oikawa H, Shima H, Kikuchi K. 2001 Tautomycetin Is a Novel and Specific Inhibitor of Serine/Threonine Protein Phosphatase Type 1, PP1. *Biochem. Biophys. Res. Commun.* **287**, 328–331. (doi:10.1006/BBRC.2001.5596)

290. Brangwynne CP. 2011 Soft active aggregates: mechanics, dynamics and self-assembly of liquid-like intracellular protein bodies. *Soft Matter* **7**, 3052–3059. (doi:10.1039/C0SM00981D)

291. Zhu L, Brangwynne CP. 2015 Nuclear bodies: the emerging biophysics of nucleoplasmic phases. *Curr. Opin. Cell Biol.* **34**, 23–30. (doi:10.1016/j.ceb.2015.04.003)

292. Liao SE, Regev O. 2021 Splicing at the phase-separated nuclear speckle interface: a model. *Nucleic Acids Res.* **49**, 636–645. (doi:10.1093/NAR/GKAA1209)

293. Liu S *et al.* 2021 USP42 drives nuclear speckle mRNA splicing via directing dynamic phase separation to promote tumorigenesis. *Cell Death Differ. 2021 288* **28**, 2482–2498. (doi:10.1038/s41418-021-00763-6)

294. Leung AKL. 2014 Poly(ADP-ribose): An organizer of cellular architecture. *JBC* **205**, 613–619. (doi:10.1083/jcb.201402114)

295. Gibson BA, Kraus WL. 2012 New insights into the molecular and cellular functions of poly(ADP-ribose) and PARPs. *Nat. Rev. Mol. Cell Biol.* **13**, 411–424. (doi:10.1038/NRM3376)

296. Leung AKL, Vyas S, Rood JE, Bhutkar A, Sharp PA, Chang P. 2011 Poly(ADP-Ribose) Regulates Stress Responses and MicroRNA Activity in the Cytoplasm. *Mol. Cell* **42**, 489–499. (doi:10.1016/j.molcel.2011.04.015)

297. Gagné JP, Isabelle M, Lo KS, Bourassa S, Hendzel MJ, Dawson VL, Dawson TM, Poirier GG. 2008 Proteome-wide identification of poly(ADP-ribose) binding proteins and poly(ADP-ribose)-associated protein complexes. *Nucleic Acids Res.* **36**, 6959–6976. (doi:10.1093/NAR/GKN771)

298. Jungmichel S, Rosenthal F, Altmeyer M, Lukas J, Hottiger MO, Nielsen ML. 2013 Proteome-wide identification of poly(ADP-Ribosyl)ation targets in different genotoxic stress responses. *Mol. Cell* **52**, 272–285. (doi:10.1016/j.molcel.2013.08.026)

299. Zhang Y, Wang J, Ding M, Yu Y. 2013 Site-specific characterization of the Asp- and Glu-ADP-ribosylated proteome. *Nat. Methods 2013 1010* **10**, 981–984. (doi:10.1038/nmeth.2603)

300. Farrar D, Rai S, Chernukhin I, Jagodic M, Ito Y, Yammine S, Ohlsson R, Murrell A, Klenova E. 2010 Mutational Analysis of the Poly(ADP-Ribosyl)ation Sites of the Transcription Factor CTCF Provides an Insight into the Mechanism of Its Regulation by Poly(ADP-Ribosyl)ation. *Mol. Cell. Biol.* **30**, 1199–1216. (doi:10.1128/MCB.00827-09)

301. Kaya-Okur HS, Wu SJ, Codomo CA, Pledger ES, Bryson TD, Henikoff JG, Ahmad K, Henikoff S. 2019 CUT&Tag for efficient epigenomic profiling of small samples and single cells. *Nat. Commun. 2019 101* **10**, 1–10. (doi:10.1038/s41467-019-09982-5)

302. Nordin A, Zambanini G, Pagella P, Cantù C. 2022 The CUT & RUN Blacklist of Problematic Regions of the Genome. **2022**.

303. Paulsen J, Liyakat Ali TM, Collas P. 2018 Computational 3D genome modeling using Chrom3D. *Nat. Protoc.* **13**, 1137–1152. (doi:10.1038/NPROT.2018.009)

304. Brown JM *et al.* 2008 Association between active genes occurs at nuclear speckles and is modulated by chromatin environment. *J. Cell Biol.* **182**, 1083–1097. (doi:10.1083/jcb.200803174)

305. Khanna N, Hu Y, Belmont AS. 2014 HSP70 transgene directed motion to nuclear speckles

facilitates heat shock activation. *Curr. Biol.* **24**, 1138–1144. (doi:10.1016/j.cub.2014.03.053)

306. Zhou R *et al.* 2022 CTCF DNA-binding domain undergoes dynamic and selective protein–protein interactions. *iScience* **25**, 105011. (doi:10.1016/J.ISCI.2022.105011/ATTACHMENT/860CB794-61E1-4DA9-ADB8-0B6A5C959253/MMC6.XLSX)

307. Kargapolova Y *et al.* 2021 Overarching control of autophagy and DNA damage response by CHD6 revealed by modeling a rare human pathology. *Nat. Commun. 2021 121* **12**, 1–15. (doi:10.1038/s41467-021-23327-1)

308. Stovner EB, Sætrom P. 2019 epic2 efficiently finds diffuse domains in ChIP-seq data. *Bioinformatics* **35**, 4392–4393. (doi:10.1093/BIOINFORMATICS/BTZ232)

309. Meers MP, Bryson TD, Henikoff JG, Henikoff S. 2019 Improved cut&run chromatin profiling tools. *Elife* **8**. (doi:10.7554/ELIFE.46314.001)

310. Naumova N, Imakaev M, Fudenberg G, Zhan Y, Lajoie BR, Mirny LA, Dekker J. 2013 Organization of the mitotic chromosome. *Science* **342**, 948–953. (doi:10.1126/SCIENCE.1236083)

311. Gibcus JH *et al.* 2018 A pathway for mitotic chromosome formation. *Science (80-.).* **359**. (doi:10.1126/SCIENCE.AAO6135/SUPPL_FILE/AAO6135S1.MP4)

312. Zhang H *et al.* 2019 Chromatin structure dynamics during the mitosis-to-G1 phase transition. *Nature* **576**, 158–162. (doi:10.1038/s41586-019-1778-y)

313. Yokoyama Y, Zhu H, Zhang R, Noma KI. 2015 A novel role for the condensin II complex in cellular senescence. *Cell Cycle* **14**, 2160–2170. (doi:10.1080/15384101.2015.1049778/SUPPL_FILE/KCCY_A_1049778_SM3224.DOCX)

314. Li Y *et al.* 2018 Novel role of PKR in palmitate-induced Sirt1 inactivation and endothelial cell senescence. *Am. J. Physiol. - Hear. Circ. Physiol.* **315**, H571–H580. (doi:10.1152/AJPHEART.00038.2018/ASSET/IMAGES/LARGE/ZH40091825660006.JPEG)

315. Kim YH, Kwak MS, Shin JM, Hayuningtyas RA, Choi JE, Shin JS. 2018 Inflachromene inhibits autophagy through modulation of Beclin 1 activity. *J. Cell Sci.* **131**. (doi:10.1242/jcs.211201)

316. Chung H, Nam H, Nguyen-Phuong T, Jang J, Hong SJ, Choi SW, Park SB, Park CG. 2021 The blockade of cytoplasmic HMGB1 modulates the autophagy/apoptosis checkpoint in stressed

islet beta cells. *Biochem. Biophys. Res. Commun.* **534**, 1053–1058. (doi:10.1016/j.bbrc.2020.10.038)

317. Iachettini S, Ciccarone F, Maresca C, D' Angelo C, Petti E, Di Vito S, Ciriolo MR, Zizza P, Biroccio A. 2022 The telomeric protein TERF2/TRF2 impairs HMGB1-driven autophagy. *Autophagy* (doi:10.1080/15548627.2022.2138687/SUPPL_FILE/KAUP_A_2138687_SM5865.DOCX)

318. Dixon JR, Gorkin DU, Ren B. 2016 Chromatin Domains: the Unit of Chromosome Organization. *Mol. Cell* **62**, 668. (doi:10.1016/J.MOLCEL.2016.05.018)

319. Zlatanova J, Caiafa P. 2009 CTCF and its protein partners: divide and rule? *J. Cell Sci.* **122**, 1275–1284. (doi:10.1242/jcs.039990)

320. Boeynaems S *et al.* 2018 Protein Phase Separation: A New Phase in Cell Biology. *Trends Cell Biol.* **28**, 420–435. (doi:10.1016/J.TCB.2018.02.004)

321. von Appen A, LaJoie D, Johnson IE, Trnka MJ, Pick SM, Burlingame AL, Ullman KS, Frost A. 2020 LEM2 phase separation governs ESCRT-mediated nuclear envelope reformation. *Nature* **582**, 115. (doi:10.1038/S41586-020-2232-X)

322. Fay MM, Anderson PJ. 2018 The Role of RNA in Biological Phase Separations. *J. Mol. Biol.* **430**, 4685–4701. (doi:10.1016/j.jmb.2018.05.003)

323. Garcia-Jove Navarro M, Kashida S, Chouaib R, Souquere S, Pierron G, Weil D, Gueroui Z. 2019 RNA is a critical element for the sizing and the composition of phase-separated RNA–protein condensates. *Nat. Commun.* **10**, 3230. (doi:10.1038/s41467-019-11241-6)

324. Guerrero G, Narendra V, Gonza E, Reinberg D, Bonasio R. 2014 CTCF regulates the human p53 gene through direct interaction with its natural antisense transcript , Wrap53. , 723–734. (doi:10.1101/gad.236869.113.with)

325. Saldaña-Meyer R *et al.* 2019 RNA Interactions Are Essential for CTCF-Mediated Genome Organization. *Mol. Cell* **76**, 412-422.e5. (doi:10.1016/J.MOLCEL.2019.08.015)

326. Li F, Chen X, Nakai K, Sun X, Zhang J, Cao C. 2022 CTCF and Its Partners: Shaper of 3D Genome during Development. *Genes 2022, Vol. 13, Page 1383* **13**, 1383. (doi:10.3390/GENES13081383)

327. Delgado MD, Chernukhin I V., Bigas A, Klenova EM, León J. 1999 Differential expression and phosphorylation of CTCF, a c-myc transcriptional regulator, during differentiation of human

myeloid cells. *FEBS Lett.* **444**, 5–10. (doi:10.1016/S0014-5793(99)00013-7)

328. Del Rosario BC, Kriz AJ, Del Rosario AM, Anselmo A, Fry CJ, White FM, Sadreyev RI, Lee JT. 2019 Exploration of CTCF post-translation modifications uncovers Serine-224 phosphorylation by PLK1 at pericentric regions during the G2/M transition. *Elife* **8**. (doi:10.7554/ELIFE.42341)

329. Kim H-S, Fernandes G, Lee C-W. 2016 Protein Phosphatases Involved in Regulating Mitosis: Facts and Hypotheses. *Mol. Cells* **39**, 654–62. (doi:10.14348/molcells.2016.0214)

330. Wlodarchak N, Xing Y. 2016 PP2A as a master regulator of the cell cycle. *Crit. Rev. Biochem. Mol. Biol.* **51**, 162–184. (doi:10.3109/10409238.2016.1143913)

331. Brautigan DL, Shenolikar S. 2018 Protein Serine/Threonine Phosphatases: Keys to Unlocking Regulators and Substrates. *Annu. Rev. Biochem.* **87**, 921–964. (doi:10.1146/ANNUREV-BIOCHEM-062917-012332)

332. Moura M, Conde C. 2019 Phosphatases in Mitosis: Roles and Regulation. *Biomolecules* **9**. (doi:10.3390/biom9020055)

333. de Castro IJ *et al.* 2017 Repo-Man/PP1 regulates heterochromatin formation in interphase. *Nat. Commun.* **8**, 14048. (doi:10.1038/ncomms14048)

334. Misteli T, Spector DL. 1996 Serine/threonine phosphatase 1 modulates the subnuclear distribution of pre-mRNA splicing factors. *Mol. Biol. Cell* **7**, 1559–1572. (doi:10.1091/mbc.7.10.1559)

335. Corkery DP, Holly AC, Lahsaee S, Dellaire G. 2015 Connecting the speckles: Splicing kinases and their role in tumorigenesis and treatment response. *Nucleus* **6**, 279–288. (doi:10.1080/19491034.2015.1062194)

336. Pavlaki I, Docquier F, Chernukhin I, Kita G, Gretton S, Clarkson CT, Teif VB, Klenova E. 2018 Poly(ADP-ribosyl)ation associated changes in CTCF-chromatin binding and gene expression in breast cells. *Biochim. Biophys. Acta - Gene Regul. Mech.* **1861**, 718–730. (doi:10.1016/J.BBAGRM.2018.06.010)

337. Tanwar VS, Jose CC, Cuddapah S. 2019 Role of CTCF in DNA damage response. *Mutat. Res.* **780**, 61–68. (doi:10.1016/j.mrrev.2018.02.002)

338. Lang F *et al.* 2017 CTCF prevents genomic instability by promoting homologous recombination-

directed DNA double-strand break repair. *Proc. Natl. Acad. Sci. U. S. A.* **114**, 10912–10917. (doi:10.1073/pnas.1704076114)

339. Hilmi K *et al.* 2017 CTCF facilitates DNA double-strand break repair by enhancing homologous recombination repair. *Sci. Adv.* **3**, e1601898. (doi:10.1126/sciadv.1601898)

340. Hwang SY *et al.* 2019 CTCF cooperates with CtIP to drive homologous recombination repair of double-strand breaks. *Nucleic Acids Res.* **47**, 9160–9179. (doi:10.1093/nar/gkz639)

341. Rogakou EP, Pilch DR, Orr AH, Ivanova VS, Bonner WM. 1998 DNA double-stranded breaks induce histone H2AX phosphorylation on serine 139. *J. Biol. Chem.* **273**, 5858–5868. (doi:10.1074/JBC.273.10.5858)

342. Natale F *et al.* 2017 Identification of the elementary structural units of the DNA damage response. *Nat. Commun.* **8**, 15760. (doi:10.1038/ncomms15760)

343. Bolderson E *et al.* 2019 Barrier-to-autointegration factor 1 (Banf1) regulates poly [ADP-ribose] polymerase 1 (PARP1) activity following oxidative DNA damage. *Nat. Commun.* **10**, 1–12. (doi:10.1038/s41467-019-13167-5)

344. Spegg V, Altmeyer M. 2021 Biomolecular condensates at sites of DNA damage: More than just a phase. *DNA Repair (Amst).* **106**, 103179. (doi:10.1016/J.DNAREP.2021.103179)

345. Mamberti S, Pabba MK, Rapp A, Cristina Cardoso M, Scholz M. 2022 The Chromatin Architectural Protein CTCF Is Critical for Cell Survival upon Irradiation-Induced DNA Damage. *Int. J. Mol. Sci.* **23**, 3896. (doi:10.3390/IJMS23073896/S1)

346. Miné-Hattab J, Liu S, Taddei A. 2022 Repair Foci as Liquid Phase Separation: Evidence and Limitations. *Genes (Basel).* **13**, 1–21. (doi:10.3390/genes13101846)

347. Stanic M, Mekhail K. 2022 Integration of DNA damage responses with dynamic spatial genome organization. *Trends Genet.* **38**, 290–304. (doi:10.1016/J.TIG.2021.08.016)